Large Deformation of Highly Compressible Peaty Ground under Embankment Loading and a Proposal/Application of New Macro Element Method for Simulating Vertical Drain/Vacuum Consolidation

NGUYEN Hong Son

June, 2015

盛土載荷に伴う高圧縮性ピート地盤の大変形と鉛直ドレーン／真空圧密シミュレーションにおける新しいマクロエレメント法の提案／適用

NGUYEN Hong Son

平成 27 年 6 月

ABSTRACT

In the view of engineering, infrastructure development such as embankment construction on soft ground including highly compressible clay/peat could be considered one of the most difficult and stimulating tasks. Numerous damages due to unexpected circumstances such as long-term settlement, differential settlement and slip failure have been reported in this type of ground. In order to avoid potential damages, pre-countermeasures such as ground improvement are important to increase ground stability and reduce residual settlements. Vertical drain method has often been used as an effective pre-construction countermeasure for soft ground, and the representative examples are; the sand drain method and prefabricated (plastic-board) vertical drain method. In recent years, vertical drain method combined with vacuum consolidation method has been widely applied especially when embankments have to be constructed quickly to shorten construction period or when very soft soils such as peat exist near the ground surface. In practical design of vertical drains, one-dimensional consolidation calculation based on Barron's theory has been widely used, and in case of combining vacuum consolidation, the reduction in pore water pressure due to vacuum loading is often replaced by an equivalent surcharge load for simplification. However, in order to account for the inward deformation characteristics of vacuum consolidation, it is desirable to perform finite element analysis in multiple dimensions. In multi-dimensional finite element analysis, directly representing the vertical drain by finite elements with high permeability requires a considerable number of elements. Therefore, a macroscopic method is needed to describe the improved effects of installing vertical drains depending on drain spacing and permeability. In addition, a suitable analysis code was requested to describe the mechanical behavior of naturally deposited soft ground considering the range of behavior from large delayed settlement to instantaneous circular slip failure.

This study investigates numerically behaviors of soft ground including highly compressible peat under embankment loading improved by vertical drain/vacuum consolidation using soil-water coupled finite deformation analysis code ***GEOASIA*** based on an equation of motion with an inertial term, onto which the SYS Cam-clay model was mounted as an elasto-plastic constitutive equation describing the soil skeleton structure. In regard to macroscopic methods, this study employs a newly proposed macro element method in addition to the mass permeability method proposed by Asaoka et al. as the most common and conventional one. As an actual example of an embankment construction site, this research is of interest to the Mukasa area on the Maizuru-Wakasa expressway (construction started in 2005; road put into service in 2014), in which a thick soft ground containing clay and peat is underlying the embankment. In this case, test embankment constructed in 2006 with ground improvement by Sand drain method and an embankment located approximately 300m from the test embankment constructed in 2012 with vacuum consolidation are focused upon. . Using of various data from the study field such as laboratory test results, site investigations, and field observations, this study aims to: (1) describe the mechanical behavior of high compressive peat within the same

theoretical framework as all other soil components from clay to sand, (2) validate the ability of the analysis methods used in this study to accurately simulate actual observed behaviors, (3) propose the effective countermeasures for the target area based on the prediction of future settlement and (4) discuss the improved effects of vertical drains/vacuum consolidation on soft ground including highly compressible peat in ensuring stability and reducing residual settlement.

This dissertation is started with a literature review that has researched about peat or highly organic content deposits. This work gives an overview of generation process, global distribution, classification for engineering purposes, typical engineering properties, and geotechnical problems involved with construction on ground containing peat. After that, this study focuses on the mechanical behavior of highly compressible peat in the Mukasa area. The results of triaxial and one-dimensional compression tests on undisturbed samples are reproduced by the model responses of the elasto-plastic constitutive equation SYS Cam-clay model to describe the characteristics of highly compressive peat based on the soil skeleton structure concept. In addition, the environmental sedimentation and the in-situ conditions are deduced based on the site investigations. It is found that, under the test embankment in the Mukasa area, as a result of deposition under continuous artesian conditions of the valley bottom created by fault movement, the peat has an extremely low consolidation yield stress and was in a state in which even a slight increase in stress would result in large-scale compression. In the following, this study confirms the ability of the soil-water coupled finite deformation analysis code ***GEOASIA*** itself, to simulate the large-scale deformation of an ultra-soft ground containing approximately 50-m-deep soft peaty soil layers under the test embankment of the Mukasa area. In this location, large-scale settlement in excess of 11 m occurred in approximately 3 years following embankment construction. While construction of the test embankment did not induce catastrophic slip failure, it dramatically impacted the surrounding ground. Field observations show that this large residual settlement was attributable to the delayed compression of the deep peaty soil layers, which were assumed at the design stage, not to be subject to settlement. The large-scale deformation of the ground observed in the approximately 4-year period starting with test embankment construction is simulated. For simplicity, in this calculation, the mass-permeability method is used as a macroscopic method to describe the improvement effect of sand drains. After confirming the ability of the soil-water coupled finite deformation analysis code ***GEOASIA***, the code is used to predict future settlement allowing continuous simulations without changing the parameters. These predictions are then used to evaluate the effectiveness of the countermeasures aimed not only at improving stability during construction, but also at reducing residual settlement. The results of these analyses were applied in the planning of large-scale repair work performed on the test embankment. And, when an embankment was subsequently constructed near the test embankment on the ground including a similar type of highly compressible peaty soil, ground improvement was conducted prior to embankment construction as a countermeasure against residual settlement. In this study, valuable field data related to these latter construction efforts is also presented.

Additionally, representing vertical drains in a numerical model using soil-water coupled finite element analysis, is a challenge when simulating particularly, vertical drain combined vacuum consolidation; the study proposes a new macro element method. The original macro element method proposed by Sekiguchi et al. can allow very accurate incorporation of the water absorption function of drains even under 2-dimnensional plane strain conditions. In this study the discharge function of vertical drains is newly added to the method by treating the water pressure in the drain as an unknown and adding a continuity equation for the drains to the governing equations. By this extension, the well-resistance phenomenon could be exhibited automatically depending on the analytical conditions. Numerical analyses are conducted after incorporating the new proposed macro element method into the analysis code ***GEOASIA***. The calculation results show that the proposed method enables highly accurate approximation in problems involving material and/or geometrical nonlinearity and multilayered ground. In addition, it is revealed that the proposed macro element method is capable of reproducing various phenomena occurring when the vacuum consolidation method is applied to clayey ground containing a middle sand layer. In the location of the middle sand layer waterproof sealing material is often wrapped to the surface of drains, in order to avoid propagation of vacuum pressure. The effects of such countermeasures can be also appropriately reproduced by the proposed method here.

Finally, by utilizing this newly proposed macro element method, simulation and investigation of the effects of ground improvement by vertical drains/vacuum consolidation on peaty ground are conducted. This dissertation focuses on the peaty ground that was improved by combination of vertical drain and vacuum consolidation under an embankment located approximately 300 m from the test embankment in the Mukasa area. The settlement value is quite smaller even at the same height of the test embankment; moreover, the settlement occurred widely on neighboring areas instead of upheaval. The results indicate that the new proposed macro element method incorporating into FEM geo-analysis program ***GEOASIA*** is capable of comprehensively and closely simulating not only the magnitude of settlement but also various ground behaviors including deformation of the surrounding ground and pore water pressure distributions. Furthermore, additional simulations are conducted by using the same analysis method and parameters to demonstrate that the settlement on surrounding areas is due to the propagation of vacuum pressure through middle sand layers. An advantage of the proposed macro-element method is that the mesh width does not have to be matched to drain spacing. In other words, it is possible to evaluate the effect of drain spacing using the same mesh. Therefore, this study conducts further calculations to evaluate the improvement effects of vertical drains/vacuum consolidation particularly focusing on various drain spacing. Here an ultra-soft ground with alternating peat and clay layers is modeled to present the typical ground where vacuum consolidation would be applied. In addition, the construction costs are estimated based on the actual construction costs in the Mukasa area in order to consider economic aspect. The analysis results pointed out that, although the use of vacuum consolidation in combination with vertical drains is effective in cases where it is necessary to limit deformation of the surrounding ground, the same reduction in residual

settlement can be achieved using vertical drains alone, provided that drains are deployed at a sufficient frequency. When applying vertical drains/vacuum consolidation on a soft ground, it is important to carefully consider not only the ground conditions (ground permeability, the presence of a middle sand layer, etc.) but also the impact on, for instance; the ground adjacent to the improved area, construction costs, and construction time. The macro-element method newly proposed in this study could quantitatively simulate/evaluate the effects of various factors and should prove to be an effective tool for making comprehensive decisions in actual practice.

ACKNOWLEDGEMENT

I would never have been able to finish this dissertation without the guidance of my committee members, helps from the partners of Soil Mechanics Group in Nagoya University, and supports from my family and friends.

First of all, I would like to express my deepest gratitude to academic supervisor, *Professor Toshihiro Noda*, for his valuable guidance, intellectual motivation, consistent encouragement, and proving me with excellent atmosphere for doing the research. He has always made himself available for instruction and support when concepts were difficult to understand despite his busy schedule. Thanks to his insight and individual lecture, I can be able to understand the essence of continuum mechanics and further gain a deeper comprehension in academic research, e.g. from configuration of material point to material and spatial descriptions of the motion by the time until essential physical meaning of vector, tensor, gradient, Jacobian in the continuum mechanics then utilize these fundamental to understand soil skeleton description in the original Cam-clay SYS Cam-clay models. This has been a great opportunity for me to do doctoral research under his guidance and learn from his research expertise. Acquiring knowledge from Prof. Noda is not only helpful to my doctoral research but also supports effectively to my work in the future.

I am also equally indebted to the one of my dissertation committee members, *Professor Masaki Nakano,* for his constructive suggestion. In the academic research, *Prof. Nakano* always smiles to encourage us to overcome and make comfortable atmosphere in any difficult situation; his positive, optimistic, and comprehensible attitude has a significant effect on me.

I am acknowledged specially for valuable advices and supportive recommendations from *Professor Feng Zhang* of Nagoya Institute of Technology who is the one of my academic committee members.

I would like to express my sincere appreciate to *Associate Professor Shotaro Yamada*, my dissertation committee member, for his great support as my sub-supervisor. His idea of new macro element method plays a significant role in this dissertation. *Associate Prof. Yamada* always gives me valuable suggestions and comprehensible explanation at any time. Special thanks to him; I can be able to catch the key points of macro element, soil experiments, vertical drain modelling and constitutive model. His conscientious and industrious spirit always encourages me in my research progress and life.

I would like to express my best regarding appreciate to *Assistant Professor Mutsumi Tashiro* for her sincere encouragement and whole hearted supports to my work, in fact this dissertation cannot be completed gently without her. She is not only my academic advisor but also my great senior friend. She has introduced me step-by-step about mechanical behaviors of peat and other soils, ways to

estimate the ground initial condition, and give me a lot of valuable experiences in numerical calculation using ***GEOASIA*** especially for embankment and vacuum consolidation. Whenever I have any confusion she always is available to explain for me. I am also extremely thankful to her family for their enthusiastic greeting and caring my family in Japan. I wish our friendship would be going strong forever.

My sincere thanks are also due to *Associate Professor Kentaro Nakai* for his kindly encouragement, helpful advices and comprehensible explanations. He always ready to clear my confusing on continuum mechanic and SYS Cam-clay soil models in anytime. Also, he not only gives me constructive recommendations for my research but also for my daily life in Japan, drinking and talking with him make me feel relaxing.

It is also my pleasure to forward my special thanks to *Assistant Professor Hideo Nonoyama* for his valuable discussion about original and SYS Cam-clay models, and his important role in management in the laboratory and Japanese national annual conferences. I also deeply thank *Mr. Takayuki Sakai*, who is the researcher at the laboratory for his helping me to overcome computer and programing errors. Heartfelt thanks to *Ms. Hitomi Yamada* for her patience and helpful working in daily life. In further, I would like express my thankful appreciate to *Dr. Motohiro Inagaki, Mr. Kouichi Yamada, Ms. Chikako Nakahori, Mr. Kakeru Takahira*, and other members of Central Nippon Expressway Company for supporting me their investigation and monitoring data as well as warm welcome and arrangement for visiting the actual site construction.

Moreover, I am also grateful to *Dr. Binbin Xu* who was former doctoral student in the laboratory for his important help in study and daily life; and *Mr. Yoshikawa* who is doctoral student for his thoughtfully guidance in utilizing of ***GEOASIA*** as well as his assistance when going to conferences and travelling. I also thank others students in the laboratory, *Mr. Derrick Ayebazibwe, Mr. Rommel Balaijo*, etc. for their enjoyment with me in the laboratory life. The former members of laboratory, *Mr. Jomel Libut, Mr. Arnold Olaget, Mr. Yusuke Ando, Mr. Hikaru Umemura, Mr. Kazunari Suzuki, Mr. Shougo Yatou, Mr. Daisuke Yamaoka, Mr. Kenta Kato,* etc. are thanked for their cooperation in the research work, their tutorial in daily life and learning Japanese basic conversation.

I would like to thank *Associate Professor Yasuo Kitane* of Structural engineering laboratory who is my second supervisor for his kindly support especially in terms of my daily Doctoral course life.

It is my honor to extend my heartfelt thanks to *Ms. Hiroko Kawahara* who is the administrative officer for international students for her kindness and constant helps and supports in many ways.

The special acknowledgement is also expressed to the *Monbusho Scholarship Program*, provided by the Japanese Ministry of Education, Science, and Culture (MEXT) for the financial supporting in this research.

I am forever indebted to my family members and friends for their unceasing support and sacrifices throughout this work to help me formulate this task in present form.

Last but certainly not least, I wish to appreciate to my wife *Ms. Mai Thi Thuy Phuong* very much for being there for me whenever I need her even a bad or a great day, cheering me up, and her great

efforts in taking care our daughter. In addition, I am immensely indebted to my daughter *Miu chan*, the wonderful gift from God that wipes away all my sorrow. Wish her healthy and happy.

NGUYEN Hong Son
Nagoya University
Nagoya, Japan

Contents

Chapter 1

Introduction

1.1. Background

Peat/highly organic soil is an accumulation of partially decomposed vegetation fragments and often referred as problematic soils for constructing infrastructures such as expressway or railway embankment, dyke, building, storage facilities, industrial zone (Terzaghi et al., 1996; Mesri and Ajlouni, 2007; Hayashi et al., 2012; Huat et al., 2014) due to its high water content, low shear strength and bearing capacity, and high compressibility including the secondary compression. In addition, its engineering properties highly depending on spatial distribution are not similar to well-known inorganic soft soil (Brawner, 1958; Lea and Brawner 1963; MacFarlane 1969; Hartlen and Wolski, 1996; Mersi et al., 1997; Mesri and Ajlouni, 2007; Huat et al., 2014). As example of geotechnical problem of the ground containing peat, Gould et al. (2002) reported four construction cases over organic soils in an urban area in the City of London, Ontario, Canada, three ones of which were classified as failure and required expensive cost for reparation. The recent slope failure during construction of embankment/dyke over peat deposit in Netherlands without sufficient adopted ground improvement were also described in Van Baar (2005) and Zwanenburg et al. (2012) (see **Photo 1. 1**). On the reconstruction of Cush Road, Co. Offaly in Ireland, Hanraha (1964) had to deal with not only large amount of long-term settlement but also upheaval and lateral displacement after 10 years of operation. In Japan, the peat deposit covers about 6% of national land area mainly distributed in Hokkaido (Hayashi et al. 2011; Huat et al. 2014). Porbaha et al., (2000) analyzed a failed embankment for the Hokuriku expressway in Niigata, while Hayashi et al., (2011) have reported the slip failure of the test embankments over a peaty ground in Hokkaido when not applying ground improvement during embanking in their studies. Similar problem statements when a test embankment construction on peaty ground was also found in the Wakasa area of Fukui prefecture in Japan reported by Hirata et al. (2010a). Even though any catastrophic slip failures were not recognized, it dramatically impacted the surrounding ground, and large-scale settlement in excess of 11 m occurred in the approximately 3 years following embankment construction.

Photo 1. 1 The example of failure embankment over peat deposit (after Zwanenburg et al., 2012)

Since the construction on peaty ground has high potential causing serious problems as above, the pre-countermeasure should be applied. Hartlen and Wolski (1996) summarized a number of methods can be utilized in practice like excavation, replacement, displacement, lightweight filling, preloading and preloading combined with vertical drainage in group of stage construction, lime/cement columns. They also stated that the selection of construction method must be considered both economic and technical aspects. In order to ensure both accelerating construction period and reducing lifecycle cost including maintenance and management costs, the pre-loading and its combination with vertical drain such as sand drain and prefabricated vertical drain has been applied as a most suitable method. While Mesri and Ajlouni (2007) generally stated that pre-loading has advantageous and economic solution in technical and environmental issues, Hartlen and Wolski (1996) noted that this vertical drainage method could be effective for avoiding instability during construction and long-term settlement. In Japan, based on approximately 50 years of construction experience of expressway, a standard practice for using vertical drain method or vertical drain together with reinforcement to improve a soft ground prior to construction of embankment has been issued to consider only problem of "stability" (Japan Highway Public Corporation, 1998; Hayashi et al., 2011). It is recognized that the residual or long-term settlement is not sufficient taken into account at the design stage, some other methods such as lightweight material replacement or overlaying construction have been dealt with through maintenance and repair after entry into operation.

Vacuum consolidation was first introduced by Kjellman in 1952 of the past century, recently becomes more popular when it was used as combination with vertical drains, as typical construction diagrams are shown in **Fig 1.1** (Shinsha et al., 2006) to reduce residual settlement, increase shear strength of soft soil, as well as to shorter construction period for embankment or surcharge loading (Bergado et al., 1998; Chai et al., 2005, 2006, 2008; Yan and Chu, 2005; Rujikiatkamjorn et al., 2007;

Mersi and Khan, 2012). This method was currently performed when the ultra-soft ground containing peaty and organic soils were encountered (Cognon et al., 1994; Ariyarathna et al., 2010; Osorio et al., 2010; Kosaka et al., 2011; Karunawardena and Toki, 2013), even though the number of literatures is much less than that for inorganic soft clay and silts, and the effect on residual settlement due to secondary consolidation/delayed compression of peat is still not clear. When applying vacuum consolidation, the negative excess pore water pressure is generated instead of positive one resulting in inward lateral deformation as the remarkable characteristic while increasing the effective stress in soil mass. In this case, in addition to increase shear strength, the stability was increased potentially by offsetting the outward deformation causing by embankment loading. Meanwhile, this inward deformation should be considered carefully because it can influence to wide area of the surrounding ground depending on ground condition.

In the practical design, however, one-dimensional consolidation calculation based on Barron's theory has been widely used, and the reduction in pore water pressure due to vacuum loading is often replaced by an equivalent surcharge load for simplification. In order to account for the inward deformation characteristics of vacuum consolidation, some researchers proposed analytical model and numerical simulation of investigation effect of vacuum consolidation (Chai et al., 2005; Indraratna et al., 2004, 2005; Tran and Mitachi, 2008). However their methods is required a large number of fine elements or less applicable to real multi-layered soft ground including clay, peat, and specially high permeable sand at middle of installed vertical drain depth. Therefore, it is necessity a macroscopic method to describe the effects of vacuum consolidation with vertical drain, then able to predict ground behaviors and design appropriate construction conditions including drain spacing, area of improvement, and duration of vacuum loading, etc. In addition, a suitable analysis code was requested to describe the mechanical behavior of naturally deposited soft ground considering the range of behavior from large delayed settlement to instantaneous circular slip failure.

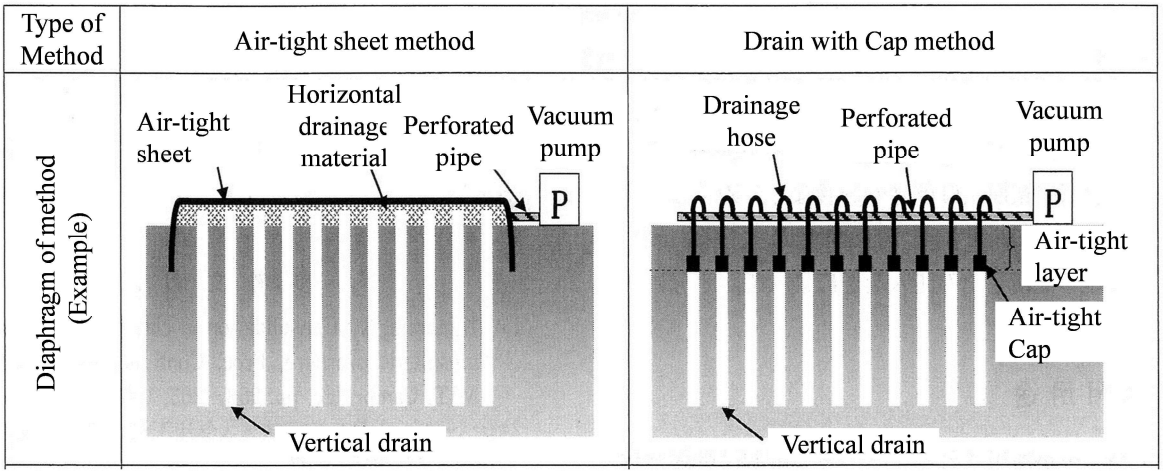

Figure 1. 1 The typical diagrams of vacuum consolidation (Shinsha et al., 2006)

About the engineering properties of peat itself, some researcher have examined experimentally and numerically. Mesri and Ajlouni (2007), focused on interpreting shear strength, permeability, compressibility and especially secondary compression (Mesri et al., 1997) using laboratory test results on undisturbed specimens. Engineering properties of Japanese peaty soil including consolidation compressibility, undrained shear strength, anisotropy characteristics, volume change of pore size during shear were published by Yamaguchi et al., (1985a, 1985b, 1987, 1992), and then was summarized in Noto (1991). In aspect of constitutive modeling, Brinkgreve et al., (1994) applied both conventional Morh-Coulomb and Modified Cam-clay models to analyze embankment over peaty ground, Tan (2008) used soft soil creep model for taking account creep effect in highway construction over peat bog, and other researchers tried to describe the anisotropy response of peat due to presenting of fibers (Sellmejer, 1994; Termaat and Topolnicki, 1994). Due to the limited experience rather than its mechanical behavior itself, peat has been regarded as unusual soil, and some kinds of exclusive model for peat have been proposed. However, peaty ground is generally not homogeneous and includes various type/condition of soils depending on the deposited environment. Therefore, suitable constitutive model is recommended to describe mechanical behavior of peat within the same theoretical framework as all other soil components from clay to sand.

1.2. Research objectives and scopes

The objectives of this study are:

- Describe the mechanical behavior highly compressible peat using the SYS Cam-clay model based on deduction of ground sedimentary condition;
- Simulate large deformations of a ground containing highly compressible peat due to a test embankment loading by soil-water coupled finite deformation analysis; Numerically investigate the effective countermeasures against residual settlement and slip failure of peaty ground;
- Propose a new macro element method in order to simulate precisely the effect of ground improvement not only vertical drain but also vacuum consolidation;
- Validate the accuracy of the proposed method by simulating an actual site of peaty ground improved by vacuum consolidation;
- Inquire into the effect of ground improvement by vertical drains/vacuum consolidation with a particular focus on the effect of drain spacing.

SYS Cam-clay model (Asaoka et al., 2002) is an elasto-plastic constitutive model that is capable to describe mechanical behavior of wide range of soils from clay, intermediate soil, to sand, and even embankment material. Therefore, results from one-dimension compression and triaxial consolidated undrained shear tests of peat were reproduced by using this constitutive model to describe movement of soil skeleton structure as its mechanical behaviors. While the initial sedimentary environment that is unique in the area of this study due to influence of artesian water pressure is deduced. After that, the simulation is carried out to simulate the effects of embankment loading on soft ground containing

high compressible peat improved by sand drains by using FEM code ***GEOASIA***; the increasing of permeability inside improved area was analyzed by attempting mass-permeability concept (Asaoka et al., 1995) for simplicity. Furthermore, effective countermeasures that are possible to apply to study field to against long-term settlement and failure are dealt with using the same material parameter of soils.

The mass-permeability concept is a simple method (Asaoka et al., 1995; Chai et al., 2001) to simulate the present of vertical drains; however the consolidation process of ground is not accurately reproduced even through acceptable ground surface settlement was shown. In order to increase the preciseness of simulation, this study extends the conventional macro element originated by Sekiguchi et al. (1986) by treating water pressure within vertical drains as unknown. This extension is verified by comparing analyses results to those from exact axisymmetric unit cell model. In addition, the advantages of this new proposed macro element are demonstrated in series of numerical analysis of vacuum consolidation together with vertical drain on assumed soft ground involving middle sand layer.

In order to validate the newly proposed macro element method, the simulation of behaviors a real soft ground containing peat that locates near the test embankment and to be improved by vacuum consolidation is performed by using ***GEOASIA*** incorporated the new macro element method. As an addition results, the effects of middle sand layer existed in improved subsoil profile can be indicated. After success in validation, the analysis is continued to numerically investigate the performance of vacuum consolidation combining with vertical drain and utilization of vertical drain only, particularly focusing on influence of drain spacing.

The scopes of this study are:

- The field study is located at Mukasa area of the Maizuru-Wakasa Expressway, Fukui Prefecture, Japan. SYS Cam-clay model are used to describe the mechanical behavior of soils including peat that encountered in this area;
- The new proposal of macro element only solves the well-resistance effects of vertical drain, the smear effect is not considered separately here but it is taken account into determination of permeability coefficient of drain by trial and error in the simulating the actual ground behaviors. In addition, the smear effect is assumed small due to high technics of prefabricated vertical drain installation.

1.3. Brief introduction of FEM code-GEOASIA

This study only using finite element geo-analysis code namely ***GEOASIA*** for performing a series of numerical simulation. The ***GEOASIA*** code that has been developing by Geotechnical Ground of Nagoya University is appropriate due to its capability handling the particular geotechnical problems within unified framework. As one of the remarkable features of ***GEOASIA***, the influence of inertial forces on geometrical deformation can be preceded. The inertia terms is represented and appears in the rate-type equation of motion by updating Lagrangian method to the usual motion equation.

FEM code-***GEOASIA*** has advantages as follows:

1) Having the breadth of application in geotechnical issues. That contains numerical simulation of mechanical laboratory experiments including oedometer test, plane strain tests, trial shear tests, hollow cylinder torsional shear tests; static/dynamic analyses of ground problems like slope instability, consolidation and delayed settlements under embankment with/without vacuum loading, liquefaction and post settlement of ground induced by earthquake, behavior of levees on soft ground concerning seepage/seismic, soft ground improvement by sand compaction pile, ground deformation including excess pore water pressure within vertical drains in soft ground treatment by vertical drain/vacuum consolidation, soil-structure interaction.
2) Capable description of natural sedimentary deposits including clay, intermediate soil, sand, as well as filling material in high accuracy with an efficient elasto-plasic constitutive model named SYS Cam-clay model (Asaoka et al. 2002, 2003). Because characteristics of soil generally include the dilatancy behavior, confining pressure sensitivity, anisotropy, and dependence of stress path, it becomes a key point when utilizing a unified soil model to predict behaviors of soil under general stress paths. By employing SYS Cam-clay model, only one set of material parameters need to reproduce the mechanical response of soil under different initial conditions.
3) The effect of inertia term is clarified. In FEM, the equation of motion acting as the equilibrium equation during deformation is one of the governing equations. A dynamic rate-type equation of motion is acquired in ***GEOASIA*** based on the two-phases mixture theory and updated Lagrangian method, that makes it able to anticipate the influence of inertia term on the geometrical deformation.
4) Unified framework for dealing with geotechnical problems. The unification here includes four aspects. First, the SYS Cam-clay model can describe the mechanical of almost natural sedimentary deposits with only one set of material parameters and various initial conditions; Second, the distinction of the deformation problems and strength problems is not necessary because it can represent the stages from initial deformation to peak point until failure after the peak; Third, quasi-static/dynamic analyses can be performed without change of the analysis code; Four, the GEOASIA can simulate and predict the entire response consistently for a given in-situ initial ground, consisting of construction of the man-made structure, consolidation settlement due to external loading, seismic response like liquefaction or failure during the seismic, and consolidation settlement after the seismic. The only soil parameters are decided at initial stage is necessary during whole calculation process. It is quite significance because it is impossible to analyze the same engineering issue with more than one ground of soil parameters.

1.4. Research outline

The dissertation is composed of six chapters and twelve appendices as follows:

In *Chapter 1*, the background, scope, objectives and outline of the research are introduced. The fundamental information of finite element method (FEM) code namely ***GEOASIA*** which is the major analysis tool using in this study is also given.

In *Chapter 2*, an overview of literature of peaty soil is early provided including environmental condition of peaty formation, global distribution of peaty soils, and classification for engineering purposes. Previous researches records that peaty soil could be considered as a problematic soil due to their extremely low shear strength and highly compressive character. Sequentially, the large-long term settlement and slip failure are highly recommended to consider when constructing on the type of soil. The later part of this *Chapter* describes the peaty soil in the field of this research that is located on Mukasa region of Maizuru-Wakasa expressway, Japan. Sedimentary environment and in-situ stress stage of deep peat layers are deduced from geotechnical investigation data. It found that deep peat layers nearby the mountain side are affected by artesian pressure due to the continuous thick alternative peat and clay layers and fault activities in geological history, meanwhile the plain area are not affected by the artesian. The triaxial and one-dimensional consolidation test results were faithfully reproduced by SYS Cam-clay model to describe the mechanical behaviors of peaty soils and determine the soil parameters.

In *Chapter 3*, the deformation of a soft ground containing highly compressive peaty soil under a test embankment loading in Mukasa region of Maizuru-Wakasa expressway is discussed. The material constants and initial in-situ conditions which were previously determined in the *Chapter 2* were put into FEM analysis to simulate the observed settlement and lateral spreading of the ground under the test embankment to confirm the capacity of soil-water coupled for peaty soil. After that, the calculation was continued to predict future settlement as well as investigate the effectiveness of countermeasures such as mass permeability method by vertical drain, slow banking, and lightweight banking material to against residual settlement and failure. Based on the results of these analyses, the ground improvement by vertical drain combined with vacuum consolidation was suggested to apply for the remaining similar ground containing highly compressive peaty soils in the project to reduce residual settlement and accelerate construction process.

In *Chapter 4*, a new expansion of macro element method with water discharge and absorption functions for vertical drain is proposed. As the extension of conventional macro element, the discharge function of drain was recently added to the method by treating water pressure inside the drain as unknown parameter, in addition, the continuity equation for drain was introduced to the governing equations. The basic performance of the proposed macro element method after incorporating into quasi-static soil-water coupled elasto-plastic finite deformation analysis was calibrated based on calculation of consolidation for an axisymmetric unit cell. The results of calculations from “exact model” and “approximated model” are almost compatible, in which the finite element with high coefficient of permeability was assigned for drain in the former, and the proposed macro element was used in the later. As an example of application, the proposed macro element was also applied to a virtual ground consisting of a middle sand layer consolidated by vacuum pressure to

simulate the well resistance phenomena due to sucking of water through middle sand. It is found that the efficacy of vacuum consolidation reduced because of well resistance caused by presence of middle sand layer; however, this behavior is not able to demonstrate by using macro element with known water pressure within drain as the original one. The results likewise show that waterproof sealing is effective for preventing loss of vacuum pressure when the middle sand layer exists in the ground. Furthermore, the method to estimate the equivalent diameter of drain (d_w) in the proposed macro element is discussed based on the three dimensional analysis, it is revealed that estimation of d_w by equalizing cross-sectional area of drain is the most agreement.

In *Chapter 5*, as verification of the proposed macro element method in the previous chapter, the simulation of an actual embankment placed on a similar ground as the *Chapter 3* that improved by vertical drain combine with vacuum consolidation was performed. The simulation results illustrate the ground deformation including centerline settlement, lateral displacement and surrounding vertical settlement, and pore water pressure are well reproduced. Unexpected settlements at the surrounding area of this actual embankment were observed in the field due to the propagation of vacuum pressure through middle sand layers, analysis results indicated that the phenomena could be prevented by installing a sheet pile at the surrounded improved area. After confirmation of capacity of the proposed macro element method, this study evaluated numerically improvement effects of vertical drain and vacuum consolidation when the embankment loading on soft ground containing peat and clay layers, particularly focusing on influence of drain spacing. From the results, it is pointed out that vacuum consolidation is highly effective in the case of limited surrounding ground deformation is required, while using an appropriate small drain space has a similar impression on reduction of residual settlement.

In *Chapter 6*, the conclusions of this study are summarized and future works are mentioned to improve the study.

In *Appendix 1*, the physical model for soil-water coupled governing equation in static condition is introduced. *Appendix 2* describes the construction of the dynamic soil-water finite deformation analysis mounted with the new proposed macro element method for simulating vertical drain.

Chapter 2

Description of mechanical behaviors of highly compressible peat by using SYS Cam-clay model

2.1. Introduction

Construction of a road embankment on very soft peaty ground is not recommended because this type of ground does not provide suitable supports to the foundation and mostly cause engineering problems (Terzaghi et al., 1996, Hayashi et al., 2012). The characteristics of peaty soils are high porosity, extreme potential of primary and secondary compressibility, low shear strength and depending on properties of contained fiber, the permeability strongly vary on porosity and stress conditions, and highly inhomogeneous spatial properties, that are different to the most inorganic soft clay. In the numerical investigation of ultra-soft peaty ground behavior under the external load such as embankment, the mechanical behaviors of peaty and organic soils have to be described clearly by a constitutive equation as an essential requirement.

In order to understand and clarify peat deposits with other type of soil, *Chapter 2* firstly given an overview of peat deposits distribution on the Earth including visual description, sedimentary environment, engineering classification, and record of geotechnical problems. After that, laboratory test results collected from boring investigation in Mukasa, Fukui Prefecture, Japan where is the research field were screened to identify type of soil including clay, sand and, particularly peat then classified into the soil layers to interpret ground layer structures. The ground layer structures and representative values of engineering properties were estimated for further analyses. Subsequently, the results from mechanical tests like eodometer and consolidated undrained trixial shear were separated for corresponding soil types based on their physical properties. Furthermore, the laboratory test results combine with site investigation to deduce the sedimentary environment stratums; it was investigated why such a massive delayed compression occurred in the deep peat layer of the area that is close to mountains, in which artesian pressure has affected.

The research utilizes the finite deformation ground analysis code ***GEOASIA*** (Asaoka and Noda, 2007; Noda et al., 2008a) mounted with the SYS Cam-clay model capable to describe mechanical behaviors of all type of soil including clay, sand, and intermediated soil as well as soil at natural or remold states (Asaoka et al., 2002) as constitutive equation for soil skeleton. Because of that, the simulation of results of oedometer and undrained triaxial shear tests on peat and soft clay samples in Mukasa area were performed in this *Chapter* using SYS Cam-clay model. Resulting from these simulation the material constants were obtained, After obtaining material constants by respond of SYS Cam-clay model and interpreting initial condition of ground with consideration of sensitivity of

soft clay and peat to disturbance during sampling (Inagaki et al., 2010), mechanical behaviors of peat as well as soft clay in field of study were described.

Mechanical behaviors and sedimentary conditions of peat in the field study have been characterized in Tashiro et al. (2015) and Nguyen et al. (2015).

2.2. Literature reviews of peat

2.2.1. Generation process of peat

Peat is identified as a highly organic soil consisting of macroscopic and microscopic fragments of decayed plant fibers (**Photo 2.1 & Fig2.1**) resulting from incomplete decomposition processes in swamps or wetlands under anaerobic conditions (Wilson et al., 1965; Hobbs, 1986; Yamaguchi et al., 1992; Kazemian et al., 2011). The color of peat ranges between light brown and black (Terzaghi et al., 1996) with distinctive odor (Craig, 1992). Peat mainly made up from organic matters which are spongy, highly compressible and combustible then possesses typical geotechnical properties comparing with inorganic clay or sandy soil originated of soil particles only (Yamguchi et al., 1992).

Photo 2. 1 The example of Peat deposit in Mukasa area, Japan

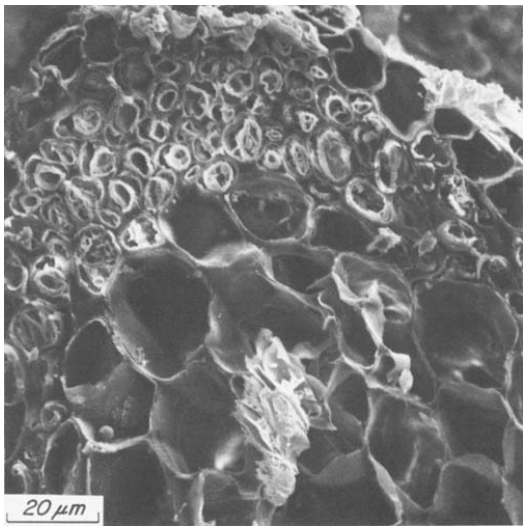

Figure 2.1 Photomicrograph of fibrous Peat (Terzaghi et al., 1996)

Peat is encountered in many countries; it covers about 5 to 8% of the land surface of the earth (Mesri and Ajlouni, 2007). Peat deposits mainly distribute in cold regions such as Canada, United State, Russia, and northern Europe. Mersi and Ajlouni (2007) estimated that tropical and sub-tropical peat in Indonesia, Malaysia, Brazil, Uganda, Zambia, Venezuela, and Zaire accounted for 8 to 11% of global peat deposit. In Japan, peat is widely distributed in Hokkaido, the northernmost main island of Japan, with area of approximately 2,000 km^2, contributing 6% of land area (Huat et al., 2014). **Table 2.1** shows the distribution of peatland throughout world by area and percent of land area.

Table 2. 1 Peatlands of the Earth (Mersi and Ajlouni, 2007; Huat et al., 2014)

Country	Peatlands (km^2)	Percent of land area
Canada	1,500,000	18
USSR (former)	1,500,000	
United States	600,000	10
Indonesia	170,000	14
Finland	100,000	34
Sweden	70,000	20
China	42,000	
Norway	30,000	10
Malaysia	25,000	8 (*)
Germany	16,000	
Brazil	15,000	
Ireland	14,000	17
Uganda	14,000	
Poland	13,000	
Falklands	12,000	
Chile	11,000	
Zambia	11,000	
Japan (*)	2000	6
26 other countries	220 to 10,000	
Scotland		10
15 other countries		1 to 9

(*) According to Huat et al. (2014)

In general, the classification of peat depends on content of organic matter, fiber, and degree of decomposition. There are several classification systems that are using for different countries based on organic content. Hobbs (1986) presented that geotechnical engineers in Russia defined peat and peaty soil as soils in which organic matter fractions exceed 50% and 10-50% respectively; in the United State of America Andrejko et al. (1983) recommended that soils with more than 75% organic matter as peat; and Hobbs (1986) suggested that peat in British is a soil containing organic matter more than 27.5%. In Canada, soil having an organic content more than 80% is called peat, and that from 60-80% is called peaty organic soil (Landva et al., 1983). Karlsson and Hansbo (1981) proposed a high organic soil with organic content more than 20% as peat in Sweden as shows in **Table 2.2**. This boundary value of organic content is also use to classify peat in Japan (Yamguchi et al., 1985) and tropical peat in Malaysia (Huat et al., 2014). In this research, the soil sample containing organic matter more than 20% is considered as peat, in which, terms of peat and organic soil can be interchangeable.

Table 2. 2 Guiding values for the classification of soils on the basics of organic content (Karlsson and Hansbo, 1981)

Soil group	Organic content in weight of dry material (< 2mm), %	Examples of designation
Low organic soils	2-6	Gyttja-bearing clay Dy (*)-bearing silt Humus-bearing, clayey sand
Medium organic soils	6-20	Clayey gyttja Silty dy (*) Humus-rich sand
High organic soils	>20	Gyttja Dy (*) Peat Humus-rich topsoil

(*) Dy denotes the stage of completely destroyed of the plant structure

As mentioned above, peat is classified on the basics of degree of decomposition or humification of remained parts of plants. For engineering purposes, Karlsson and Hansbo (1981) suggested that peat can be divided into three main types in accordance with the von Post scale as seen in **Table 2.3.**

- ***Fibrous peat*** is low decomposed and clear plant structure, brown to brownish yellow in color. The material remain in the hand has a fibrous structure if sample is squeezed in the hand. This group falls in H1 – H4 on the von Post scale.
- ***Pseudo-fibrous peat*** is moderately decomposed and unclear to relative clear plant structure, usually brown in color. If sample is squeezed in the hand, more than haft of peat mass remains between the figures. The material remaining in the hand has a more or less mushy consistency, but with clear fibrous structure. In according to von Post scale, this type of peat is in range H5 – H7.
- ***Amorphous peat*** is highly decomposed and invisible plant structure, with brown to brownish black in color. When squeezing sample in the hand, only few more solid components such as root fibers and wood remnants can be remained in the hand at mushy consistency. This group is H8 – H10 in the von Post scale.

Table 2. 3 Classification of peat on the basis of decomposition on the von Post scale (Karlsson and Hansbo, 1981)

Designation	Group	Description
Fibrous peat	H1 – H4	Low degree of decomposition. Fibrous structure. Easily recognizable plant structure, primarily of white mosses
Pseudo-fibrous peat	H5 – H7	Intermediate degree of decomposition. Recognizable plant structure
Amorphous peat	H8 – H10	High degree of decomposition. No visible plant structure. Mushy consistency

There is another classification system for Canadian peat proposed by Radforth (1969) based on the structure of peat rather than its organic content or decomposed process. Peat is divided into three main categories which are amorphous-granular, fine-fibrous (fiber diameter ≤ 1mm), and coarse-

fibrous. The amorphous-granular peat is similar to clay in grain structure where water in pore is locked in an absorbed condition around particles, meanwhile two later types of peat hold free condition for pore water in the mass, and the concept of "woody" is put to these types of peat.

Peat generated in the humid region like swamps where usually lack of oxygen and acidic pore water causes delay of oxidation. In this condition of environmental deposition, procedure of decomposition is slower and accumulation is faster than that of dry area. Because of absenting free oxygen the dead plants or vegetation are fermentation and putrefaction rather than decomposition by evolution of organic gaseous, such as methane as obvious evidences. Peat formation occurs wherever these conditions are favorable without regard to altitude or latitude, but almost peat area locates in the cold and temperate regions as mentioned in **Table 2.1** (Hartlen and Wolski, 1996). The peatland is highly complicated system and its development is altered based on the environments regarding water supply, temperature, and supply of nutrients. A typical generation process of peat in a lake normally consists of three stages with different types of peat were described by Hobbs (1986), and showing in **Fig. 2.2**. In the first stage, peatlands develop by filling lake, basin, or valley by sediments under the ground water level controlling. Rich nutrient is supplied by run-off and percolating groundwater promotes the expanding of vegetation. The marsh-like scenery commonly referred as fen peat is adopted at the end of this stage. Such fen peat is underlain by very soft organic mud and organic clay in general manner. In the second stage, transitional peat is formed due to the raising growth of peatland extent on direct precipitation for water supply. The peat is ordinarily mixed and woody. In the last stage, the growth of peatland is more distant the maximum physical limits of the groundwater and water supply depends only on direct precipitation. Peat itself acts as a reservoir holding water above groundwater level. This type of peat is termed as raised bogs and acid in character.

Huat et al., (2014) stated that peat deposits in the tropical region are commonly referred as basin and valley peat for that occurrence in highland and lowland area respectively. Lowland or valley peat is usually found in poorly drained depression or basin areas; meanwhile, basin peat is often encountered on the inward edge of the mangrove swamps along a coast.

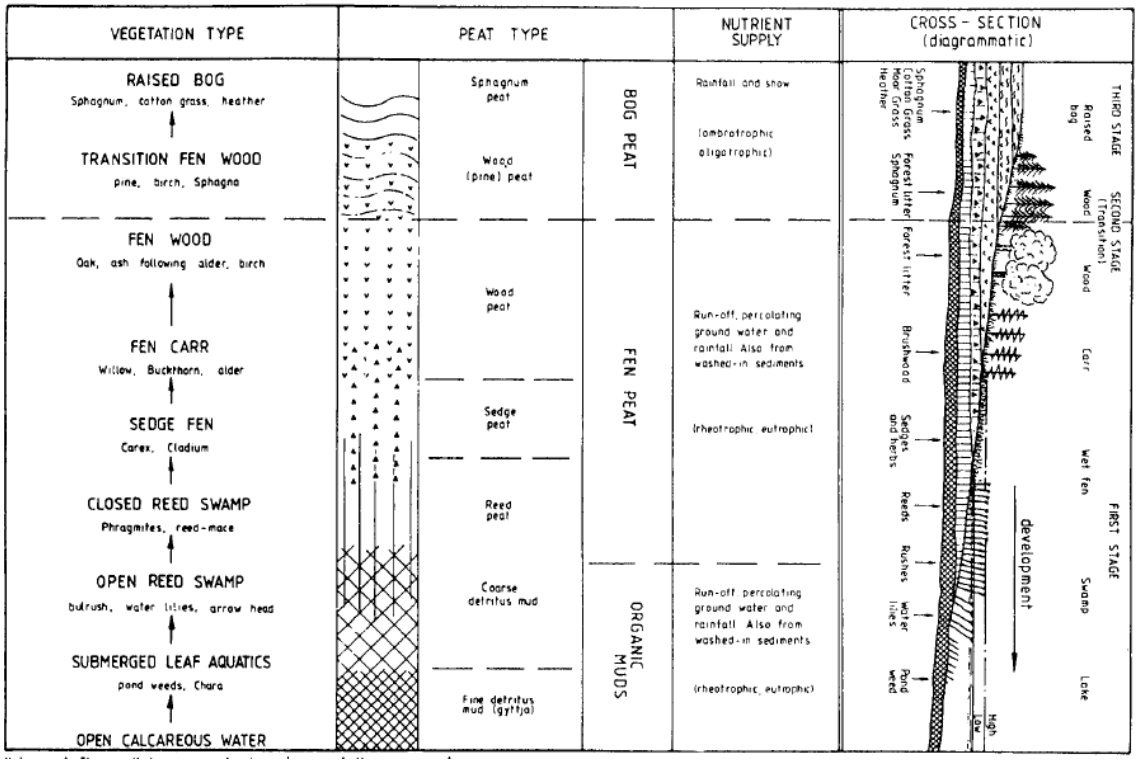

Figure 2.2 Vegetation and peat succession by lake filling (Hobbs, 1986)

2.2.2. Engineering properties of peat

The engineering properties of peat and organic soils as well are extremely variable mainly depending on the amount of organic matter or degrees of decomposition, and its structure (Hartlen and Wolski, 1996). Although peat possess distinctive engineering properties with those of inorganic soils like clay and sand, the same basic mechanism and factors could be used to determine both behaviors of peat and inorganic soils (Mersi and Ajlouni, 2007). The peat's engineering properties consisting of organic content, water content, liquid and plastic limits, particle density etc., has been interpreted accurately from laboratory experiments and field observations; however the potential for biodegradation of peat in laboratory environment has been considered carefully in testing and interpretation of experimental results, previously noted by Mersi et al. (1997).

Organic content: This is the most important factor affecting on engineering properties of peat. As mentioned earlier, the soil containing more than 20% of organic content is considered as peat. **Table 2.4** shows a summary of peat's engineering properties collected from literatures, in which organic content of peat varies from 20% to 99%. In general, the amount of organic matter indirectly determined from the loss of ignition method as percentage of mass after drying by oven using **Eq. 2.1** proposed by Skempton and Petley (1970).

$$H\,(\%) = 100 - 1.04(100 - Li) \tag{2.1}$$

Where: H is organic content; Li is loss if ignition

Water content: The method using to determine the water content of peat is same as that using for inorganic soil. Peats usually have an extreme high natural water content which can be ranged from 100% to surpass the value of 1500% as several typical peats tabulated in **Table 2.4**.

Consistency limits: In the view of civil engineers, the consistency limits mainly indicate liquid and plastic limits of soil, and the same determination method can be used for peats. In addition, peats contain the amount of dead plant fragments then their consistency properties highly depend on the type of organic matter, degree of decomposition, and clay mineral as well (Huat et al., 2014). The liquid limit of peat in temperate region ranges from 200% to 1500% which is reported by Hobbs (1986). The typical consistency limits of peat are also shown in **Table 2.4**.

Density of soil particle: For peats and organic soils, the density of soil particles can be tested using the boiling bottle or gas jar methods which are frequently utilized for inorganic soils. Generally the particle density of peat is smaller than that of mineral soils depending on the organic components. The cellulose (pure peat) has particle density ranges from 1.40 g/cm^3 to 1.50 g/cm^3, while mineral particles have density around 2.70 g/cm^3. Hobbs (1986) illustrated the relationship between soil particle density peat and its organic content as shown in the **Eq. 2.2**. The particle density of typical peats varies in the range of 1.40 – 1.80 g/cm^3 as shown in **Table 2.4**.

$$\rho_s = \frac{3.8}{0.013 \cdot H + 1.4} \tag{2.2}$$

Where ρ_s is solid particle density, H is organic content (same notation as **Eq. 2.1**)

Permeability: Peat sediments ordinarily exist at very high initial void ratio with the pore diameter of undisturbed sample at initial stage in the variation of 100μm – 0.1μm (Yamguchi et al., 1985). Therefore, properties of the pure peat often possess high initial permeability that is typical in range of 100 to 10,000 times higher that of soft clay or silts (Mersi and Ajlouni, 2007). However, the permeability of peat reduces dramatically under the change of compression load or effective vertical stress due to the reduction of void ratio indicated by laboratory measurements (Hanrahan, 1954, Lefebvre et al., 1984, Yamguchi et al., 1985, Santagata et al., 2008); under the typical high embankment load, the permeability of peat even decrease to smaller than that of clay deposit (Miyakawa, 1960). The linear relationship between permeability coefficient in logarithm and void ratio has been supposed (e.g. Mersi and Ajlouni, 2007).

Table 2.4 Engineering properties of typical peat summarized from literatures

Peat type	Water content	Liquid limit	Plastic limit	Particle density (ρ_s)	Organic content	Void ratio	References
	%	%	%	(g/cm^3)	(%)		
Amorphous (Canada)	200-600			1.62-1.65	77.5-87.8		Adam (1965)
Fibrous (Canada)	355-425			1.73	84.1		
Amorphous (Canada)	600			2.0	25.1		Wilson et al., (1965)
James bay Fibrous (USA)	660-1591			1.53-1.68	66.7-99.9	11.61 -27.53	Lefebvre et al., (1984)
	1000-1340			1.37-1.55	95.9		Ajlouni (2000)
	1000-1340			1.50-1.64	96.0	18.0-23.5	Mersi and Ajlouni (2007)
Middleton peat (USA)	623-846			1.53-1.65	90-95	10.1-14.2	Mersi et al., (1997)
	510-850			1.47-164	93-95		Ajlouni (2000)
	510-850			1.53-1.65	90-95	8.3-14.2	Mersi and Ajlouni (2007)
Ohmiya peat (Japan)	300-1200			1.60-2.30	27.2-79.2	7.0-18.0	Yamaguchi et al., (1985)
Ishikari peat (Japan)	718-921			1.7-2.0	53.0-77.7	11.5-17.6	Yamaguchi et al., (1992)
Hokkaido peat (Japan)	369-679			1.54-2.11	41.8-90.6	10	Hayashi et al. (2011)
Peaty	152-240				44.0-65.0		Boulanger et al., (1998)
Peat (Netherlands)	520			1.69	55.3		Zwaneburg (2005)
	200-600				25-95		Zwaneburg et al., (2012)
High organic content soil	129-390	228-406	114-253	1.95-2.2	33.4-63.6	4.28-5.49	Santagata et al., (2008)
Hokkaido peat (Japan)	259-913				13.7-90.6	7.8-13.8	Hayashi et al., (2012)
Sri Lanka peat	110-470				60.0-70.0		Karunawardena (2007)
Ireland peat	700-1400			1.10-1.80		25	Hanrahan (1954)
	650-1350				93.0-98.0		Osorio et al., (2010)
Australia peat	168-247	259-305	125-207	1.53	63.0-68.0		Whitlow (2000)
Turkey peat	136-322	148-315		1.73-2.13		2.19-4.68	Ulusay et al., (2010)
West Malaysia peat	200-700	190-360	100-200	1.38-1.70	65.0-97.0		Huat et al., (2014)
East Malaysia peat	150-2207	210-550	125-297		50.0-98.0		
Kalimantan peat (Malaysia)	467-1224			1.50-1.77	41.0-99.0		
Adria peat (Italy)	330-421			1.55-1.58	68.0-75.0	5.15-6.84	Cola and Cortellazzo (2005)
Correzzola peat (Italy)	606-790			1.46-1.60	70.0-72.0	10.25-11.84	

2.2.3. Geotechnical problems on peaty ground

In the view of geotechnical engineer, peat is taken into account as problematic soil (Santagata et al., 2008; Kazemian et al., 2011). This type of soils mostly causes serious instability problems for foundation and considerably large and long-term settlement for embankment construction in many years (Terzaghi et al., 1996; Hayashi et al., 2012). **Fig. 2.3** illustrates representative geotechnical problem when constructing building on peaty ground even using pile foundation, and the damage existing infrastructure nearby an embankment due to upheaval of peat ground when they settle, in according to Huat et al., (2014).

Large scale and long-term settlement could be considered as the significant geotechnical problem on the ground consisting peat because peat usually has extremely high initial void ration and compression properties. In the initial stage of construction, the consolidation process may be faster than soft clay, but delayed dissipation of pore water pressure would be occurred due to rapidly decreasing permeability resulting in residual settlement in long time after completion of construction. The future decay of organic matter which is assumed to process at slower rate after subjected by external load is an additional reasonable factor to increase secondary compression (Mersi et al., 1997). Excessive settlement has influenced on the serviceability of structure or required additional countermeasures of road embankment constructed on peaty ground, as several cases reported by Lea and Brawner (1963), Hanrahan (1964), Edil and Simon-Gilles (1986), Osorio et al. (2008), and Hirata et al. (2010a).

Slope instability or slip failure is often subjected to the geotechnical problem of construction of infrastructures such as embankment, dyke on peat deposits because peat has generally low undrained shear strength (Brawner, 1958) particularly in the early stage of construction, and very low permeability after load application and subsequent compression. The slip failure is possible to reduce in long-term because the shear strength of peat significantly increases after dissipated large amount of pore water (Lea and Brawner 1963; MacFarlane 1969; Mersi and Ajlouni 2007). For instance, Van Baar (2005) and Zwanenburg et al., (2012) noted the recent failures occurring on dyke and embankment constructed on peaty ground in the Netherlands; a large failure of Grand Canal embankment built on Irish peat (see **Photo 2. 2**) was reported by Pigott et al. (1992); and the failure of an embankment on peaty ground in the Kameda Interchange for Hokuriku expressway in Niigata, Japan during loading using multi-loading stage was described by Porbaha et al. (2000).

In conjunction with previously mentioned problems, the large horizontal displacement and surrounding ground upheaval are possible to make damage to the existed infrastructures like building, drainage system, or even cultivated field…etc. nearby certain constructing project, these engineering problem can be pictured in mid as **Fig. 2.3**(**c**). Hanraha (1964) reported the observation of heavy damage of the Cush Road, Co. Offaly in Ireland consisted of ground upheaval, and large, long-term lateral displacement.

An additional engineering problem can be occurred on peaty deposits is the appearance of gas formation in the ground due to the decomposition and oxidation of remained plant matters for a very

long time. Vonk (1994) discovered the existence of a gas formation in peat bog underlain by an embankment when measuring excess pore water pressure by cone penetration hole, he also supposed that this gas can cause the increasing of excess pore water pressure, by the means of that the stability of ground can be affected during construction, however the mechanism of this suspicious failure has not been studied in detail.

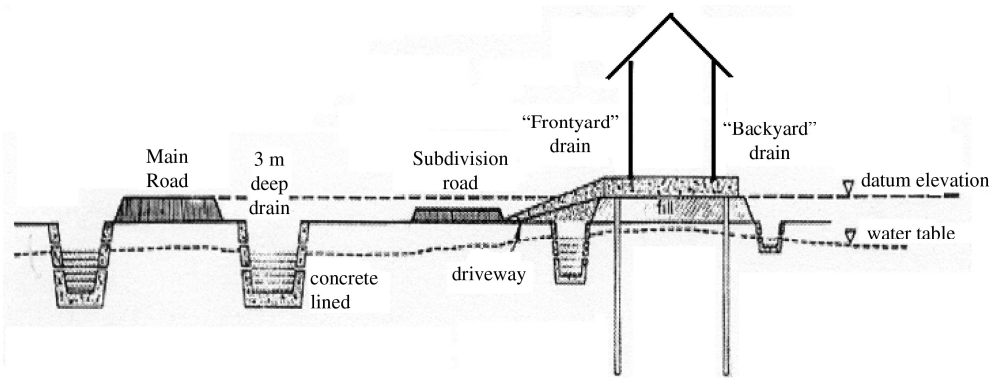

(a)

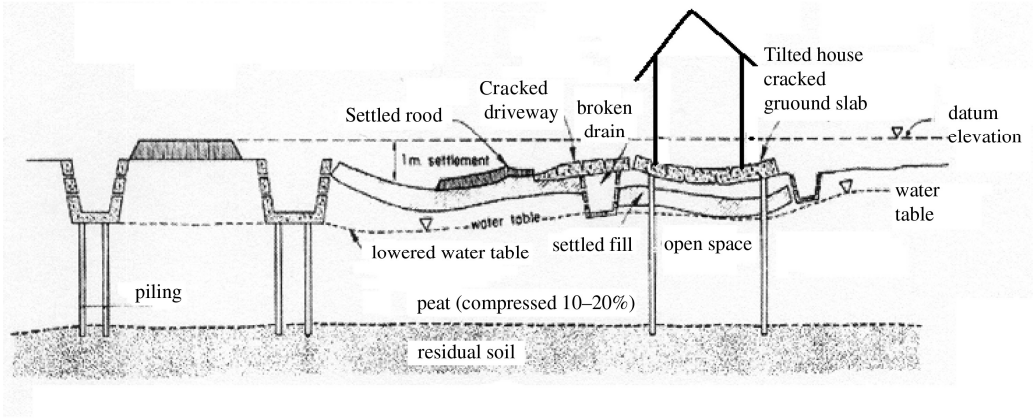

(b)

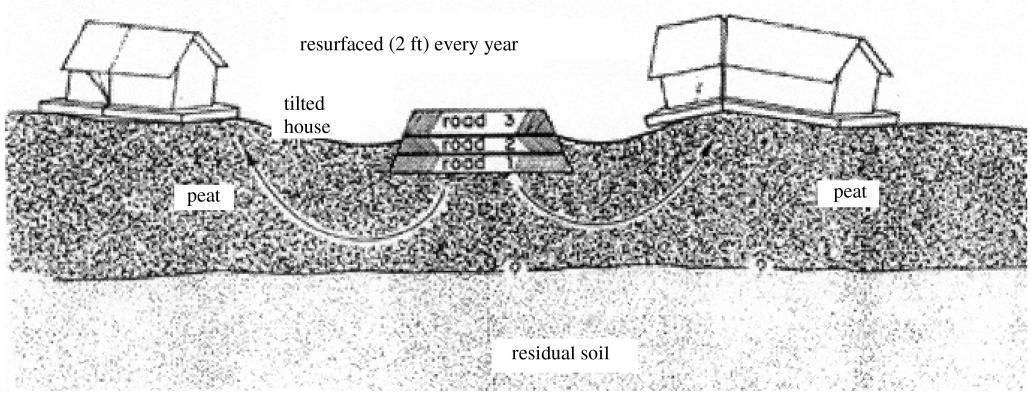

(c)

Figure 2.3 Typical engineering problems on peaty ground (Huat et al. 2014)

(a) Typical layout for housing immediately after completion of construction; (b) Several years after completion of construction; (c) Sketch of problem due to upheaval of peat near roads when they settle.

Photo 2. 2 Failure on Grand Canal embankment constructed on peat (Pigott et al. 1992)

2.3. Characteristics of Peaty soils in the study area

2.3.1. Introduction to the study area

This research deals with the peaty ground in the Mukasa area, Wakasa-cho, Fukui Prefecture, center of Japan, nearby the Sea of Japan. Mukasa area is a part of new construction of the Maizuru-Wakasa expressway connecting the Chugoku expressway with Hokuriku expressway and passing through Fukuchiyama, Maizuru, Obama, and Tsuruga as seen in **Fig. 2.4**. The Maizuru-Wakasa expressway is planned to employ in Fiscal Year 2014.

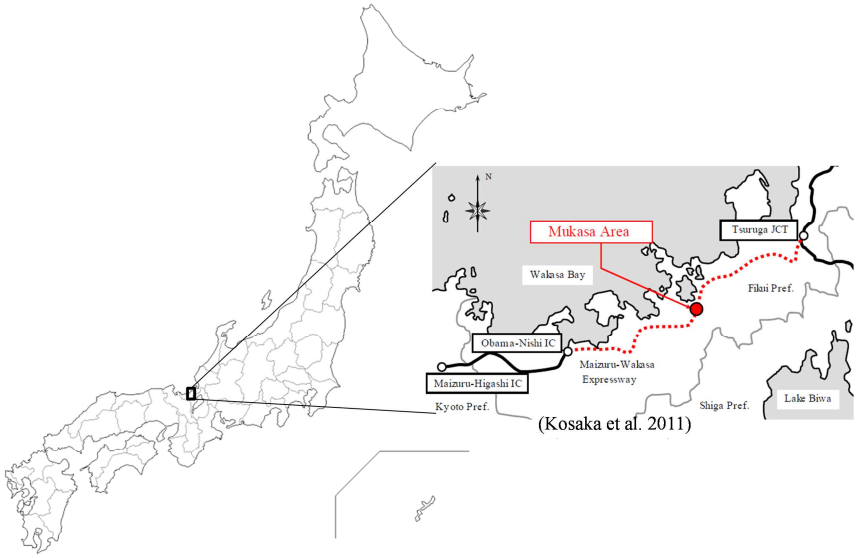

Figure 2.4 Location map of this research (Kosaka et al., 2011)

Fig. 2.5 shows the geomorphological map of Mukasa area that locates within a triangular region lying between the Kumagawa and Mikata faults known as the San'en triangle. The research area lies at the bottom of a typical downed valley bounded on three sides by mountains. Peat deposits were found predominately from the lowest level of the valley to the depth of about 50m with alternated cohesive and sandy soil layers. This humic soil is classified as low-moor peat, containing a relatively high proportion of clay and sand in addition to organic component, hypothesizing that this peat was deposited in the condition of abundant water. Because this region has cold climate, the formation of localized ultra-soft peaty ground was formed due to insufficient decomposition of organic matters such as dead plants. Considering the fact that the current region's topography was created by fault motion occurring after the Mid-Pleistocene era (Nakae et al., 2002), and the peat was accumulated at the annual rate of 1mm/year (Japanese Geotechnical Society, 2004), resulted in the unique stress state of the peat deposited under an artesian pressure that will be discussed latter.

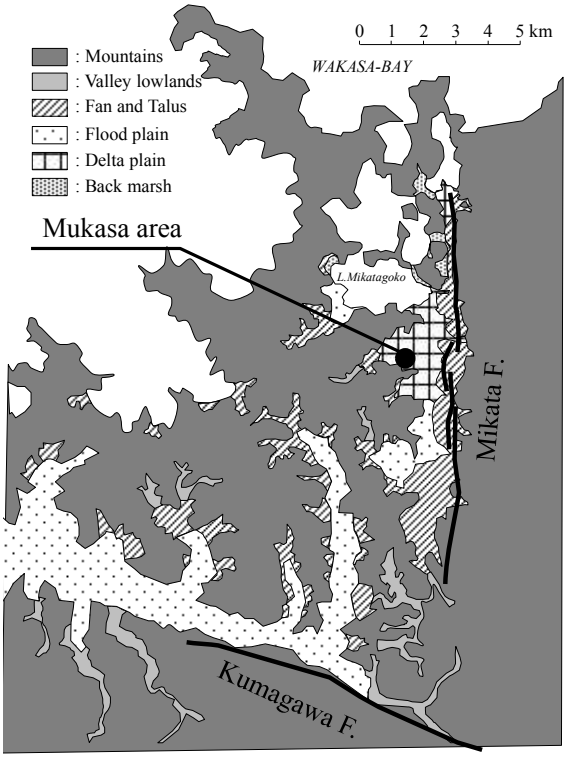

Figure 2.5 1:50,000 geomorphological land classification map "Nishizu Kumagawa" (After the Geological Survey of Japan, 2001)

Structure of geologic strata in the Mukasa area in a longitudinal direction is presented in **Fig. 2.6**. The approximate 50m depth peaty soft ground is composed of mostly alluvium peat together with alluvium clay, several thin layers of alluvium sand alternating in the middle. There are existences of continuous cohesive soft soil layers (peat and clay) from the ground surface to approximate 50m depth at the right and left side forward to mountain areas meanwhile thin layers of sand more regularly and a diluvium peat deposit places in the deep instead of deep alluvium peat appear at the

center area. At the bottom of the profile, a layer of diluvium gravel that is considerably to exist at the bottom of whole the profile.

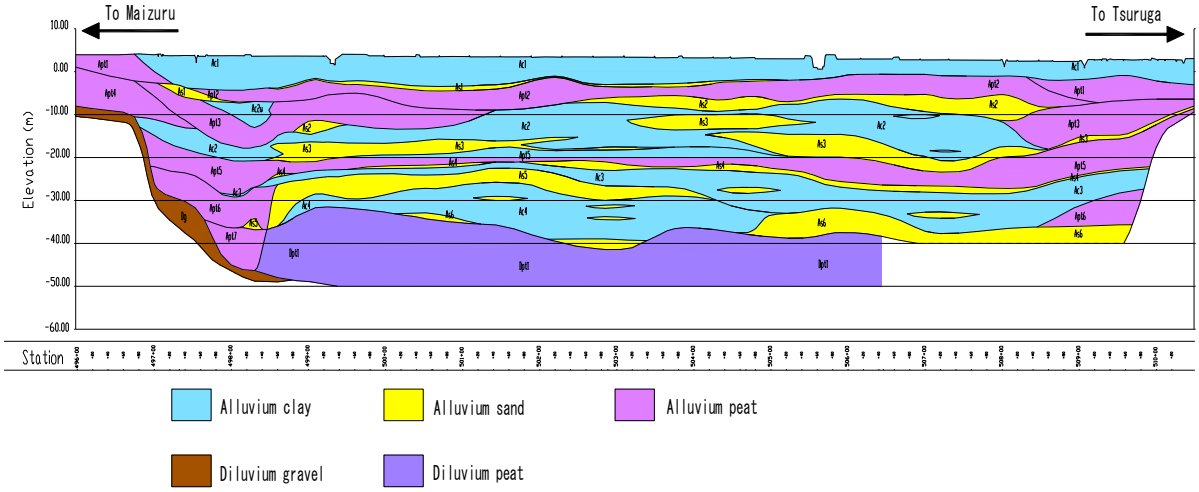

Figure 2.6 Stratum structure in the Mukasa area (longitudinal direction)

2.3.2. Geotechnical investigation data

Fig. 2.7 illustrates positions of the boring investigation that consists of 11 boreholes performed at 10 positions (denotes from A to J) around section A and section B which are the scopes of this research. In section A, the test embankment was constructed in February 2006 for the purposes of identifying and selecting appropriate countermeasures arising due to the softness of the ground. While, another embankment loading combined with vacuum consolidation was performed in section B in January 2012 to accelerate the construction process. The distance between two sections is only about 300m, and the same height of embankments was desired for them in designed criteria. The boring was taken twice at the position D, the first time was in 2007, and the second was in 2009. The boring investigations were done both before and after construction of embankments for determining designed soil parameters and inspecting the change of soil properties. The undisturbed sampling of cohesive soils was taken during each boring period. Index tests, classification tests, and mechanical tests were performed in the geotechnical laboratory on undisturbed samples to interpret soil profiles and decide the soil parameters.

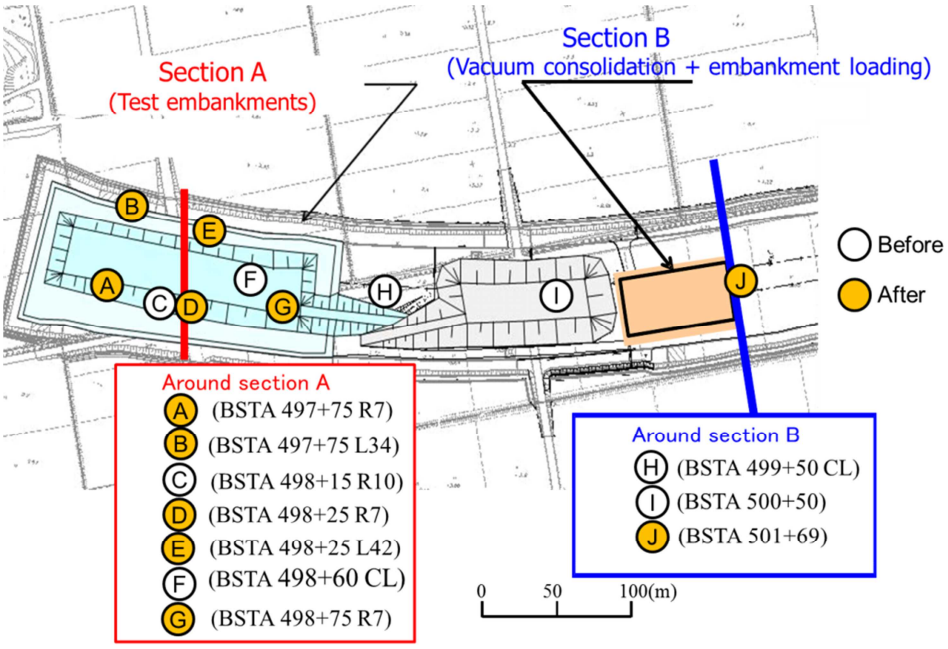

Figure 2.7 Layout of boring investigation

The profile of the ground from the section A to the section B is demonstrated in **Fig. 2.8**. The distance between two sections is approximate 300m. It can be seen that the ground composition in the Mukasa area is extremely complex and does not comprise horizontal strata of deposited materials. From this profile, the alluvium soft clay and peat exist similar in both two sections at the shallow depth due to the same deposition condition.

Continuous alluvium peat layers appear to the depth of approximate 50m in section A, whist there are few thin layers of alluvium sand alternated in the middle, and a diluvium peat layer is distributed abundantly from boundary of the section A to B. This causes the differences in soil properties examined in the following part. The peat layer, which contains pieces of wood and sand, is not only heterogeneous but characteristically tends to undergo changes in water content (i.e., desiccation and swelling) as a result of stress release during sampling or slight disturbances during sample preparation (Noto, 1991). Regarding to the peaty ground in the Mukasa area, it was extremely difficult to classify the condition and type of samples based solely on sampling depth.

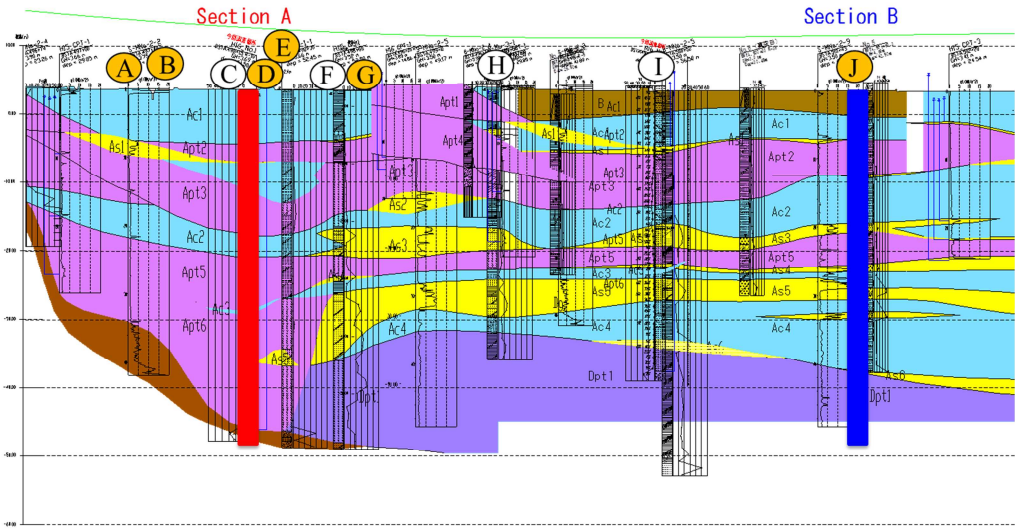

Figure 2.8 Soil profile between the sections A and B

Therefore as many test results as possible for samples before and after embankment construction in the vicinity of cross sections targeted for analysis were collected. The "types" of soil with their representative values and layer boundaries had been classified by evaluating a numerous physical experiments such as particle density, natural moisture content, liquid/plastic limits, and ignition loss which are inherent to type of soil and peat as well. Because sedimentary environments were slightly different from the two sections, the soil classification was done separately for the ground directly under each section. **Figs. 2.9(a) & (b)** show the soil type classification based on the physical laboratory test results corresponding to the soft ground in sections A & B. After all physical test results were screened, the representative or mean values of soil properties for each layer were determined for each section as tabulated in **Table 2.5**. It can be seen that the similar values for the shallow layers such as Ac1, Apt2, and Ac2 due to the same type of soil and deposition conditions; there are some soil's types in section B but not occur in section A and vice versa at the middle depth of the ground; and downward to the bottom the same type of soil is considered for both Apt7, Apt8 in section A and Dpt1, Dpt2 in section B because their mean values are closed to each other, however they are deposited in different initial condition. Peat's values of Atterberg limits, ignition loss are higher and soil particle density are lower those of clay, appropriate with the review engineering properties of peat over the world in **Table 2.4**. Especially those properties of deep peat layers which are Apt5, Apt6, Apt7, and Apt6 possess very highly compressibility and low shear strength, therefore large-scale deformation is possible to occur in section A.

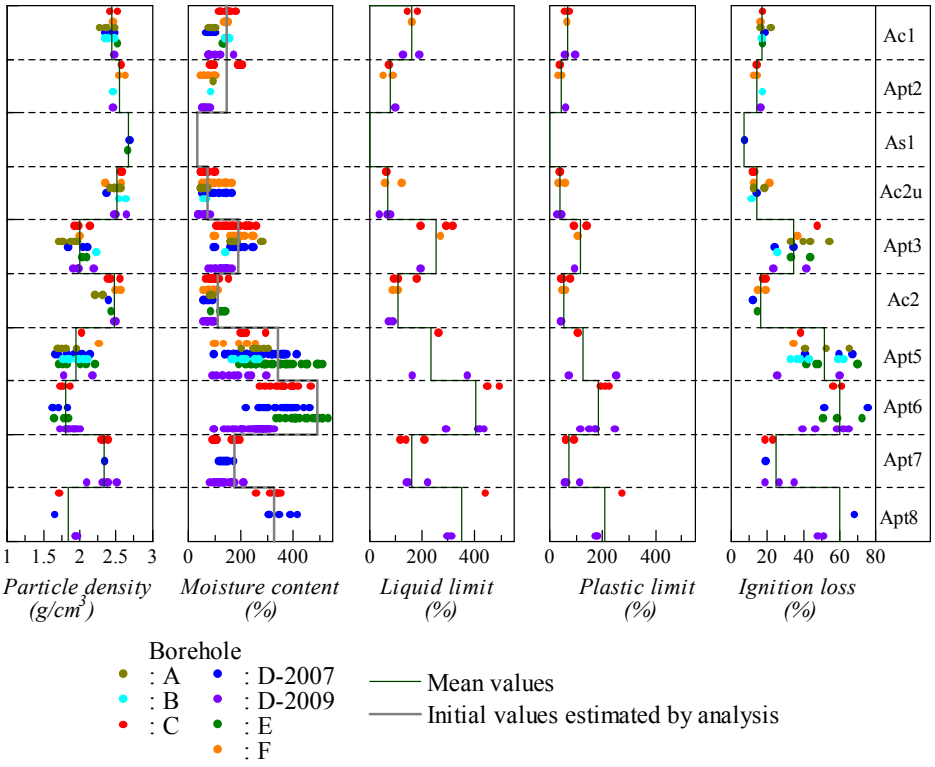

(a) In section A

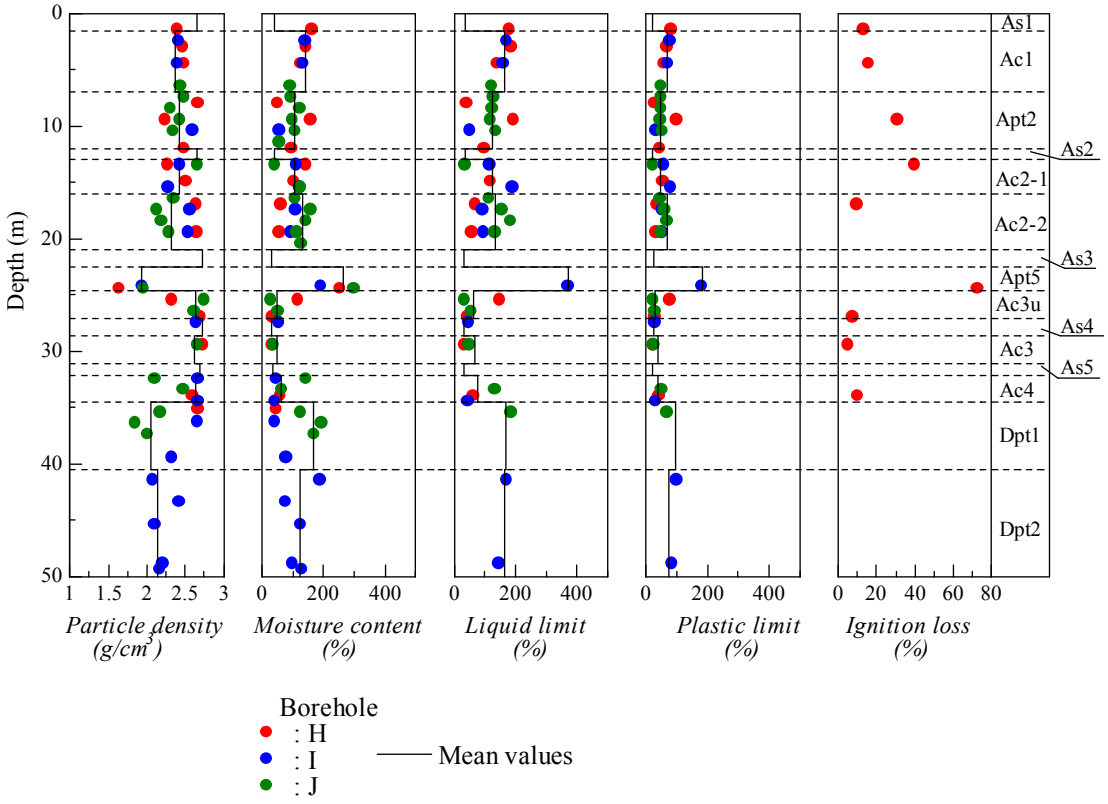

(b) In section B

Figure 2.9 Laboratory test results classified by soil types

Table 2.5 Representative values of physical properties

Soil types	Particle density		Water content		Liquid limit		Plastic limit		Ignition loss
	(g/cm^3)		(%)						
	Section A	Section B	Section A	Section B	Section A	Section B	Section A	Section B	
Ac1	2.45	2.38	137.0	139.8	162.2	163.0	68.9	70.1	17.3
Apt2	2.55	2.42	145.0	108.3	79.15	106.0	43.8	48.9	14.3
As1,As2	2.68	2.65	35.0	39.5	-	35.0	-	20.5	-
Ac2u	2.51	-	73.0	-	71.4	-	40.2	-	14.0
Ac2 (*)	2.47	2.42	110.0	108.3	107.1	106.0	50.4	48.9	16.0
Ac2-2	-	2.17	-	132.5	-	135.0	-	67.2	34.8
Apt3	2.00	-	190.0	-	255.5	-	113.4	-	35.0
Apt5	1.95	1.84	333.0	267.0	235.1	369.9	125.6	185.6	51.5
As3,As4, As5	-	2.66	-	30.5	-	30.5	-	23.4	-
Ac3u,Ac3, Ac4	-	2.57	-	50.8	-	63.8	-	29.2	-
Apt6	1.81	-	492.0	-	406.7	-	185.4	-	60.0
Apt7	2.34	-	162.0	-	164.5	-	73.3	-	25.0
Apt8	1.84	-	360.0	-	351.0	-	209.7	-	60.0
Dpt1	-	1.96	-	170.0	-	168.5	-	96.6	-
Dpt2	-	2.16	-	123.0	-	165.2	-	73.8	-

(*) Denote the representative values of soil layer Ac2-1 in section B

After that, results of mechanical tests including oedometer and consolidated undrained trialxial for undisturbed samples were divided into each layer by type of soil in order to interpret its mechanical behaviors. **Fig. 2.10**, for example, shows the compressive curves resulting from oedometer tests were separated into each soil layer. Red and blue colors stand for soil samples in section A and B, respectively. Although the curves are comparable, those curves representing for post-construction are higher in consolidation yield stress and smaller in initial specific volume to compare with those of pre - construction.

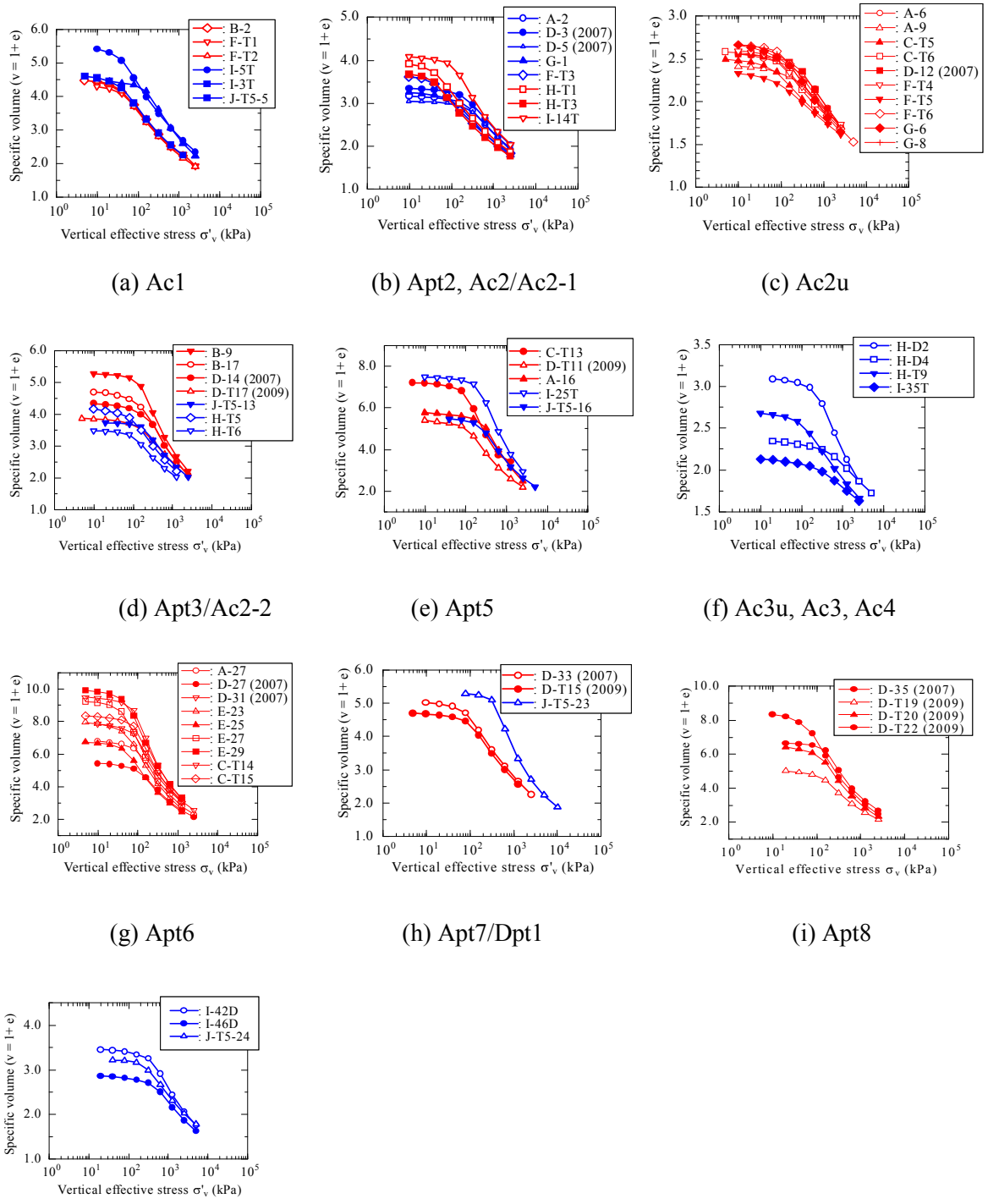

Figure 2.10 Oedometer test results were divided into corresponding soil type

Consolidation yield stress (p_c) determined from oedomter test results are plotted together with overburden effective pressure (σ'_{v0}) that was estimated based on assumption of normally hydrostatic pressure with water level at ground surface. In section A, the p_c increases regularly from the surface to the depth of around 30m then decreases to the end of deep peat layers. Besides, the p_c are even smaller

than σ'_{v0} in the deep peat layers, so the soil in this case could be considered as under consolidated stage (**Fig. 2.11(a)**). These phenomena not literally reported consider the distinctive features of the ground in this section. In contrary to section A, p_c are bigger than σ'_{v0} and linearity increase with depth (**Fig. 2.11(b)**) indicates the soils in the state of over-consolidated in deep depth in section B. The distribution in section B is similar to many others ground generally. Due to the unique distribution of p_c and their values are smaller than that of deep peat in section B (**Fig. 2.10(h)**) even same type of soil, the large and long-term settlement has been occurring after the completion of embankment, meanwhile small long-term settlement is possibility to occur in section B.

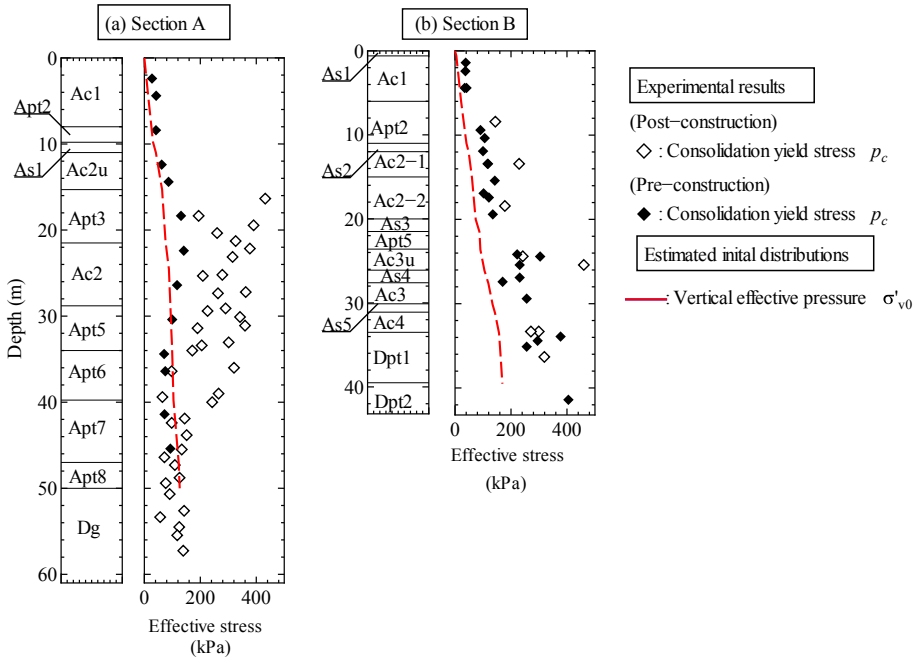

Figure 2.11 Distribution with depth of consolidation yield stress and vertical effective pressure

2.3.3. Interpretation of the sedimentary environment and initial stress state

In section A locating nearby the mountain side, the unique state ($p_c < \sigma'_{v0}$) of the greater than 30-m-deep peat layer resulted from the layer remaining unconsolidated over this time. As such, it could be deduced that the deep peat layer is under artesian conditions causing by the faults movement. For ensuring the present of artesian pressure, in October of 2009 (approximately 3 years after completion of the embankment) a standpipe piezometer was installed from the crown of the test embankment to directly measure the water pressure of the Diluvial gravel (Dg) layer lying directly under the deep peat layer. It was found that the water pressure at a depth of 60 m was approximately 100 kPa greater than the normal range of hydrostatic pressures. The results of this measurement of the Dg layer and the distribution of pore water pressure with depth prior to embankment construction are both presented in **Fig. 2.12(a)** (right). Based on the fact that the pore water pressure before and after embankment construction both lie on essentially the same line, it could be assumed that the artesian pressure of the

Dg layer did not change following embankment loading. Given that a continuous As1 layer exists at an approximate depth of 11 m, it was estimated that the layers deeper than As1 are affected by the artesian pressure, and the water pressure distribution prior to embankment loading was estimated as the solid blue line shown in **Fig. 2.12**(**a**) (right). It was deduced that the artesian pressure is caused by the fact that, due to fault motion, the Dg layer forms a continuous layer that is lowest at the valley bottom and slopes upward as it approaches the mountainous areas.

Fig. 2.12(**a**) (left) shows the estimated initial in-situ effective overburden pressure, taking artesian pressure into consideration (dash red line). The measured consolidation yield stresses before and after embankment establishment are presented in the same figure for reference. When artesian pressure is taken into consideration, the ($p_c > \sigma'_{v0}$) relationship is found to exist for all layers. If the maximum effective stress experienced in the past is assumed to be equivalent to the consolidation yield stress, it can be imagined that the deep peat layers in section A have maintained an extremely low effective overburden pressure and a high void ratio even during deposition of the overlying strata. It is believed that this is attributable to a progressive increase in artesian pressure resulting from ongoing subsidence of the Dg layer in the vicinity of the valley bottom and uplift on the mountain side. As a consequence, test embankment loading resulted in an effective stress that readily exceeded the consolidation yield stress of the deep peat layer, despite its extreme depth (> 30 m). It is further speculated that, given the layer's extremely high initial void ratio and compressibility, substantial time was required for dissipation of the excess water pressure.

In opposition, it was confirmed in both in situ (measured pore water pressure) and laboratory experiment investigations that the ground under section B is only minimally affected by the artesian conditions and, therefore, the deep peat layers possess sufficiently large consolidation yield stress (**Fig. 2.12**(**b**)). In addition, it was confirmed that alternating clay and sand layers exist in the middle of the ground profile. However, laboratory experiments demonstrated that the shallow Ac1 and Apt2 layers below both the test embankment in section A and the present section B comprise soil of similar type and condition since they are not affected by artesian conditions. Considering the points above, it is predicted that, although there may be problems associated with the stability and settlement of the shallow ground layers, there is little possibility that the embankment in section B will undergo the same kind of large-scale delayed settlement as the test embankment (section A).

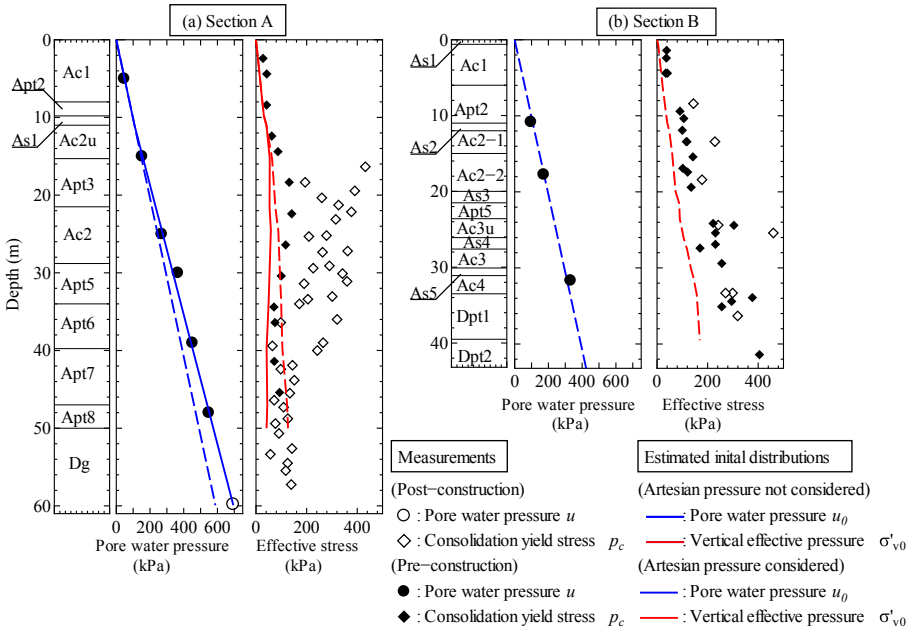

Figure 2.12 Estimated initial distributions of pore water pressure and vertical effective pressure

2.4. Description of mechanical behavior of the peat based on SYS Cam-clay model

2.4.1. Estimation of material constants by simulating the laboratory test results using SYS Cam-clay model

In order to estimate the material constants of soil layers, back analyses the results of oedometer and consolidated undrained triaxial tests for undisturbed soil samples from each layer particularly peat were simulated using the response of the SYS Cam-clay model to describe behaviors of structure, overconsolidation, anisotropy of soil skeleton. The SYS Cam-clay model consists of totally 12 soil parameters which can be separated into two categories. The category of 5 elasto-plastic material constants including compression index $\tilde{\lambda}$, swelling index $\tilde{\kappa}$, critical state constant M, specific volume at mean effective stress p' = 98.1 kPa on normal consolidation line (NCL) N, and poisson's ratio ν , which are directly come after original Cam-clay model and can be interpreted by conventional triaxial shear and oedometer tests. The second category composes 7 evolution parameters containing the parameter representing for loss of overconsolidation m, degradation parameters of soil structure (a, b, c_s), development of stress induced anisotropy b_r and limitation of rotation m_b. The parameters in later category are acquired by simulating the response of undisturbed samples with undrained triaxial and consolidation tests after getting the elasto-plastic material constant together with some given value representing the states of sample in the experiments. The optimal parameters are obtained by trial-and-error method. Pay attention to the advanced characteristic of SYS Cam-clay model is that for a given soil, only one group consisting of above 12 material constants is needed to represent the soil response under different conditions.

This procedure of simulating laboratory test results was applied to all soil types existed in the Mukasa area comprising of peat, clay, and sand. The examples of simulation results are presented in the **Fig. 2.13** and **Fig. 2.14** for both the shallow peat (Ac1) and deep peat in section A (Apt6) and in section B (Dpt1). The line with circle points are the experiments results and the solid lines without point depict the response of SYS Cam-clay model. A good agreement between model response and experimental results shows that soil parameters are simulated faithfully. The material constants are tabulated in **Tables 2.6 & 2.7** representing for soils in section A and B, respectively. However, given that actual values from mechanical tests were not available for all ground layers in section B, a number of ground layers (i.e., As1 and As2; Apt2 and Ac2-1; Ac3u, Ac3, and Ac4) were assumed to be of the "same type" based on the results of physical tests. In addition, because mechanical tests were not performed on samples collected from the middle sand layers As3, As4, and As5, these layers were assigned material constants for silica sand no. 6 to represent typical sand. In addition, due to highly inhomogeneity, the sensitivity to disturbance and high compressibility of the in-situ peat, experimental results that could not be considered to be homogeneous element behavior with soil of same type, such as a result of Dpt1 under the highest confining pressure as shown in **Fig. 2.14** (**b**), were not taken it into consideration to decide the material constants by simulation.

Although the ground contains sensitive clays and peats with the liquidity index greater than one, which easily lose strength by remolding and change the state to slurry, all samples of the triaxial tests referred in this study were carried out in the usual manner, because the self-standing specimen could be made from the undisturbed samples. However, fairly lower unit weight of peat than general soils and the artesian pressure effects were not considered in the test. Therefore, some of the tests were carried out in normal-consolidated state under the confining pressure determined only by sampling depth. Particularly in the case of the deep peat layer samples in section A, the stress path from shear tests under confining pressures greater than the in-situ overburden pressure were not smooth and were found to be convex downward. This may be attributable not only to the heterogeneity of the samples, but also the fact that residual excess pore water pressure existed in the samples prior to the onset of shear, as evidenced by the dramatic decline in permeability accompanying the compression of peat samples. Test results that could not be considered to exhibit homogeneous element behavior were not subject to simulation.

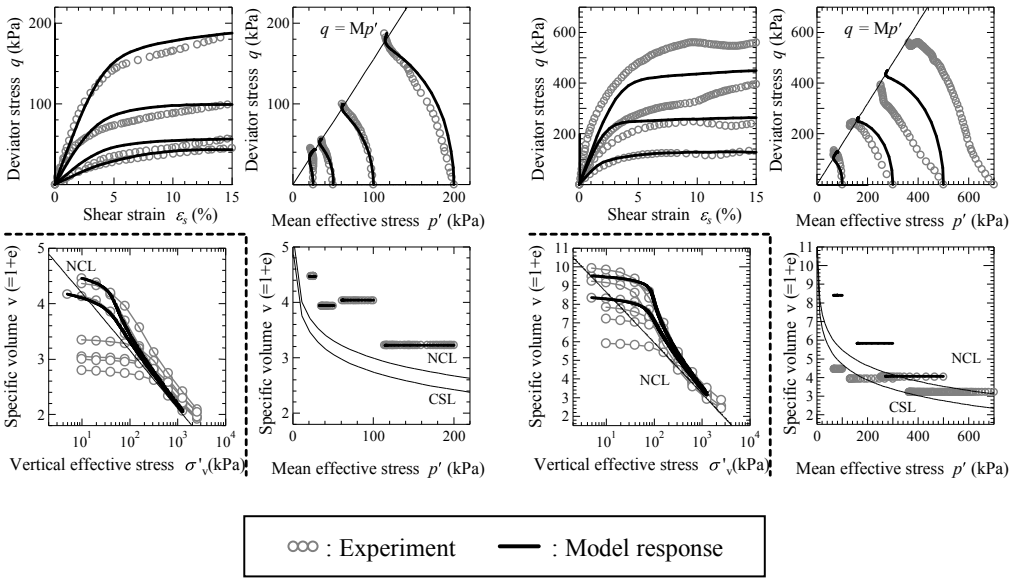

(a) Apt1 (b) Apt6

Figure 2.13 Examples of results of laboratory tests and simulations using SYS Cam-clay model for soil samples in section A

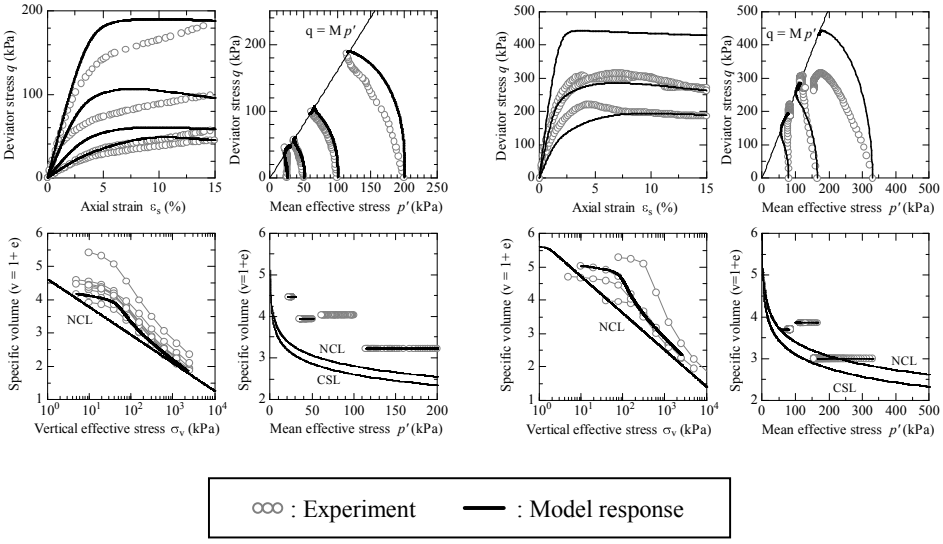

(a) Ac1 (b) Dpt1

Figure 2.14 Examples of laboratory test results and of simulation using the SYS Cam-clay model for soil samples in section B

Table 2.6 Material constants for ground in section A

Soil layer	Ac1-1 Ac1-2	Apt2	As1	Ac2u	Apt3	Ac2	Apt5	Apt6	Apt7	Apt8
Elasto-plastic parameters										
Compression index $\tilde{\lambda}$	0.46	0.21	0.15	0.19	0.72	0.3	0.68	1.21	0.47	1.04
Swelling index $\tilde{\kappa}$	0.1	0.05	0.02	0.04	0.06	0.03	0.15	0.1	0.05	0.1
Critical state constant M	1.55	1.7	1.0	1.2	2.3	1.6	2.0	1.6	1.7	2.0
Specific volume at p'=98.1 kPa on NCL N	3.0	2.3	2.1	2.0	3.9	2.2	3.7	5.5	2.8	5.0
Poisson's ratio ν	0.4	0.4	0.3	0.4	0.4	0.4	0.35	0.4	0.4	0.4
Evolution parameters										
Degradation of overconsolidation state m	3.0	3.0	0.05	3.0	3.0	3.0	1.0	3.0	3.0	3.0
Degradation of structure a	0.45	0.45	1.0	0.32	0.1	0.23	0.25	0.4	0.29	0.4
b	0.8	1.0	1.0	0.8	0.8	0.8	0.9	0.8	0.8	0.8
c_s	0.2	0.2	1.0	0.1	0.2	1.0	0.1	0.2	0.3	0.3
Evolution of rotation b_r	0.3	0.25	3.5	0.3	0.1	0.2	0.2	0.2	0.1	0.2
Limit of rotation m_b	1.0	1.0	0.7	1.0	1.0	1.0	1.0	1.0	1.0	1.0
Density of soil ρ_s (t/m^3)	2.45	2.55	2.68	2.51	2.00	2.47	1.95	1.81	2.34	1.84

Table 2.7 Material constants for ground in section B

Soil layer	As1 As2	Ac1	Apt2 Ac2-1	Ac2-2	Apt5	As3 As4 As5	Ac3u Ac3 Ac4	Dpt1	Dpt2
Elasto-plastic parameters									
Compression index $\tilde{\lambda}$	0.15	0.37	0.31	0.39	0.73	0.05	0.24	0.48	0.40
Swelling index $\tilde{\kappa}$	0.020	0.055	0.040	0.045	0.045	0.012	0.030	0.050	0.045
Critical state index M	1.00	1.55	1.20	2.40	2.35	1.55	1.50	2.55	2.10
NCL intercept N	2.05	2.90	2.75	2.88	4.10	1.98	2.35	3.40	2.90
Poisson's ratio ν	0.30	0.40	0.40	0.35	0.40	0.30	0.40	0.30	0.40
Evolution parameters									
Degradation index of overconsolidation m	0.05	2.00	2.00	2.00	2.00	2.20	1.80	1.50	2.00
Degradation index of structure a	1.00	0.37	0.40	0.25	0.35	1.00	0.50	0.30	0.40
b	1.00	0.80	0.80	0.90	0.90	1.00	0.95	0.90	0.90
c_s	1.00	0.20	0.10	0.20	0.20	1.00	0.15	0.25	0.25
Rotational hardening index b_r	0.10	3.50	0.05	0.03	0.07	3.50	0.05	0.05	0.10
Limitation of rotational hardening m_b	1.0	1.0	1.0	1.0	1.0	0.7	1.0	1.0	1.0
Soil particle density ρ_s (t/m^3)	2.65	2.38	2.42	2.17	1.84	2.66	2.57	1.96	2.16

2.4.2. Estimation initial conditions

The initial in-situ conditions prior to embankment construction were deduced based on the natural water content and the results of consolidation tests on undisturbed samples with regarding soil disturbance. The natural water content measured in all laboratory tests, including mechanical tests, are presented in **Fig. 2.9**. With respect to the ground in the Mukasa area, although samples were collected from locations very near to each other, in some cases, samples collected after embankment loading had higher natural water content than samples collected before embankment loading. Even in the case of samples taken from the same borehole, in some instances, extremely wide variability in the natural water content was observed within a single stratum, (e.g., Apt5 and Apt6). In this study, the soil-water coupled finite deformation analysis described below were performed using natural water content values lying between the mean and maximum values and values that most closely reproduce the observed settlement were determined for each layer by trial-and-error. The estimated initial water content values before test embankment construction in section A are shown as gray solid lines in **Fig. 2.9**(**a**). In addition, examples of deduced in-situ compression curves, deduced distributions of initial

conditions with depth in section A, and those distributions in section B are presented in **Figs. 2.15, 2.16 and 2.17**, respectively. With regard to the initial conditions before embankment construction, it was assumed in this study that the void ratio, degree of structure, degree of anisotropy, and stress ratio were uniform within each layer irrespective of depth, and generated a depth distribution of overconsolidation ratios based on the effective overburden pressure and the consolidation yield stress p_c at the center of each stratum. In section A, because sufficient sample data for the ground near the surface could not be collected, assumed that the 0 to 8-m-deep layer (Ac1-1 and Ac1-2) was composed of the same material and assigned slightly lower water content to the 0 to 3-m-deep layer (Ac1-1).

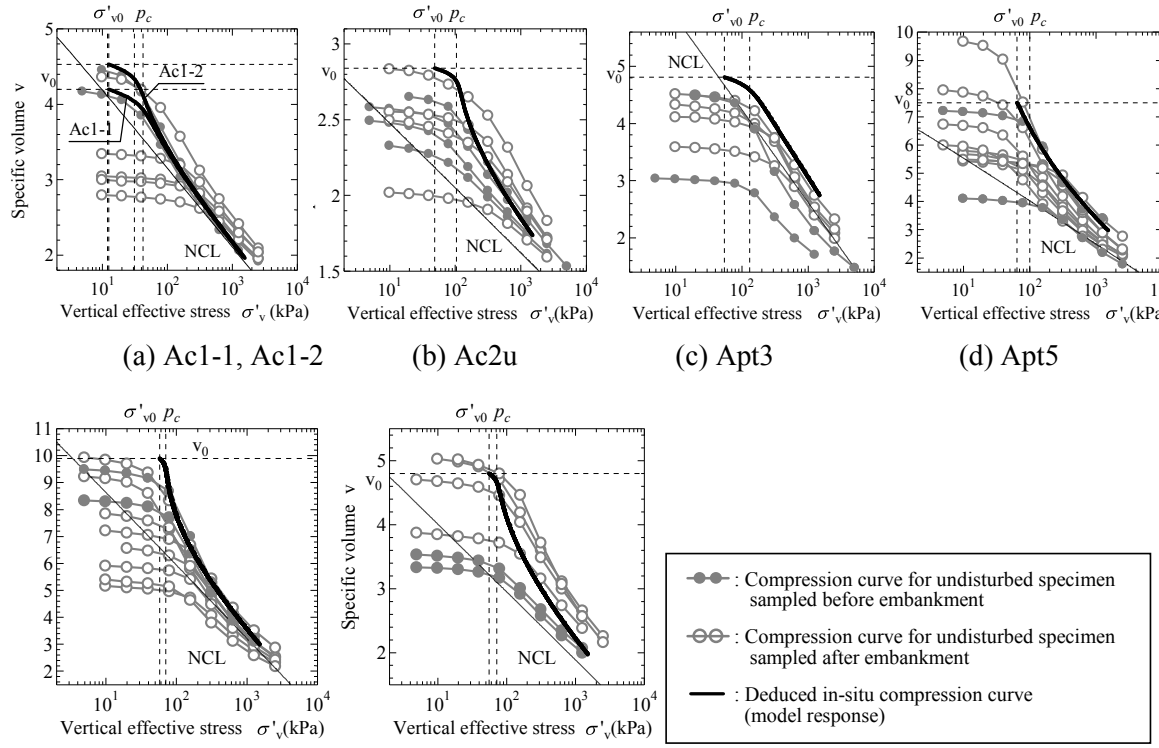

Figure 2.15 Examples of deduced in-situ compression curves

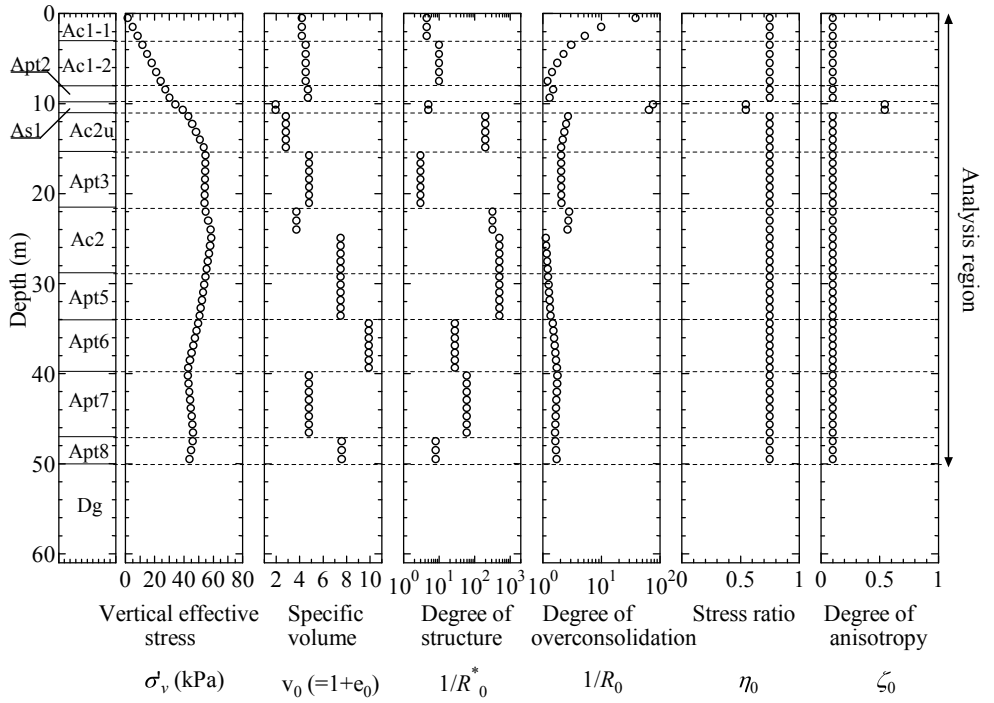

Figure 2.16 Distribution of deduced in-situ initial conditions in section A

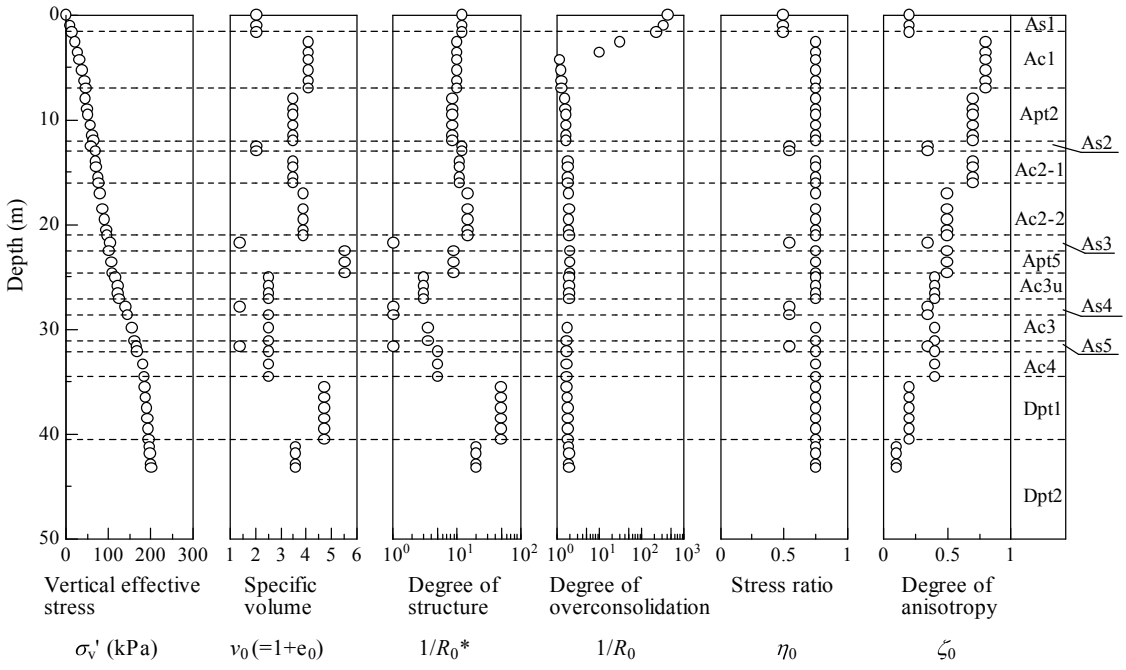

Figure 2.17 Distribution of deduced in-situ initial conditions in section B

2.4.3. Discussion on the mechanical behaviors peat

After obtaining material constants by respond of SYS Cam-clay model and interpreting initial condition of ground, mechanical behaviors of peat as well as soft clay in Mukasa area could be discussed. It can be seen that the stress-strain relationship is ductile for clay and peat even though the slope of the compression curve in the region before the consolidation yield stress is generally low. These characteristics were modeled in the SYS Cam-clay model as a material having a high Poisson ratio and relatively rapidly-developing anisotropy. The in-situ deep peat layer in particular was predicted to undergo substantial compression as a result of even a slight increase in stress above the consolidation yield stress. In the framework of elasto-plastic constitutive equation for soil skeleton, these characteristics were represented for a material having a small initial consolidation ratio and a high degree of structure, a large compression index, and exhibiting rapid degradation of structure. Here, the degree of structure refers to the degree of soil bulkiness. Soil with high degree of structure can maintain higher void ratios under the same stress state and withstand greater stress states with the same void ratio than fully remolded soil (soil without structure) (Asaoka et al., 2002; Asaoka, 2003).

2.5. Brief summary

The first part of this *Chapter* gives a short review of peat deposits relate to environmental generation, global distribution, engineering classification, typical engineering properties, and geotechnical problems of peaty ground when developing infrastructure. The second part introduces characteristics of the peaty ground in Mukasa area, Japan on which large deformation of embankments were monitored during and after construction. By screening a plenty soil investigation data including field and laboratory tests, the representative engineering properties of all soil layer mainly containing peat and clay were determined, then distinctive sedimentary environment was deduced. The last part shows the material constant of peat in Mukasa, its ground initial conditions, and discusses about peat's mechanical behaviors resulting from simulation of laboratory test results based on SYS Cam-clay model. The findings can be listed as following:

1) A soil considered as a peat has been incomplete decomposed plant fragments, the color ranges from light brown to black with distinctive odor. Peat deposits mainly generated in humid or abundant water regions where usually lack of oxygen, in this condition the dead vegetation decomposes slower and accumulated faster than that of dry area. Due to generated environment, peat deposits normally distribute abundantly in cold regions such as Canada, United Sate, Russia, Scandinavia, Britain or in a small area in tropical region such as Indonesia, Malaysia, Sri Lanka.
2) Peat is generally classified based on the organic content. Although there are some different bounded values using among many countries, a soil containing at least 20% of organic matter is classified as peat. In addition, peat could be divided into fibrous, pseudo-fibrous, and amorphous peat based on the degree of decomposition.

3) Engineering properties of peat can be determined regularly in the same way with inorganic soft clay, however the potential of biodegradation of peat in laboratory need to be considered. The distinctive engineering properties of peat are extremely high natural water content, and Atterberg limits; very low density of soil particle; dramatically decreasing of permeability under external load.
4) Because peat has above special engineering properties, the extreme high compression and low shear strength can be predicted. Therefore, many geotechnical problems occurred when constructing on peaty ground has been record, including large-scale and long-term settlement, circular slip failure, and ground uplift in vicinity. In addition the influence of gas formation inside peaty ground could be an engineering problem.
5) In the field of this study, Mukasa area, Japan, soil characteristics and initial conditions of two grounds under two embankments were investigated based on site and laboratory investigation. Those grounds were noted as section A under the test embankment and section B under the target embankment improved by vacuum consolidation method. In section A, the cause of the large-scale delayed compression of the deep peat layer was first examined by deducing the sedimentary environment of the stratum in question. As a result, it could be confirmed that valley bottom was created through fault motions under artesian pressure of 100 kPa. In addition, it was estimated that subsidence of the valley bottom was accompanied by a progressive increase in artesian pressure and that the deep peat layer deposited while maintaining a high void ratio under low effective stress. It was believed that test embankment loading resulted in a stress state readily exceeding the consolidation yield stress, causing a characteristic large-scale compression of the peat layer and a dramatic reduction in permeability due a decrease in the void ratio, leading ultimately to delayed dissipation of excess water pressure. On the other hand, effect of artesian pressure was not found in the section B at 300m far from section A, and the existing of several thin sand layers in the middle causes deep peat layers are overconsolidated state presented by higher consolidation yield stress. Therefore the large-scale deformation and large residual settlements might be not possible to occur in section B.
6) The mechanical behaviors of the peat were described in the same theoretical framework with all other soil components from clay, to sand, to embankment material based on simulation of oedometer and undrained triaxial tests using SYS Cam-clay model. In addition, taking into consideration the sensitivity to disturbance and the heterogeneity of peat layers, initial in-situ conditions were deduced by simulating the observed settlement of each layer under the center of the embankment. As the results, peat could be modelled as a material having a high Poisson ratio, relatively rapidly-developing anisotropy, a small initial consolidation ratio, a high degree of structure, a large compression index, and exhibiting rapid degradation of structure.

Chapter 3

Large-scale deformation of ultra-soft peaty ground under embankment loading and effective countermeasures against residual settlement and failure

3.1. Introduction

As the description on the previous *Chapter 2* the ground at section A in the Mukasa area, comprises an approximately 50-m-deep soft peat-containing deposit with N-values varies from 0 to 1, and is an extremely rare example of ultra-soft ground. In advance of construction of the Maizuru-Wakasa expressway slated to be completed in FY2014, a test embankment was constructed in February 2006 over the ground in this section for the purposes of identifying and selecting appropriate countermeasures to problems arising due to the softness of the ground. While construction of the test embankment did not induce catastrophic slip failure, it dramatically impacted the surrounding ground, resulting in a maximum uplift of approximately 1 m and a maximum horizontal displacement of approximately 2 m in the vicinity of the toe of the embankment. This caused the waterway to slant and cracks to form on the ground surface (**Photo. 3.1**). Ground deformation due to the embankment was observed as far as approximately 100 m from the toe of the embankment. Because nearby paddy fields could no longer retain water as a result of this slanted ground, work was performed to re-level the fields by scraping surface soil. By the time the target embankment height of approximately 7 m was finally achieved, the embankment had already reached a total thickness (the sum of embankment height and settlement) of 15 m (Hirata et al., 2010a). Approximately three years after establishment of the test embankment, settlement had reached 11 m.

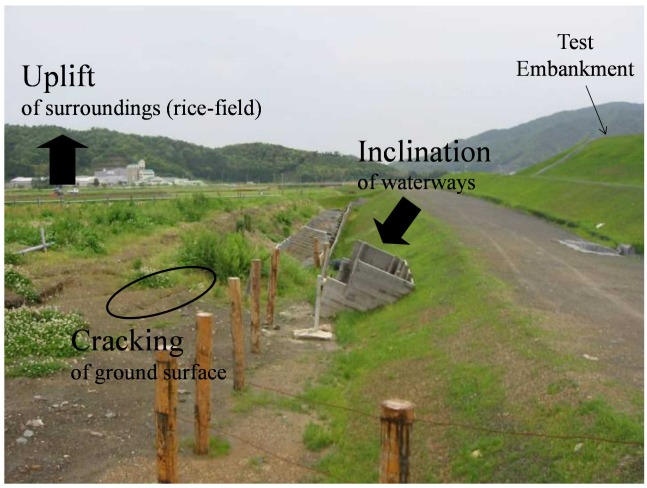

Photo 3. 1 Deformation of ground around toe of embankment

Embankment loading on thick deposits of soft ground in general, not just peat, results in the risk of both failure and settlement, necessitating the implementation of preventative countermeasures. The vertical drain method is one effective countermeasure that promotes consolidation settlement and strengthening of soft ground. While it is widely recognized that the vertical drain method is effective in improving stability during embankment construction, the verdict regarding its effectiveness in preventing residual settlement is mixed, with clear evidence of its efficacy in some cases (Noda et al., 2005b) but not in others (Mochinaga et al., 1984). It is generally found to be ineffective at reducing residual settlement in the case of peaty ground (Root, 1958; Lea and Brawner, 1963). In the context of expressway construction in Japan, based on approximately 50 years of construction experience, it has become standard practice to use the vertical drain method and make other ground improvements prior to embankment construction only when "stability" is an issue (Japan Highway Public Corporation, 1998). Residual settlement is generally not taken into consideration at the design stage but is instead treated as something to be dealt with through maintenance and repair after entry into service.

As can be seen in **Figs. 3.1** and **3.2**, the test embankment in the Mukasa area comprised three sections, one of which was improved using cardboard drains, one with sand drains, and one with no ground improvement. The drain lengths were determined based on stability analysis. At the point that embankment construction was completed, it was concluded that the impact of ground improvements by drain on residual settlement was unknowable. This is because the ground composition in the Mukasa area is extremely complex, and the thickness of the soft layer underlying test embankments can differ substantially. It was therefore concluded that it would be impossible to directly compare the impact of the presence or absence of a drain. In reality, however, it was noticed that the unimproved deep peat layer, which had been assumed at the design stage not to be subject to settlement, had undergone substantial compression as a result of embankment loading. Furthermore, this settlement did not appear to be approaching convergence approximately three years after completion of the embankment.

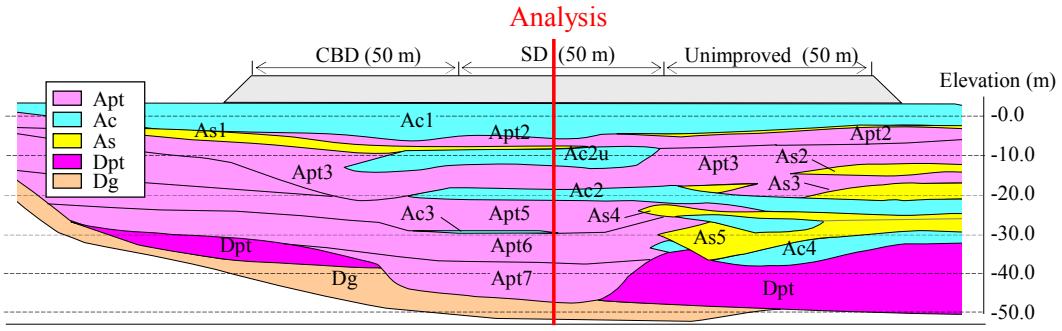

CBD: Card Board Drain, SD: Sand Drain, Apt: Alluvial peat, Ac: Alluvial clay, As: Alluvial sand, Dpt: Diluvial peat, Dg: Diluvial gravel.

Figure 3.1 Schematic of test embankment and underlying soil strata (longitudinal direction)

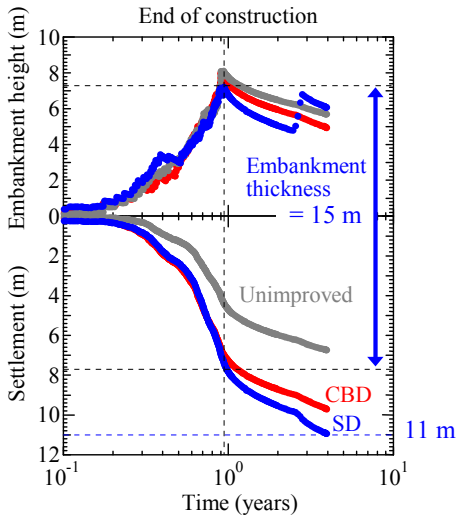

Figure 3.2 Ground surface settlement for test embankments

In this *Chapter*, the sand drain (SD)-improved section of the test embankment was focused, which is underlain by the thickest layer of soft ground and has experienced the greatest magnitude of settlement. The sedimentary environment underlying this section has been deduced in the *Chapter 2*; it was investigated why such massive delayed compression occurred in the deep peat layer, which had been assumed in the design stage not to be subject to settlement. This *Chapter 3*, utilizing the ground analysis code developed by the authors' research group, the large-scale deformation of the ultra-soft peaty ground observed in an approximately 4-year period from the start of embankment loading was simulated. After verifying the validity of the simulation, the calculation was conducted continuously without changing any parameters in order to predict future settlement behavior. Based on additional simulations, it was evident that drain installation, light weight embankment, and loading speed reduction are effective methods for improving the stability during loading and reducing residual settlement after construction on ultra-soft peaty ground.

A numerical analysis of the Mukasa test embankment was previously performed by Hirata et al. (2010a). They performed a calculation based on soil-water coupled infinitesimal deformation theory, employing an elasto-plastic constitutive equation capable of handling anisotropy (Sekiguchi and Ohta, 1977) to model the clay and peat, and modeling the sand and the embankment as linear elastic materials. Based on precise simulation of the loading history, they were able to reproduce the observed deformation up to completion of the test embankment and to evaluate countermeasures aimed at preventing the ground deformation in the vicinity of the embankment during its construction, but did not attempt to predict future deformation. In contrast, the present study employed the soil-water coupled finite deformation analysis code ***GEOASIA*** (Asaoka and Noda, 2007; Noda et al., 2008a) based on an equation of motion with an inertial term rather than a force equilibrium equation, onto which the SYS Cam-clay model (Asaoka et al., 2002) capable of describing the structure, overconsolidation, and anisotropy of the soil skeleton structure was mounted as an elasto-plastic constitutive equation describing the soil skeleton. This analysis code enabled to accomplish the

following: (1) as investigated in the previous *Chapter* it was able to describe the mechanical behavior of peat within the same theoretical framework as all other soil components from clay, to sand, to embankment material, i.e., within the same elasto-plastic theory capable of describing movement of the soil skeleton structure; (2) it was able to investigate the major factors contributing to large-scale settlement by deducing initial in-situ conditions (Inagaki et al., 2010), while taking into consideration the sedimentary environment and sensitivity of peat to disturbance; and (3) by consistently considering the range of behavior from large delayed settlement resulting from progressive failure of the soil skeletal structure (Tashiro et al., 2011) to instantaneous circular slip failure (Noda et al., 2008b; Takaine et al., 2010; Nakano et al., 2010; Yamada and Noda, 2013), it was able to identify the conditions resulting in and evaluate the efficacy of countermeasures against each of these phenomena.

The results of analyses in this *Chapter* were subsequently applied to the design of a culvert box to replace a portion of the test embankment, resulting in the construction of box with 1.2-m free board and the replacement of the adjacent embankment with lighter material in order to reduce differential settlement. In addition, when an embankment was subsequently constructed near the test embankment on similar ultra-soft ground, drains were installed deeper to reduce residual settlement. Valuable field data related to these subsequent efforts was presented in the contents of this study and, based thereupon; the need for preparatory work prior to embankment construction on soft ground aimed at reducing residual settlement was demonstrated. In addition, a part of this study has been published on Tashiro et al. (2015).

3.2. Simulation and prediction of ground deformation

3.2.1. Analysis conditions

In this study, the soil-water coupled analysis based on finite deformation theory was conducted under 2-dimensional plane strain conditions. The cross section subject to analysis is presented in **Fig. 3.3** along with N-values depth distribution and monitoring positions. The finite element mesh and boundary conditions (immediately following embankment establishment) used in the analysis are shown in **Fig. 3.4**. Although the actual thicknesses of the ground layers were observed to vary in the horizontal direction; for simplicity, it was assumed that all layers were uniformly horizontally stratified and extended the thicknesses for each layer measured under the center of the embankment. However, the two hard layers (As4 and Dpt) with relatively high N-values located in the bottom-right corner of the cross section were included in the model as simplified trapezoidal strata. In the vertical direction, the model included all layers down to Apt8, with the Dg layer being considered the basement stratum; in the horizontal direction, the model included all regions affected by the embankment loading (width 400 m, height 50 m). The embankment and ground were assumed to be fully saturated. The water pressure at the embankment-ground boundary was constantly set to zero (atmospheric), and a constant water pressure distribution assuming artesian conditions was set for the bottom, right and left boundaries. The loading history was simulated by adding elasto-plastic elements

on top of the ground (Takaine et al., 2010). For simplicity, it was assumed that the embankment was extended laterally at a constant rate, and simulated the historical change in height of the crown in the center of the embankment based on a series of 4 loading events (**Fig. 3.5**). As laboratory tests for the embankment material, As4, and Dpt were not conducted, taking into consideration the N-values shown in **Fig. 3.4**, we applied an initial state equivalent to that of No. 6 medium-density silica sand as a general sand material (Tashiro et al., 2011). Material constants of all soil layers and initial in-situ conditions of ground were deduced and presented in *Chapter 2* (see **Table 2.6** and **Fig. 2.16**).

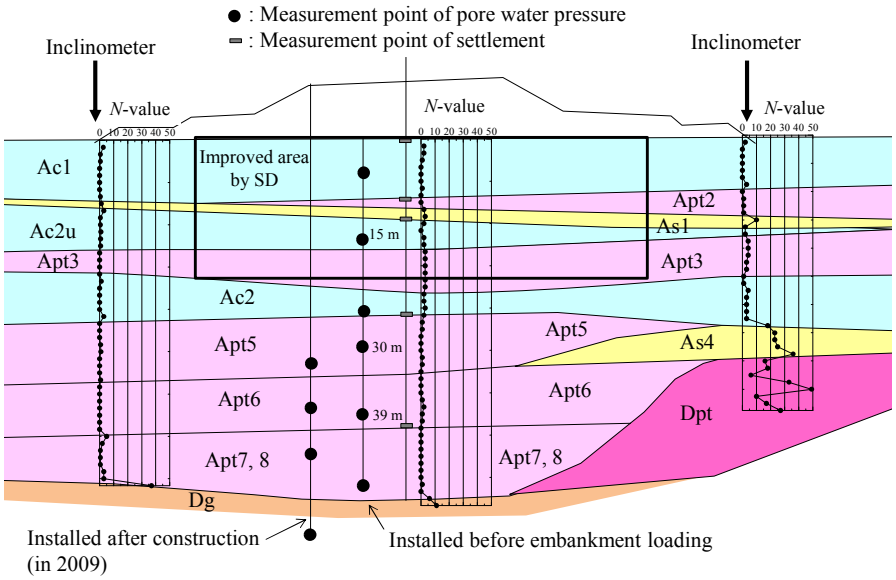

Figure 3.3 Geological structure and *N*-values of ground (cross section)

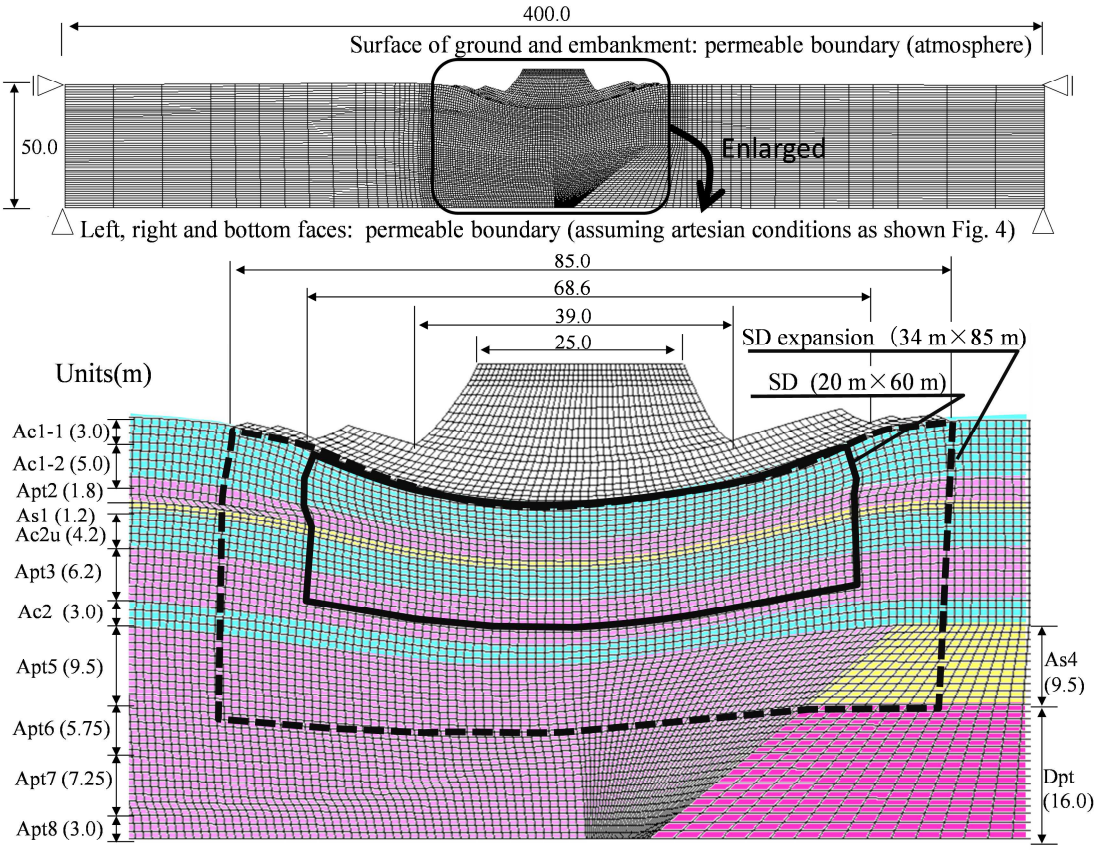

Figure 3.4 Finite element mesh (after embankment construction)

The coefficients of permeability used in the analyses are presented in **Table 3.1**. The coefficients of permeability for the ground were chosen from within the range observed in consolidation tests for undisturbed samples based on their ability to reproduce the ground deformation observed up to the present. With regard to the highly compressible peat layer, the e-ln*k* relationship expressed in **Eq. 3.1** was employed to describe the decrease in permeability k with decreasing void ratio e. The improvement effect of sand drains was simply modelled based on a mass-permeability concept proposed by Asaoka et al. (1995), in which only the mass-permeability of ground with drains is determined by back analysis to consider the acceleration effect of consolidation resulting from the drains installation, instead of modelling the each effect of drains spacing, permeability of drains, disturbance due to drain installation and other factor. In this study, the value of 100 times as large as the original coefficients of permeability as shown in **Table 3.1** were assigned to finite elements corresponding to the improved area.

$$\mathrm{e} = C \ln \frac{k}{k_0} + \mathrm{e}_0 \qquad (3.1)$$

Table 3. 1 Coefficient of permeability used in soil-water coupled finite analysis

	k_0 (cm/sec)	C
Embankment	1.0×10^{-5}	No change in permeability
Ac1-1	4.0×10^{-3}	
Ac1-2	1.0×10^{-7}	
Apt2	1.0×10^{-6}	
As1	1.0×10^{-3}	
Ac2u	1.0×10^{-6}	
Apt3	1.0×10^{-6}	

	k_0 (cm/sec)	C
Ac2	1.0×10^{-6}	No change in permeability
As4	1.0×10^{-6}	
Dpt	1.0×10^{-8}	
Apt5	5.0×10^{-4}	0.169
Apt6	1.0×10^{-5}	0.639
Apt7	1.1×10^{-5}	0.212
Apt8	1.5×10^{-5}	0.794

3.2.2. Reproducing the observed ground deformation

Comparisons of observed values and simulated results are presented in **Figs. 3.5** to **3.9**. Through a process of trial and error, the initial void ratios and permeability coefficients for each ground layer were adjusted so that the model would reproduce the actual settlement observed for each layer directly below the centerline of the embankment in the approximately four-year period (up to March, 2010) starting with test embankment construction. It could be demonstrated that the analysis code ***GEOASIA*** was capable, for the most part, of reproducing not only the surface settlement and horizontal displacement of the nearby ground surface, but also the pore water pressure during embankment construction and two years after completion of the embankment.

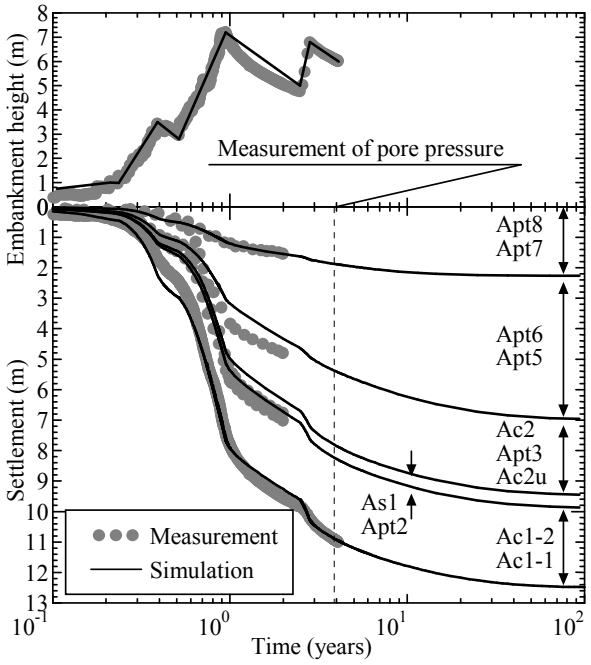

Figure 3.5 Simulations and predictions of settlement directly below center of embankment

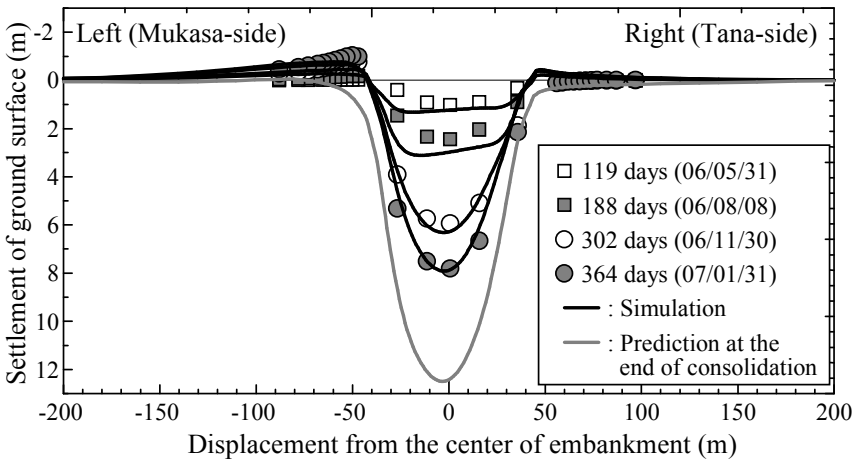

Figure 3.6 Settlement of ground surface

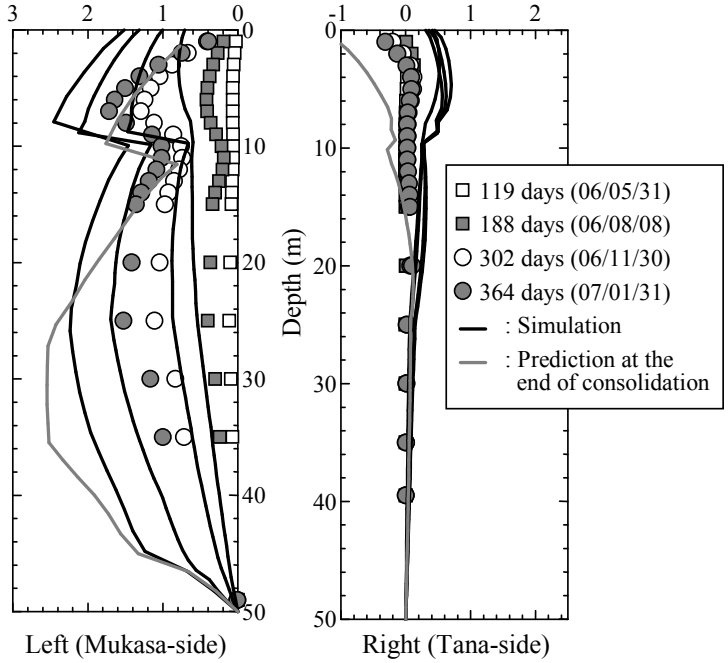

Figure 3.7 Lateral displacement at toe of embankment

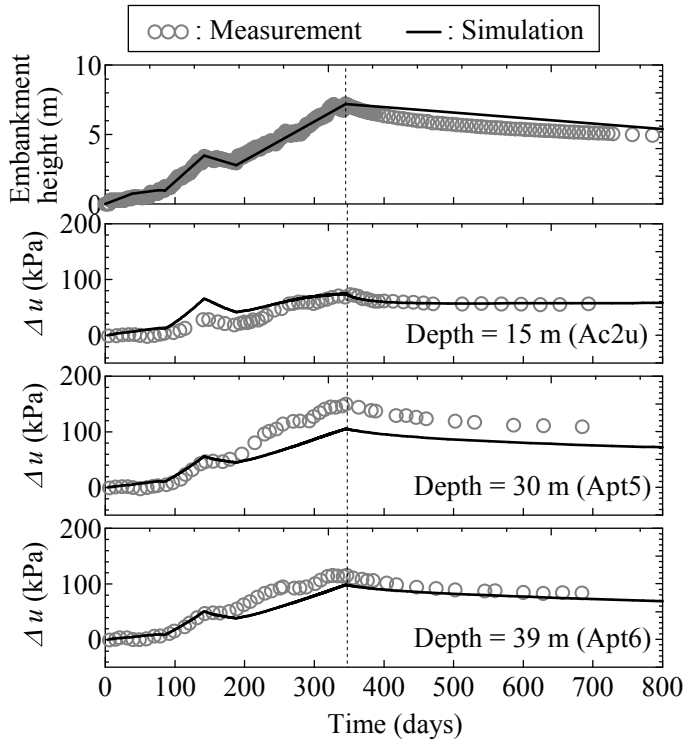

Figure 3.8 Change of pore water pressure in primary stage of embankment loading

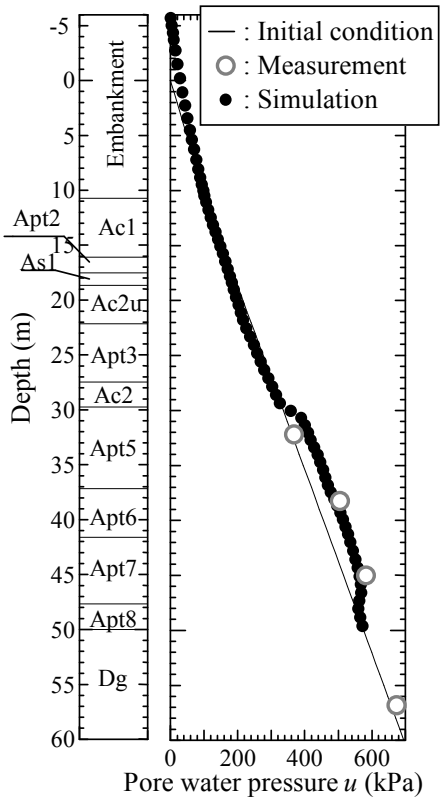

Figure 3.9 Distribution of pore water pressure about 2 years after end of construction

3.2.3. Prediction of residual settlement

Next, without changing the parameters determined through the above-described reproduction of observed settlement, the numerical analysis was continued in order to predict future settlement behavior. Defining the end of consolidation as the point where the settlement rate of the embankment center falls to 1 mm/year, it is predicted that an additional settlement of 1.52 m will occur over the next approximately 66 years.

Fig. 3.10 shows the distribution of shear strain at the end of embankment construction and at the end of consolidation. It is evident from these simulations that the large-scale deformation of the ground near the embankment during embankment loading is due to slip deformation of the shallow peat layer in unimproved areas and that the long-term residual settlement is caused by delayed compression occurring in the deep peat layer after completion of the embankment. The difference in lateral deformation on the left and right sides of the embankment is attributable primarily to the presence of hard layers (As4 and Dpt) deep in the soil profile. **Fig. 3.11** shows the behavior of finite mesh elements in the middle of the deep Apt6 layer. The deep peat layer, which initially possesses large voids, is readily compressed because of its low consolidation yield stress. It can further be seen that the permeability of the deep peat layer becomes extremely poor as the void ratio becomes smaller, resulting in delayed dissipation of excess water pressure.

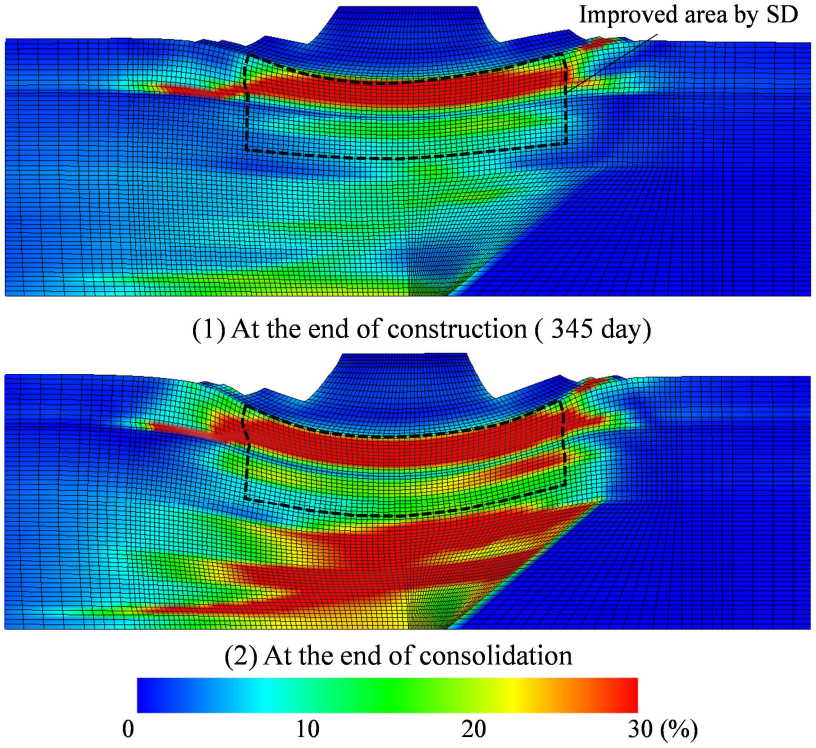

Figure 3.10 Distribution of shear strain

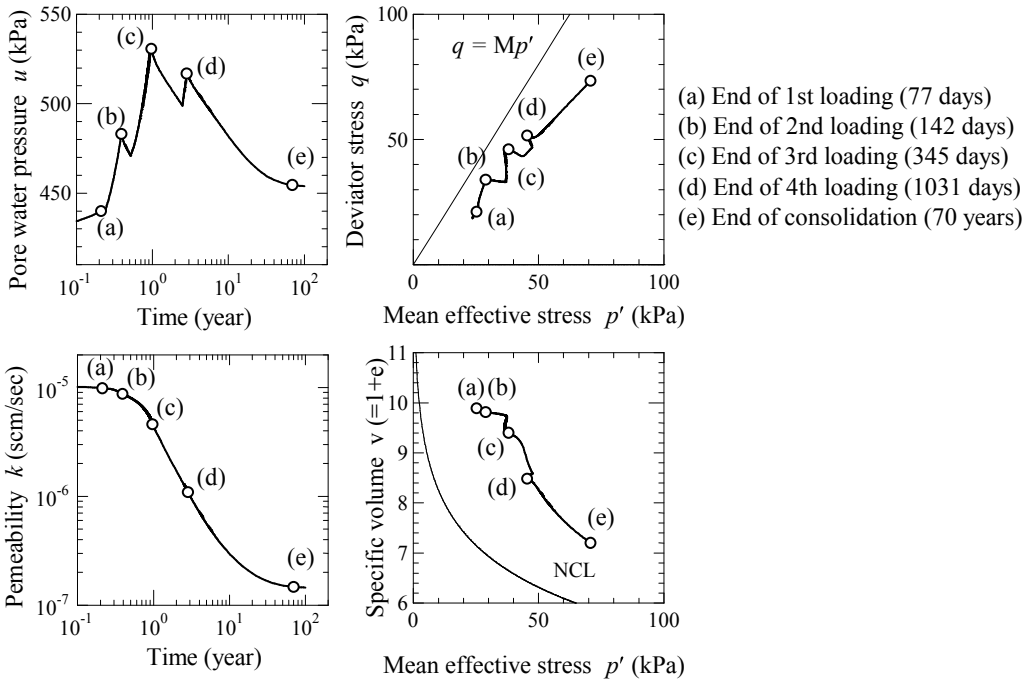

Figure 3.11 Behavior of element at center of Apt6 layer

3.3. Investigation of effective countermeasures against settlements/failure of peaty ground

By using the parameters determined in the course of reproducing observed settlement, and partially changing the analysis conditions, numerical analyses were conducted to identify the conditions resulting in large residual settlement and slip failure of ultra-soft ground containing peat, and to evaluate the efficacy of various countermeasures. In subsequent analyses, for simplicity, monotonic loading was assumed utilizing the loading speed calculated (*LRc*) using **Eq. 3.2** in term of embankment thickness per day.

$$LRc = LRa \times \Delta \tag{3.2}$$

Here, *LRa* equals to 3.0 cm/day representing the actual construction rate, and Δ is the operating ratio that is determined from construction rate at the other embankment site in the Mukasa area based on factors such as weather and availability of embankment materials; and the value of 0.783 was estimated for this operating ratio.

3.3.1. Effects of mass permeability improvement by vertical drain installation

In order to evaluate the effectiveness of the ground improvements by sand drains installed in the test embankment, the following three cases were investigated. Case-1 represents the improvement conditions that were actually implemented (based on the analysis described above).

Case-1: SD installed in test embankment (length 20 m, width 60 m).

Case-2: No SD installed.

Case-3: SD installed over extended area (length 34 m, width 85 m, see **Fig. 3.5**).

Fig. 3.12 shows (a) ground surface settlement directly under the center of the embankment, (b) residual settlement after presumed entry into service approximately 2 years after completion of the embankment, and (c) horizontal displacement directly under the toe of the embankment (only the left side).

Settlement in the early stages of embankment loading is smallest in Case-2. However, as illustrated in **Fig. 3.13**, a large-scale circular slip including deep ground layers suddenly occurred as a result of prominent undrained shear, causing a sudden large-scale settlement in which the crown of the embankment ended up being lower than the current ground surface. Based on these results, it could be concluded that installation of the SD in the test embankment in the Mukasa area was effective at preventing a catastrophic slip failure. Furthermore, because the analysis code ***GEOASIA*** employed in this study is formulated based on an equation of motion with an inertia term rather than a force equilibrium equation, it is capable of modeling instantaneous circular slip without problems, as in Case-2, even if that handle failure via stress control (Noda et al., 2008b; Takaine et al., 2010; Nakano et al., 2010; Yamada and Noda, 2013).

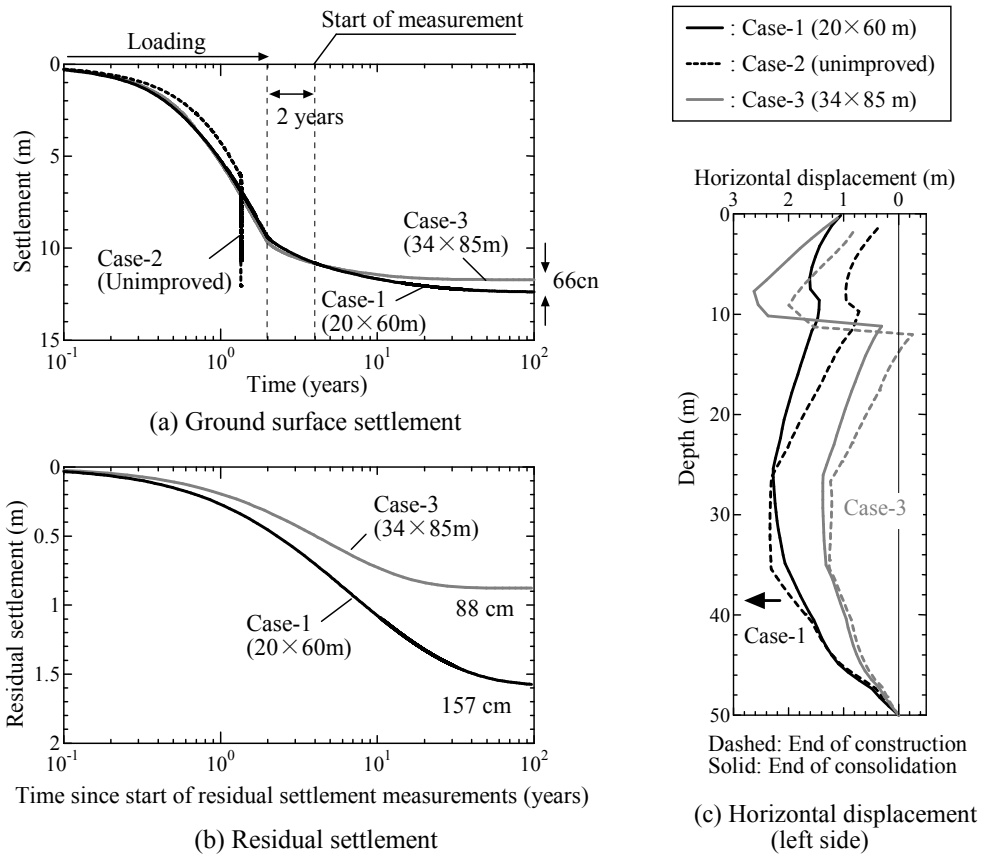

Figure 3.12 Effect of mass permeability improvement

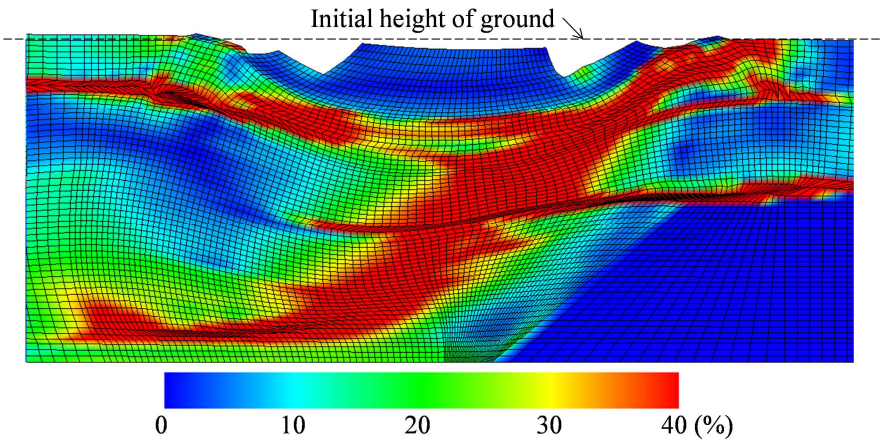

Figure 3.13 Circular slip during loading for Case-2 (unimproved by SD)

Based on a comparison of Case-1 and Case-3, it can be seen that expansion of the drain-improved area results in earlier settlement convergence and a reduction of residual settlement by approximately 50%. In addition, total settlement of the ground was reduced due to suppression of the deformation caused by undrained shear strain, particularly in the deep peat layer. However, because settlement of the improved area takes place earlier, substantial deformation also occurs in the shallow ground of unimproved areas near the toe of the embankment. It is believed that, when the drain installment areas

are expanded, increasing the area of counterweight fill or decreasing the loading speed in the early stages of embankment construction, as discussed in section **3.3.2** below, would be effective at counteracting such deformation.

3.3.2. Effects of slow banking method

During test embankment construction, the loading speed was controlled based on the embankment height. However, because settlement progressed rapidly during construction, the actual loading speed increased, resulting in large-scale deformation of the surrounding ground. Based on this experience, to ensure stability during actual construction, the loading speed was regulated based on the embankment thickness, effectively slowing the loading rate.

Taking this into consideration, in this study the impact of slow banking on Case-3 above (expanded drain installment area) was examined. The results of this simulation are presented in **Fig. 3.14**. Because slow banking promotes drainage while loading, it not only reduces deformation of the shallow ground but is also effective in reducing residual settlement. However, in cases where construction cannot be carried out over a sufficiently long period due to various local constraints, there is a need to evaluate other construction methods. In fact, a portion of the embankment in the Mukasa area was constructed using the vacuum consolidation method.

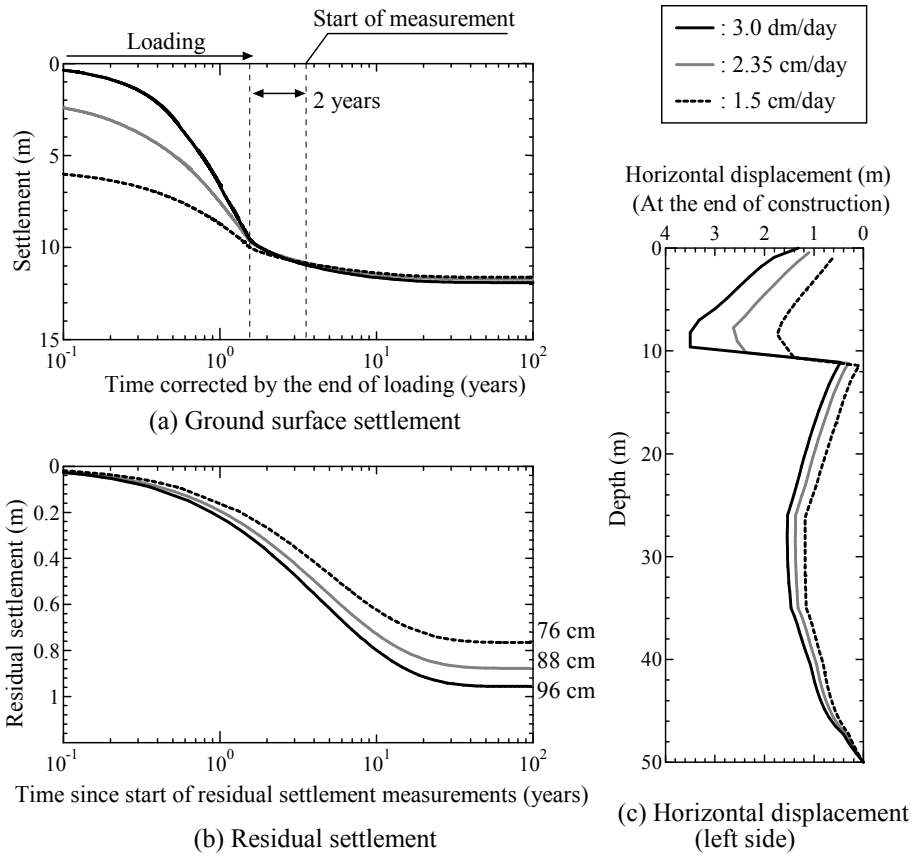

Figure 3.14 Effect of slow banking method

3.3.3. Effects of lightweight banking material

In the Mukasa area, prior starting operation a section of the SD-improved embankment (STA498) was scheduled to be replaced with a culvert box in order to restore a local road and waterway that had been blocked by construction of the test embankment. In this study, in advance of designing the culvert box and reducing the embankment load near the box, the residual settlement expected to result from the load reduction was estimated. For simplicity, the load reduction was modeled by removing finite elements corresponding to the embankment. And, extending the calculation on the actual case shown in **Fig. 3.5**, simulations were conducted to examine the impact on the subsequent behavior of instantaneously reducing the load at a point approximately 3 years after the end of loading. The results of these simulations are presented in **Fig. 3.15**. It was found that greater load reduction results in earlier convergence of settlement and less residual settlement. Load reduction was also demonstrated to reduce surrounding settlement of the ground near the toe of the embankment, albeit only slightly. If the load is reduced to that of an embankment constructed using Foamed Cement Banking (FCB) material, the residual settlement is predicted to be on the order of 1m.

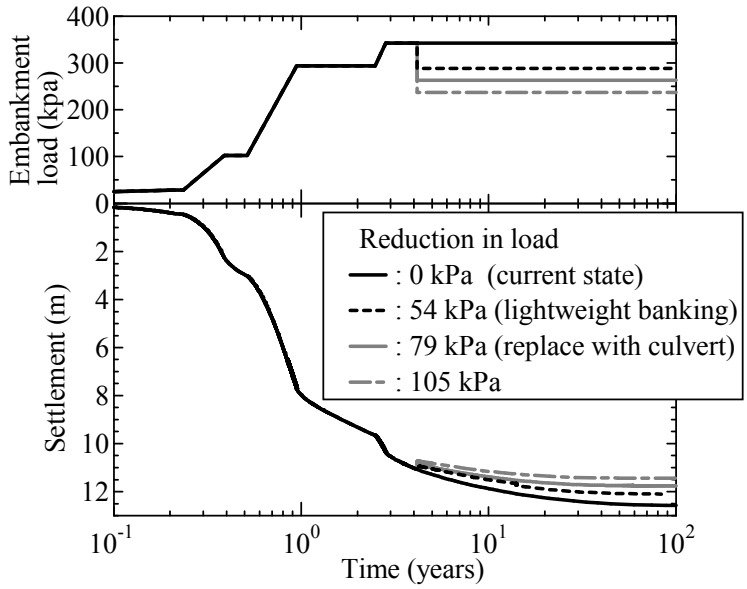

Figure 3.15 Effect of lightweight banking method

These simulation results were applied to the design and actual construction of a culvert box with a 1.2 m freeboard capable of tolerating the predicted residual settlement. In addition, a large portion of the backfilled embankment spanning approximately 50 m was replaced with lightweight FCB material. **Photo 3.2**(**a**) shows the test embankment after load reduction construction.

3.4. Results and discussion related to field observation

The results of field observations of ground surface settlement after culvert box replacement of the test embankment (STA498) are shown in **Fig. 3.16**(**a**). In the figure, “height of embankment” refers to

the historical change in height of the embankment in the lightweight, backfilled area adjacent to the culvert box. In the analysis shown in **Fig. 3.15**, the load was reduced instantaneously under 2-dimensional plane strain constraints assuming uniformity in the third axis. In contrast to the simulation, the actual construction work involved partial removal of the test embankment in a series of steps followed by construction of the culvert box and a lightweight embankment with a rectangular cross section. Given that the actual loading history differs from that of the simulation, it is not possible to directly compare the simulation and field observation results. Nevertheless, the results of the field observations confirm that embankment lightening is effective in achieving earlier convergence of settlement and reducing residual settlement.

Photo 3.2(**b**) shows the second embankment located approximately 1.1 km (STA509) from the Mukasa test embankment (or section A). In addition to being an extremely large-scale embankment with a design height of 11.5 m, the embankment is underlain by an approximately 45-m-thick soft peat layer similar to that under the test embankment. Taking the test embankment experiences into consideration, 34-m-deep plastic vertical drains (PVD) were installed prior to embankment construction as a countermeasure against residual settlement. Furthermore, because the pace of embankment construction had to be accelerated due to the construction of a nearby tunnel, 16-m-deep PVD was additionally installed and a vacuum consolidation method employed to ensure stability (Kosaka et al., 2011). The results of field observations of ground surface settlement under this embankment are presented in **Fig. 3.16**(**b**). Although large-scale settlement exceeding 11 m, similar to that observed for the test embankment, occurred during embankment construction, the presence of deep drains promoted consolidation of the deep peat layer and substantially reduced the magnitude of residual settlement. In addition, deformation of the nearby ground was reduced through vacuum consolidation. As in the case of the test embankment, a portion of this embankment was replaced by a culvert box. However, given the small residual settlement, there was no need to lighten the surrounding embankment.

Based on a comparison of the two embankments above, it could be concluded that the conventional design principles, that settlement can be coped with by providing sufficient freeboard and sinking allowance as long as stability can be achieved, did not completely apply to the ultra-soft peaty ground in the Mukasa area. When loading soft ground containing clay or peat with a load exceeding the soil's consolidation yield stress, it is necessary to not only ensure stability during embankment construction but also to implement countermeasures prior to construction against subsequent residual settlement.

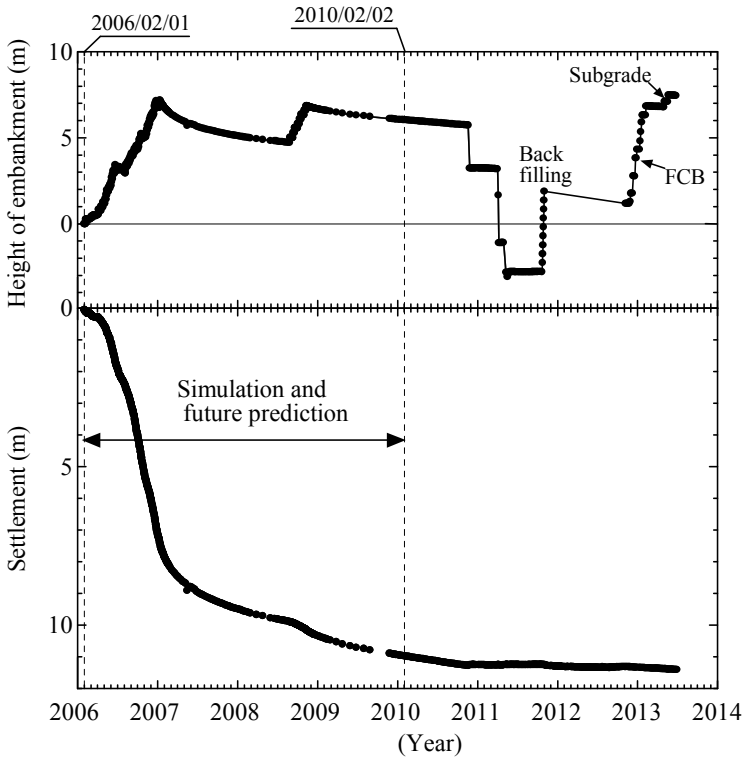

(a) STA498 (test embankment)

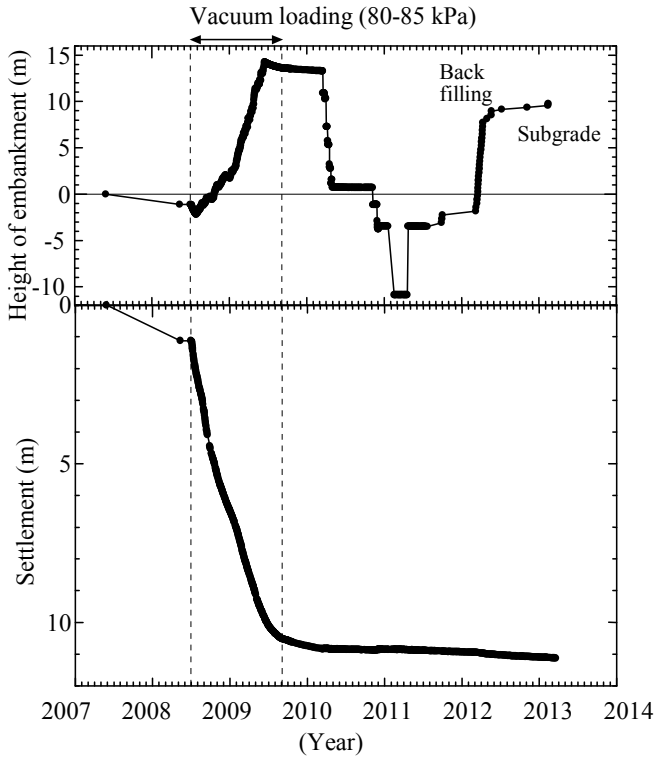

(b) STA509

Figure 3.16 Observation results for two embankments replaced by culvert box

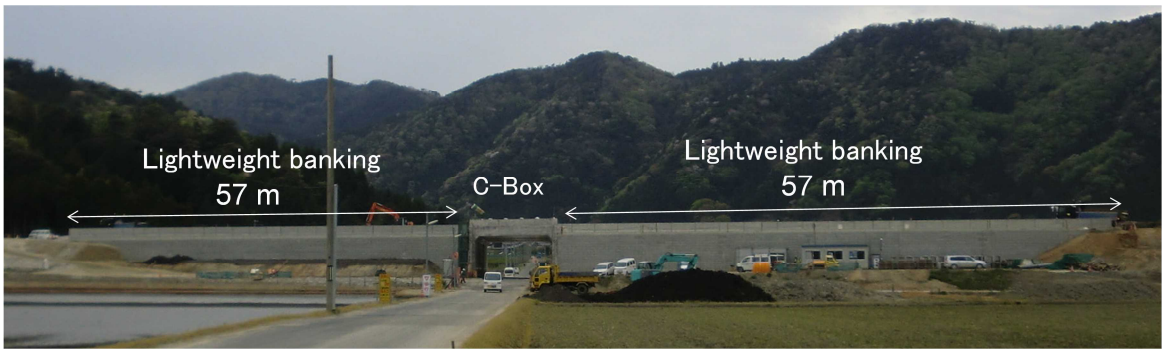

(a) Residual settlement not considered (STA498 test embankment, taken in 2013)

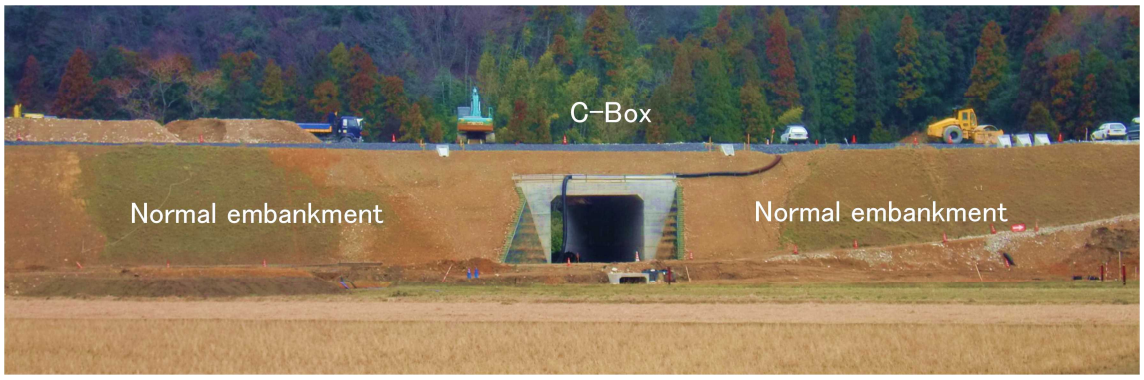

(b) Residual settlement considered (STA509, taken in 2013)

Photo 3. 2 Different countermeasures after construction based on whether or not residual settlement was considered

3.5. Brief summary

In advance of construction of the Maizuru-Wakasa expressway on the ultra-soft peaty ground in the Mukasa area, a test embankment was constructed on section A to select countermeasures for the problems associated with construction on soft ground. Although catastrophic slip failure did not occur during loading, the large-scale settlement that did occur was accompanied by substantial deformation of the adjacent ground. The study in this *Chapter* focused on the SD-improved test embankment section underlain by the thickest soft layer with a depth of approximately 50 m. In this section, the overall settlement exceeded 11 m approximately three years after embankment construction, and did not appear to be approaching convergence due to large-scale delayed compression of the greater than 30-m-deep peat layer, which was assumed in the design stage not to be subject to settlement, the overall settlement.

The large-scale deformation of the ultra-soft peaty ground observed in the approximately four-year period (up to March, 2010) starting with test embankment construction was simulated using the ground analysis code ***GEOASIA*** developed by the authors' research group. The mechanical behavior of the peat was described within the same theoretical framework as all other soil components from

clay, to sand, to embankment material. In addition, taking into consideration the sensitivity to disturbance and the heterogeneity of the peat layers, the initial in-situ conditions were deduced by simulating the observed settlement of each layer under the center of the embankment. As a result, it could be demonstrated that the analysis code ***GEOASIA*** was capable, for the most part, of reproducing not only the large-scale deformation of the surrounding ground that occurred during embankment loading, but also the observed pore water pressures during embankment construction and the approximately 2-year period following construction. Allowing the simulations to continue without changing the parameters obtained from the simulation of the observed behavior resulted in prediction of an additional 1.52 m of residual settlement in the next approximately 66 years.

The ground analysis code ***GEOASIA***, which takes inertial forces into consideration, enables simultaneous investigation not only of long-term settlement behavior resulting from degradation of the soil skeleton structure, but also circular slips and failures that occur instantaneously. Taking advantage of this feature of the analysis code, the effectiveness of countermeasures in ensuring stability and reducing residual settlement was also investigated. Due to its extremely low consolidation yield stress, when peat is subjected to a substantial load under undrained conditions, large lateral deformation, or in some instances slip failure, can occur. Even under drained conditions, sudden large-scale compression occurs, leading to significant deformation of the surrounding ground. Through a series of analyses, it was demonstrated that improvement of the permeability by drains and that lowering the loading speed as much as possible and, as an even more drastic countermeasure, lightening the load are effective not only for increasing stability during construction, but also for reducing the amount residual settlement.

Large-scale repair work was performed on the test embankment based on the results of these analyses. Furthermore, when an embankment was subsequently constructed near the test embankment on similar ultra-soft ground, installation of deeper drains and vacuum consolidation were conducted taking into consideration the residual settlement. The results of field observations of both embankments presented in this study emphasize the importance of implementing countermeasures aimed at both ensuring stability during construction and, taking future maintenance into consideration, reducing residual settlement when subjecting soft ground containing clay and/or peat to loads exceeding consolidation yield stress of the ground.

Chapter 4

Proposal of a new macro element method with water absorption and discharge functions for vertical drains

4.1. Introduction

It is well known that soil-water coupled elasto-plastic finite element analysis is one of the most important tools for analyzing problems involving ground deformation and failure. It goes without saying that a challenge faced when simulating the vertical drain (VD) method using this numerical analysis approach, is how to represent the VD in the numerical model. The simplest method is to model the VDs with finite elements after dividing the mesh finely in the improved region (e.g., Borges et al., 2008). While this is an ideal approach from the standpoint of being able to precisely calculate stress, strain and water flow, it is problematic in that it requires 3-dimensional analysis and simultaneous evaluation of a vastly increased number of elements. The corresponding approach for analysis under 2-dimensional plane strain conditions is to distribute thin, highly-permeable elements vertically or permeable boundaries in the ground. In this case, because wall-like drains are created, special manipulation of some type is required to match the progress of consolidation between under 3-dimensional condition and under 2-dimensional plane strain condition (e.g., Shinsha et al. 1982; Hird et al., 1992; Indraratna et al., 2004). There is a mass permeability concept as a technique that does not require increasing the mesh density by assigning the macroscopic permeability to the improved ground in order to consider the acceleration effect of consolidation resulting from the VD method. While this offers a simple way to present the problem, it still requires a means of deciding the mass-permeability of the ground with the drains. Asaoka et al. (1995) proposed a back-analysis method for determining the mass permeability of ground with drains. Chai et al. (2001) reported a method for calculating the vertical macroscopic coefficient of permeability of ground based on the drain diameter and arrangement. However, the problem with these methods is that, even though they are able to simulate the settlement behavior of the ground surface, they do not necessarily accurately reproduce the consolidation process in the ground. Sekiguchi et al. (1986) proposed a different approach to simulating the VD method with the goal of reducing computational cost. Specifically, they attempted to express the accelerated consolidation associated with the VD method by assigning a water absorption function of drains to each element in the drain-improved region. They can be considered as a type of homogenization method that enables the reproduction of accelerated consolidation effects due to drains at the macroscopic level without dealing with the heterogeneity that occurs around individual drains. Sekiguchi et al. (1986) used the term “macro element method” to refer to this approach. It is a useful method that allows very accurate incorporation of the water absorption function of drains even under 2-dimensional plane strain conditions. Sekiguchi et al. (1986) validated

their proposed method through experiments conducted on a test embankment under which the soft ground was improved by installation of sand drains. Based on this approach, Asaoka et al. (1995) proposed the aforementioned method for determining the mass-permeability of drain-improved ground. Takeyama et al. (2008) and Arai et al. (2008) performed simulations of vacuum consolidation using the same method. Hirata et al. (2010b) included the well resistance coefficient proposed by Yoshikuni and Nakanodo (1974) and/or Yoshikuni (1979) into the macro element to simply account for the consolidation delay resulting from well resistance. Also, Chai et al. (2013) discussed several methods to incorporate VD effects into soil-water coupled finite element method including the original macro element method.

One of main objective in this *Chapter 4* is to newly extend the function of the original macro element method. Specifically, treating the water pressure in the drain, which has been specified as an analytical condition in previous versions of the method, as an unknown is proposed. In the proposed method, a continuity equation for drains is added to the governing equations in order to compensate for the increased an unknown. In previous versions of the macro element method, as a consequence of approximating the drain permeability as infinity, the pore water absorbed into drains would simply vanish. In the proposed method, however, this pore water is transported to the ground surface through drains with finite permeability. That is to say, the proposed macro element method newly obtains a discharge function for the drain while retaining the water absorption function included in previous versions. Analysis showed that, in simulations with this rational expansion, a well resistance spontaneously occurs under certain conditions. Furthermore, in previous versions of the macro element method, it was necessary to match the mesh division width to the drain spacing or an integral multiple thereof. If this restriction was removed, it would be possible to use the same mesh to investigate the effect of the drain spacing. In this paper, a formulation whereby the solution is not constrained by the mesh division width is conducted.

The structure and objective of the present *Chapter* are as follows. First, the new macro element method that incorporates water absorption and discharge functions for VDs is formulated. Next, using a soil-water coupled elasto-plastic finite element analysis code based on finite deformation theory incorporating the above formulation, calculation results for an axisymmetric unit cell model surrounding a single drain are shown to ascertain the baseline performance and approximation accuracy. Then, a series of simulation results for vacuum consolidation of ground containing a middle sand layer are shown to demonstrate the advantage of treating the water pressure in the drain as an unknown. In addition, mesh sensitivity is also verified for the same analytical target. Finally, the conversion methods of equivalent diameter of a single band-shaped vertical drain that are modelled in macro element are investigated by comparison with 3D model, in which higher permeability is assigned for element representing vertical drain. The dependence of well resistant phenomenon that occurs when using band-shaped vertical drain on its thickness is also investigated numerically by applying the new macro element method.

In fact, some contents of this *Chapter* could be seen in Yamada et al., 2015.

4.2. Formulation of a new macro element method equipped with a water absorption and discharge functions for vertical drains

4.2.1. Soil-water coupled elasto-plastic finite element governing equations and macro element method

Asaoka et al. (1994, 1997b) proposed a quasi-static soil-water coupled elasto-plastic finite element method based on finite deformation as an extension of the method of Akai and Tamura (1978), which is of the type proposed by Christian and Beohmer (1970). Extending this approach by the introduction of macro elements is considered herein.

The governing equations for the numerical analysis methods above are represented as follows.

$$\mathrm{K}\left\{\dot{\boldsymbol{v}}^{N}\right\}-\mathrm{L}^{\mathrm{T}}\dot{u}=\left\{\dot{\boldsymbol{f}}\right\} \tag{4.1}$$

$$-\mathrm{L}\left\{\dot{\boldsymbol{v}}^{N}\right\}=\sum_{i=1}^{m}\alpha_i(h-h_i)\rho_w g \tag{4.2}$$

Eqs. 4.1 and **4.2** represent a spatially discretized rate-type equilibrium equation and a soil-water coupled equation, respectively. By solving these equations simultaneously, the node velocities $\left\{\dot{\boldsymbol{v}}^{N}\right\}$ and the representative value of the pore water pressure u u at each element are obtained. Here, K represents the tangent stiffness matrix, L is the matrix for converting $\left\{\dot{\boldsymbol{v}}^{N}\right\}$ to the elemental volume change rate, $\left\{\dot{\boldsymbol{f}}\right\}$ is the nodal force rate vector, h and h_i represent the total head corresponding to the water pressure for the element in question and neighboring elements, respectively, ρ_w is the density of water, g is the magnitude of the gravitational acceleration, α_i is the coefficient of pore water flow to adjacent elements, and m is the number of faces for each element. The left side of **Eq. 4.2** represents the compression rate for soil elements and the right side represents the rate of pore water flow from soil elements.

In the macro element method, since the influence of the drain on the rigidity and the mass of the element is assumed to be negligibly small, **Eq. 4.1** is employed directly. On the other hand, in order to introduce the water absorption function of vertical drains to the each element, the term $\dot{Q}_D$, which represents the rate of water influx from the soil to the drain, is added to the right side of **Eq. 4.2**.

$$-\mathrm{L}\left\{\dot{\boldsymbol{v}}^{N}\right\}=\sum_{i=1}^{n}\alpha_i(h-h_i)\rho_w g+\dot{Q}_D \tag{4.3}$$

4.2.2. Model for pore water influx from soil to drain

In the macro element method, a representative value of the water pressure in the drain u_D is assigned at the center of the element in addition to the representative value of the pore water pressure u. A model for calculating the rate of pore water influx from soil to the drain $\dot{Q}_D$ is introduced based on the difference between these two water pressures, given by

$$\dot{Q}_D=\kappa(u-u_D)\ \left(=\kappa(h-h_D)\rho_w g\right) \tag{4.4}$$

where h and h_D represent the total heads corresponding to u and u_D, respectively. The coefficient of pore water flow from the soil to the drain is denoted as κ and must be specified to appropriately represent the effects of the drain spacing and diameter. Sekiguchi et al. (1986) specified a κ based on the assumption that mesh division width was matched to the drain spacing or an integral multiple thereof for drain arrangement in a square pattern, and validated the performance of the model. In this proposal, while basically following the derivation process of Sekiguchi et al. (1986), the author derived a specific κ that enables the mesh division width to be assigned independently of the drain arrangement and spacing.

First, an axisymmetric unit cell model surrounding a single drain is concerned, as illustrated in **Fig. 4.1**. Using $r_w(=d_w/2)$ as the radius of a circular drain, $r_e(=d_e/2)$ as the radius of the model, r as the distance to the center axis, z as the height from the bottom, t as time, $f(r)$ as the first eigenfunction from the solution by Barron (1948), and $u_w(z,t)$ as the water pressure in the drain, it was assumed that the distribution of water pressure $u(r,z,t)$ in the area surrounding the drain ($r_w \le r \le r_e$) can be approximated as follows:

$$u(r,z,t) = g(z,t)f(r) + u_w(z,t) \tag{4.5}$$

$$f(r) = \ln\frac{r}{r_w} - \frac{r^2 - r_w^2}{2r_e^2} \tag{4.6}$$

where, $g(z,t)$ is a function describing the change in water pressure in the drain with height.

Next, the mean water pressure $\bar{u}(z,t)$ within the horizontal cross-section of the axisymmetric unit cell model ($r \le r_e$) at a height z is defined by the following equation.

$$\bar{u}(z,t) = \frac{2\pi\int_0^{r_e} u(r,z,t)rdr}{\pi r_e^2} \tag{4.7}$$

Substituting **Eqs. 4.5** and **4.6** into **Eq. 4.7**, the following equation is obtained.

$$\bar{u}(z,t) = g(z,t)\frac{n^2-1}{n^2}F(n) + u_w(z,t) \tag{4.8}$$

$$F(n) = \frac{n^2}{n^2-1}\ln n - \frac{3n^2-1}{4n^2}, \quad n = \frac{r_e}{r_w} \tag{4.9}$$

When **Eqs. 4.5** and **4.6** are used to describe the water pressure distribution, the rate of pore water influx from the soil to the drain per, $\dot{Q}_D^*(z,t)$ can be expressed by the following equation:

$$\begin{aligned}\dot{Q}_D^*(z,t) &= 2\pi r_w dz \frac{k}{\rho_w g}\frac{\partial u}{\partial r}\bigg|_{r=r_w} \\ &= \frac{2\pi k dz}{\rho_w g}\frac{r_e^2}{r_e^2 - r_w^2}g(z,t),\end{aligned} \tag{4.10}$$

where k is the permeability coefficient of the ground. By deleting $g(z,t)$ from **Eqs. 4.8** and **4.10**, $\dot{Q}_D^*$ can be re-expressed by the following equation, using $\overline{u}$ and u_w.

$$\dot{Q}_D^*(z,t) = \frac{2\pi k dz}{F(n)\rho_w g}(\overline{u}(z,t) - u_w(z,t)) \tag{4.11}$$

In other words, the equation describes how much pore water flows into the drain per improved area $\pi r_e^2 dz$ per unit time. Next, the rate of influx into the drain $\dot{Q}_D^*$ is converted to a per-element basis $\dot{Q}_D$. In addition, u and u_D in **Eq. 4.4** are considered as corresponding to $\overline{u}$ and u_w in **Eq. 4.11**, respectively. Furthermore, defining V as the volume of one element, when the ratio of $\dot{Q}_D^*$ to $\dot{Q}_D$ is assumed to be the same as the ratio of $\pi r_e^2 dz$ to V, the flow coefficient κ in Eq. (4) can be expressed as follows.

$$\kappa = \frac{8kV}{F(n)d_e^2\rho_w g} \tag{4.12}$$

In finite deformation analysis, the element volume V is matched to the actual volume. In addition, the permeability coefficient k of the ground is allowed to change with the ground's void ratio (although, in this *Chapter*, change in the permeability coefficient is not taken into consideration). Meanwhile, d_e and d_w are employed as material constants that always have the same value irrespective of element deformation.

By formulating the water-flow coefficient κ using the element volume V, the mesh division width can be separated from the drain arrangement and spacing. In previous formulation of the macro element method, when performing calculations under plane strain conditions, attention needed to be paid to how the depth direction was defined. However, if the formulation proposed in this *Chapter* is used, no constraint is placed on depth (it is simply necessary to utilize a unit depth). Furthermore, as can be seen in **Eq. 4.12**, the flow coefficient does not depend on the ground hardness.

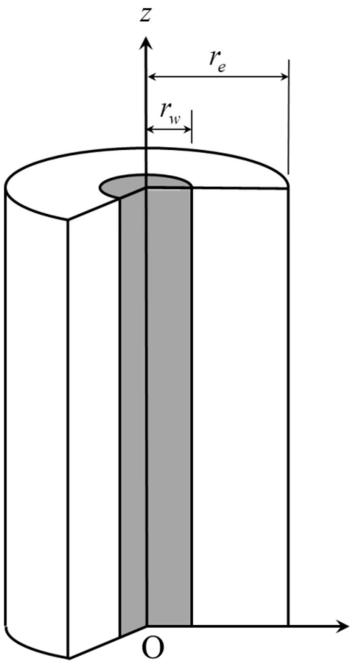

Figure 4.1 Axisymmetric unit cell model surrounding a single drain

4.2.3. Soil-water-drain coupled equation

The equation obtained by substituting **Eq. 4.4** into **Eq. 4.3** is called the "soil-water-drain coupled equation."

$$-\mathrm{L}\left\{\boldsymbol{v}^{N}\right\}=\sum_{i=1}^{m}\alpha_i(h-h_i)\rho_w g+\kappa(h-h_D)\rho_w g \tag{4.13}$$

In previous versions of the macro element method, $\left\{\boldsymbol{v}^{N}\right\}$ and u are obtained by simultaneously solving **Eqs. 4.1** and **4.13**. In such cases, the total head h_D or corresponding water pressure in the drain u_D in **Eq. 4.13** is specified by the analyst as a type of permeable boundary condition. For example, in the case of a problem involving consolidation due to loading, the water pressure in the drain is specified as hydrostatic pressure. In contrast, in the case of a vacuum consolidation problem, a pressure that is a designated amount below the hydrostatic pressure is specified. Meanwhile, when the discharge function for drains is insufficient, i.e., when well resistance occurs, it is difficult for the analyst to assign the water pressure in the drain in advance. Therefore, in this *Chapter*, the water pressure in the drain u_D is treated as an unknown.

4.2.4. Continuity equation for drains

In order to obtain the water pressure in the drain u_D as a part of solution, it is necessary to compensate as many equations as increased unknowns. In the present *Chapter*, for the region over which the macro-element method is to be applied, a continuity equation for drains is formulated, on the assumption that the initial mesh for macro elements are approximately divided in a vertical

direction and each element contained a virtual drain as shown in **Fig. 4.2**. And it is assumed that the water flow within the drain can be approximated by Darcy's law. Furthermore, based on the assumption that the change in drain volume relative to the change in element volume is negligibly small, the continuity equation for drains is formulated as follows:

$$\kappa(h-h_D)\rho_w g = \sum_{j=1}^{2}\beta_j(h_D-h_{Dj})\rho_w g \tag{4.14}$$

where h_{Dj} is the total head of the drain contained in the macro elements above and below the macro element in question. The left side of **Eq. 4.14** represents the amount of pore water flowing from the soil to the drain per unit time. The right side of the equation represents the amount of water flowing to the macro elements above and below the macro element in question via the virtual drain per unit time. The coefficient of water flow through the virtual drain β_j is constructed as follows so as to allow for mesh deformation in finite element problems:

$$\beta_j = \frac{k_w}{l^j}\frac{\boldsymbol{l}^j}{l^j}\cdot\boldsymbol{n}^j\frac{s^j}{n^2} \tag{4.15}$$

where $\boldsymbol{l}^j$ represents the vectors connecting element centers, l^j represents the magnitudes thereof, and $\boldsymbol{n}^j$ and s^j are the outward-facing normal vector and area for boundary surface j of the element. Equation (15) is obtained by replacing k^i with k_w and multiplying s^j by the ratio of the drain cross-sectional area to the improved area $1/n^2$ in the pore water flow coefficient α_i between the elements whose specific shapes are shown in **Appendix A1**. As in the case of κ, when calculating β_j, in addition to using the current value for $\boldsymbol{l}^j$ and $\boldsymbol{n}^j$ in finite deformation problems, d_e and d_w are treated as material constants for which the same value is always used even if the element undergoes deformation.

In previous versions of the macro element method, as a consequence of approximating the drain permeability by infinity, pore water entering a drain simply disappeared. In contrast, in the method proposed in this *Chapter*, pore water entering a drain is discharged to the ground surface according to the continuity equation for drains. The addition of **Eq. 4.14** to the governing equations signifies the addition of a discharge function to the macro element method. Along with this extension, k_w is added to the list of macro element method material constants.

Under certain initial conditions, when **Eq. 4.14** is solved in conjunction with **Eqs. 4.1** and **4.13**, in order to simultaneously obtain the water pressure in the drain u_D, the nodal displacement velocities $\{\boldsymbol{v}^N\}$ and the pore water pressure u, it is necessary to assign hydraulic boundary conditions for the drain in addition to the boundary conditions required for general soil-water coupled analysis. In this case, the same treatment applied to **Eq. 4.2** is applied to **Eq. 4.14** (See **Appendix A8**). In addition, it is necessary to assign an initial value for the water pressure in the drain. Unless there is a specific reason, this is set to the ground water pressure.

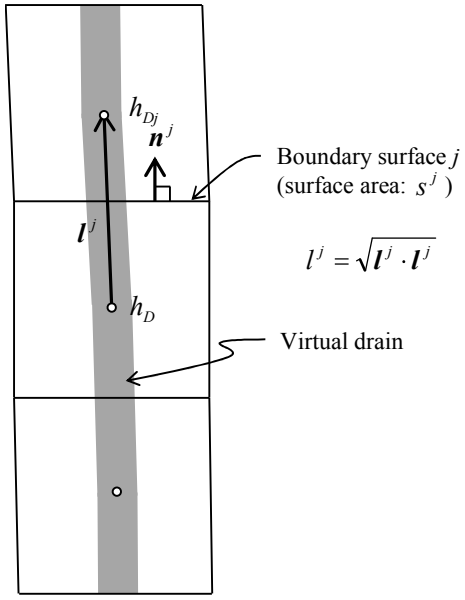

Figure 4.2 Virtual drain contained in mesh elements

4.2.5. Calculation of material constants of drain (d_e, d_w, and k_w)

As mentioned earlier, the proposed macro element method contains three material constants d_e, d_w, and k_w. These are introduced when constructing the axisymmetric soil-to-drain pore water flow model illustrated in **Fig. 4.1**. Meanwhile, as shown in **Fig. 4.3**, the improved region associated with a single drain is generally not circular and the drain material is often distributed in a band. When applying the macro element method, it is necessary to calculate d_e based on the drain arrangement and spacing, and to calculate d_w based on the drain shape. Various methods have been proposed for converting those based on simple calculations employing the solution from Barron (1948). The question of which method is optimal warrants discussion elsewhere. Here, the representative methods are briefly referred. First, with regard to the conversion to the equivalent diameter d_e, the following equations, obtained by equating the area of the real improved region for a single drain and the horizontal cross-sectional area of the axisymmetric unit cell model, are often used:

$$d_e = \frac{2}{\sqrt{\pi}} d \quad \text{: Square pattern} \tag{4.16}$$

$$d_e = \sqrt{\frac{2\sqrt{3}}{\pi}} d \quad \text{: Triangular pattern} \tag{4.17}$$

where d is the drain spacing. The followings are examples of equations for converting band-shaped drains to columnar drains:

$$d_w = \frac{2(a+b)}{\pi} \tag{4.18}$$

$$d_w = 2\sqrt{\frac{ab}{\pi}} \tag{4.19}$$

$$d_w = \frac{(a+b)}{2} \tag{4.20}$$

where a and b are the width and thickness, respectively, of a band-shaped drain. **Eqs. 4.18**, **4.19** and **4.20** are derived by equalizing outer circumference (Hansbo, 1970), the cross-sectional area, and the average value of the width and the thickness (Rinxer et al., 1986) of a drain, respectively.

Care must be taken when assigning a value to k_w. It should be kept in mind that k_w is a drain material constant substituted into a problem set up as illustrated in **Fig. 4.1**. When the permeability coefficient of a drain $\tilde{k}_w$ is measured experimentally or determined by other means, k_w must fulfill the following relationship in order to ensure that the discharge capacity assigned to a single drain, before and after conversion, with respect to the cross-sectional area of the improved region is equivalent to the measured value:

$$\frac{a_w}{a_e} k_w = \frac{\tilde{a}_w}{\tilde{a}_e} \tilde{k}_w \tag{4.21}$$

where $\tilde{a}_e$ and $\tilde{a}_w$ are the cross-sectional area of the improved region for a single drain and the cross-sectional area of the drain prior to conversion, respectively, and a_e and a_w are respectively the horizontal cross-sectional area of the axisymmetric unit cell model and the cross-sectional area for a circular drain after conversion. Accordingly, it is only when $a_e = \tilde{a}_e$ and $a_w = \tilde{a}_w$ (i.e., when **Eq. 4.16** or **4.17** is used to obtain d_e, or when **Eq. 4.19** is used to obtain d_w) that $k_w = \tilde{k}_w$.

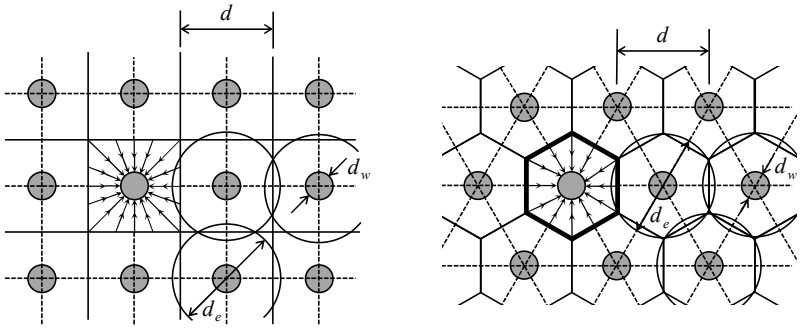

(a) Square pattern (b) Triangle pattern

Figure 4.3 Drain arrangement and equivalent circle

4.2.6. Removal of supplementary conditions

Sekiguchi et al. (1986, 1988) added the following conditions to the original macro element method.

1) The mesh division width and depth must be matched to the drain spacing or be an integral multiple thereof when drains are deployed in a square pattern.
2) Macro elements situated transversely adjacent to non-improved regions are designated "transitional macro elements," while the remaining macro elements are designated "basic macro elements." The transitional elements mediate the direct flow of pore water from transversely adjacent regular elements to the drain.
3) There is no exchange of pore water via soil between transversely adjacent macro elements, hence $\alpha_i = 0$ in the horizontal direction.

All of the above conditions are the consequence of assuming $\partial u / \partial r = 0$ where $r = r_e$ for the pore water pressure distribution in **Eqs. 4.5** and **4.6**, i.e., the rate of horizontal water flow at the outer boundary of an axisymmetric unit cell model is zero, assumed when constructing the soil-drain influx model. As mentioned earlier, in view of the advantage of the proposed method in determining the effect of the drain spacing using the same mesh, remove constraint 1). In addition, based on the expectation that the flow of pore water from non-improved regions to improved regions, and the influence of the drains on the non-improved regions, will be accounted for by pore water flow between soil's elements represented in the soil-water-drain coupled equation itself, the author has decided not to use the transitional macro elements 2). Constraint 3) also has been removed because the author considers that the engineering value of including the water flow resulting from the horizontal heterogeneity in the pore water pressure distribution homogenized at the macro scale is greater than the value of strictly fulfilling the conditions assumed when constructing the model for pore water influx from soil to drain. In order to ensure the validity of removing these supplementary conditions, it is essential, at the very least; to confirm that mesh division width will have little influence on the analysis results. This point is discussed in the section 4.4.4 of this *Chapter*.

4.3. Verification of the proposed macro element method

This section demonstrates the work of on the basic performance and verification of accuracy of the proposed macro element method based on calculations of consolidation for an axisymmetric unit cell model as illustrated in **Fig. 4.1**.

4.3.1. Analysis conditions

Some calculations were performed after incorporating the proposed macro element method into the quasi-static soil-water coupled elasto-plastic finite element method based on the finite deformation theory of Asaoka et al. (1994, 1997b). For the constitutive model of the soil skeleton, the SYS Cam-clay elasto-plastic constitutive model (Asaoka et al. 2002) based on the soil skeleton structure concept was employed. This constitutive model can describe the work of the structure, overconsolidation and anisotropy by introducing a superloading yield surface (Asaoka et al. 1998, 2000), a subloading yield surface (Hashiguchi, 1978, 1989; Asaoka et al., 1997a), and rotational hardening (Sekiguchi and Ohta,

1977; Hashiguchi and Chen, 1998) into the Cam-clay model (Roscoe and Burland 1968), respectively, and reproduce the mechanical behavior of a wide range of soils including clay, intermediate soil and sand.

A 20-m-thick ground layer under single drainage condition in which a circular drain is installed down to the bottom was modeled. The drain was assigned a diameter d_w of 0.05 m, an equivalent diameter d_e of 1.5 m, and a permeability coefficient k_w of 5.0×10^{-2} cm/s. Two types of analytical models were applied to this setup. The first was the axisymmetric model shown in **Fig. 4.4**, in which the drain and the surrounding ground are discretized to a mesh. With respect to the drain in this model, only the water absorption and discharge functions were considered. Therefore, the same mechanical characteristics were assigned to all elements, although a higher permeability coefficient was assigned for the elements corresponding to the drain than for those representing the ground. This analytical model is referred to as the "exact model." The second model, illustrated in **Fig. 4.5**, is a plane strain model in which the horizontal direction is not divided to a mesh. The water absorption and discharge functions are approximated using the macro element method. This analytical model is referred to as the "approximate model." In the approximate model, although the analytical domain in the horizontal direction is set to a width of 0.25 m in order to create a square mesh, the specification of the analytical domain in the horizontal direction does not influence the analytical results under the above analytical conditions. The material constants assigned to the macro element method are summarized in **Table 4.1**.

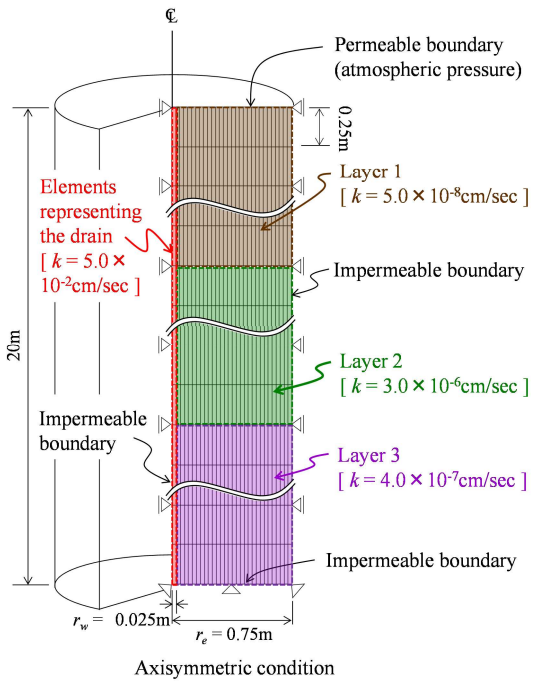

Figure 4.4 Finite element mesh and boundary conditions (exact model)

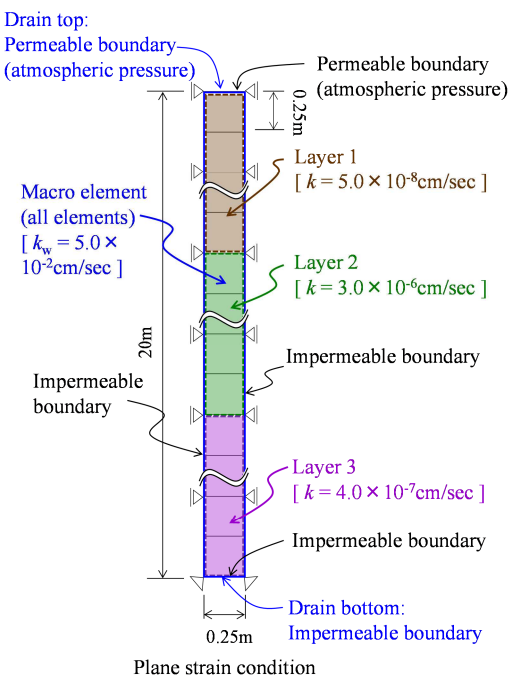

Figure 4.5 Finite element mesh and boundary conditions (approximate model)

Table 4. 1 Material constants of macro element method

Equivalent diameter d_e (m)	1.5
Diameter of circular drain d_w (m)	5.00×10^{-2}
Coefficient of permeability of circular drain k_w (cm/sec)	5.00×10^{-2}

In both the analysis models, horizontal displacement was fixed for the sides of the analyzing domain and both the vertical and horizontal displacements were fixed for the bottom. In terms of the hydraulic boundary conditions, the sides and bottom were specified as impermeable boundaries, while the ground surface was specified as a permeable boundary (atmospheric pressure). Similarly, for boundary conditions of the macro element method in the approximate model, the bottom was specified as an impermeable boundary while the ground surface was specified as a permeable boundary (atmospheric pressure). The ground surface was vertically loaded with a uniform distribution at a fixed rate over a ten-day period until a final load of 150 kN/m^2 was reached. Thereafter, the load was kept constant.

The material constants and initial conditions adopted for the ground are shown in **Table 4.2**. As can be seen in **Figs. 4.4** and **4.5**, the model ground comprises 3 layers. Although the same mechanical characteristics were assigned to all ground layers, permeability coefficients were different for each layer as shown in **Table 4.3**. The values shown in **Table 4.2** were determined based on the assumption of typical alluvial clay. The initial conditions were fixed to the values in **Table 4.2** throughout the ground layers. The initial distribution of stress condition was determined by accounting for the self-weight under applying a slight load to the ground surface (9.81 kN/m^2). The initial water pressure distribution was set to be hydrostatic. The overconsolidation ratio was calculated based on the conditional equation that the quantities of state variables must satisfy (Noda et al., 2005a).

Table 4. 2 Material constants and initial conditions for the ground

	Clay
Elasto-plastic parameters	
Compression index $\tilde{\lambda}$	0.300
Swelling index $\tilde{\kappa}$	0.020
Critical state index M	1.60
NCL intercept N	2.51
Poisson's ratio ν	0.30
Evolution parameters	
Degradation index of overconsolidation m	5.00
Degradation index of structure a	0.80
b	1.00
c_s	0.30
Rotational hardening index b_r	0.01
Limitation of rotational hardening m_b	1.00
Soil particle density ρ_s (t/m^3)	2.754
Evolution parameters	
Specific volume v_0	3.20
Stress ratio η_0	0.375
Degree of structure $1/R^*_0$	12.0
Degree of anisotropy ζ_0	0.107

Table 4. 3 Permeability coefficient for each ground layer

Layer 1	k (cm/sec)	5.00×10^{-8}
Layer 2	k (cm/sec)	3.00×10^{-6}
Layer 3	k (cm/sec)	4.00×10^{-7}

4.3.2. Analysis results

Fig 4.6 shows the time-settlement relationships. For the exact model, the figure shows the mean amount of settlement for all ground surface nodes. The approximate model predicted essentially the

same time-settlement curve as the exact model. For comparison purposes, **Fig. 4.6** also shows the results for the case when the water pressure in the drain in the macro element method is not treated as an unknown but given as a hydrostatic pressure, using the approximate model. It is evident that treating the water pressure in the drain as an unknown results in delayed consolidation.

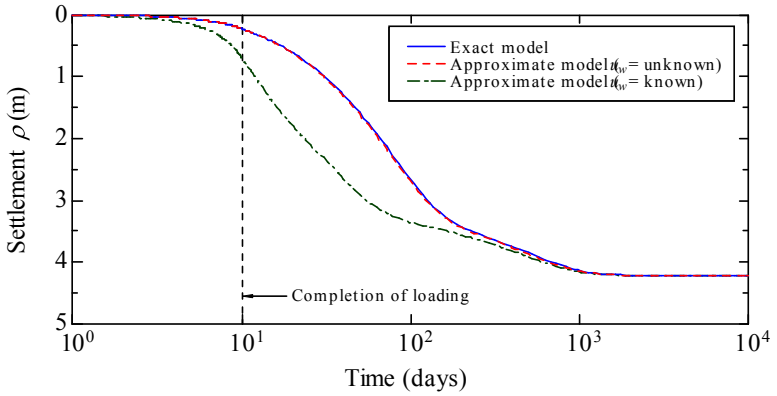

Figure 4.6 Verification of the proposed method in terms of settlement behavior

Fig. 4.7 shows the excess pore water pressure distribution in the ground and the excess water pressure distribution in the drain for both the exact and approximate models. For the exact model, the excess pore water pressure in the ground is the average value weighted by the volume for all transversely adjacent elements. Both the approximate and exact models yielded essentially the same distribution. The higher the permeability for a given ground layer, the earlier the excess pore pressure dissipated. The fact that the uneven distribution of pore water pressure in the ground shown in **Fig. 4.7** was obtained for the approximate model reflects the water absorption function of the macro element method. The same calculations based on mass-permeability concept do not result in such uneven pressure distribution because pore water pressure dissipation progresses from the area near the permeable boundary. It is also evident from **Fig. 4.7** that the excess pore water pressure in the drain is not zero. Based on this figure, it can be concluded that the delayed consolidation that occurs when the water pressure in the drain is treated as an unknown in the macro element method results from the well resistance. Naturally, the occurrence of the well-resistance phenomenon in the approximate model is a consequence of assigning a finite discharge capacity to the drain in the macro element method.

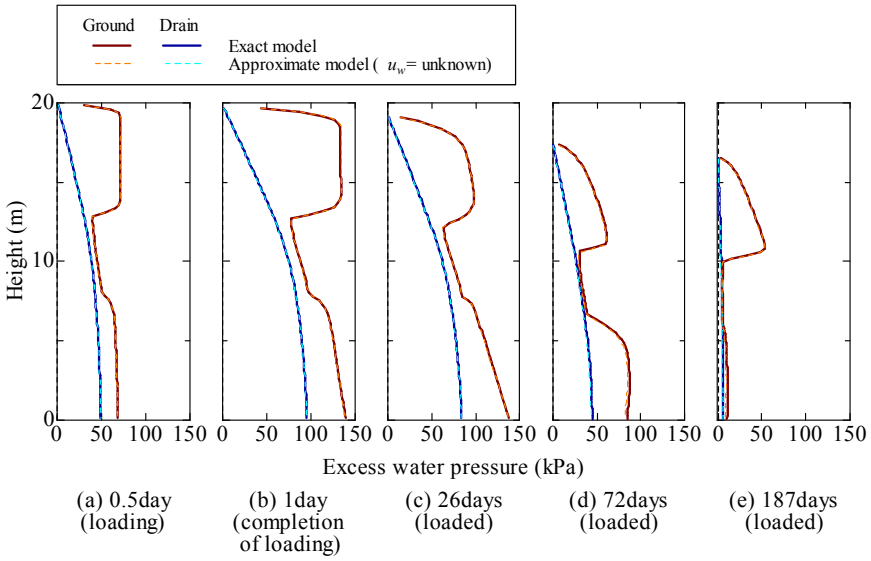

Figure 4.7 Verification of the proposed method in terms of excess pore water pressure behavior

Fig. 4.8 shows isochrones of the specific volume v , the overconsolidation ratio $1/R$, and the degree of structure $1/R^*$ for both the exact and approximate models. The values for the exact model represent the volume weighted means for each Gaussian point. At each time point, the approximate model closely approximates the mean values obtained using the exact model. Furthermore, the problem has strong material nonlinearity because the overconsolidation ratio after completion of consolidation is essentially unity (i.e., the consolidation yield stress is exceeded across all layers). In addition, geometric nonlinearity cannot be ignored in the problem because the settlement in excess of 20% of the ground thickness occurs.

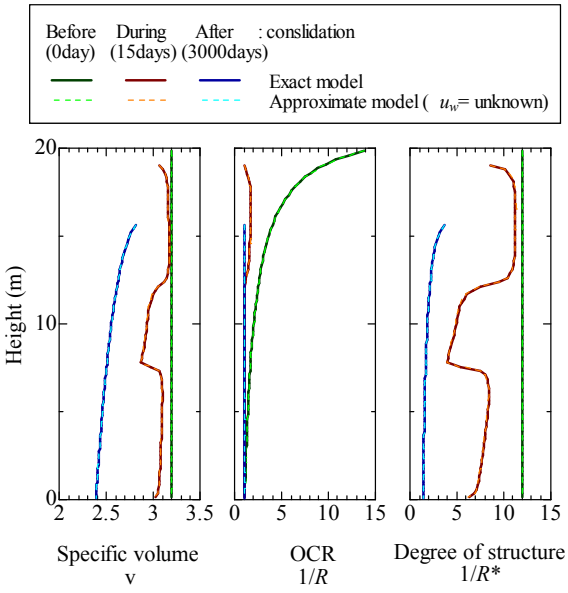

Figure 4.8 Verification of the proposed method in terms of various state variables

As explained earlier, treating the water pressure in the drain as an unknown and obtaining its value as a part of solution enables the well-resistance phenomenon to occur automatically and with high precision, even in multilayered ground. The macro element method can be applied to problems involving material as well as geometric nonlinearity and can approximate changes in the internal state variables brought about in the improved region.

4.4. Simulation of a clayey ground containing a middle sand layer improved by vacuum consolidation

When the vacuum consolidation method is applied to ground composed of soft clayey layers containing a middle sand layer, the effects of depressurization are sometimes less than expected because a large quantity of water is absorbed from the sand layer. This can be considered a type of 'well-resistance phenomenon' that occurs because water the sucking of water exceeding the discharge capacity of the drain occurs in the sand layer. Here, the proposed macro element method is applied to virtual ground and attempt to reproduce this phenomenon as well as the effects of a countermeasure against the sucking of water. Finally, mesh size sensitivity is also verified.

4.4.1. Analysis conditions

For this analysis, the same analysis code as in the previous section was used. The finite element mesh and boundary conditions are shown in **Fig. 4.9**. Assuming plane strain condition, analyses were conducted with respect to half cross section. A ground was modeled as two clay layers sandwiching a 3 m thick highly permeable sand layer. The pore water pressure at the ground surface was always set at zero (atmospheric pressure). Another sand layer was assumed to be present below clay layer 2, and, accordingly, a permeable boundary condition (constant head) was assigned to the bottom of the model. The left-hand side of the half cross section was specified as an impermeable boundary. Meanwhile, the right-hand side of the model was specified as a permeable boundary (constant head) on the assumption of connectivity of the model with the ground.

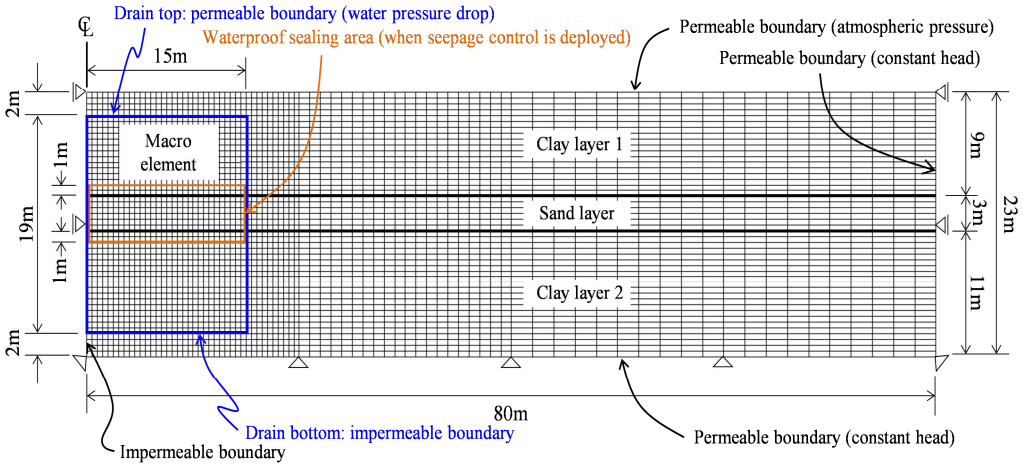

Figure 4.9 Finite element mesh and boundary conditions

The material constants and initial conditions for each layer are shown in **Table 4.4**. The clay layers 1 and 2 were assigned material constants corresponding to typical alluvial clays, and the sand layer was assigned material constants for silica sand. The initial conditions were determined in the same manner as in the previous section

Table 4. 4 Material constants and initial conditions for the ground layers

	Clay 1	Sand	Clay 2
Elasto-plastic parameters			
Compression index $\tilde{\lambda}$	0.300	0.086	0.286
Swelling index $\tilde{\kappa}$	0.020	0.003	0.024
Critical state index M	1.60	1.35	1.50
NCL intercept N	2.51	1.95	3.00
Poisson's ratio ν	0.30	0.40	0.10
Evolution parameters			
Degradation index of overconsolidation m	5.00	0.20	1.00
Degradation index of structure a	0.80	5.00	0.35
b	1.00	1.00	1.00
c_s	0.30	1.00	0.40
Rotational hardening index b_r	0.01	5.000	0.030
Limitation of rotational hardening m_b	1.00	0.55	1.00
Soil particle density ρ_s (t/m^3)	2.754	2.787	2.754
Coefficient of permeability k (cm/sec)	1.0×10^{-7}	5.0×10^{-2}	1.5×10^{-8}
Evolution parameters			
Specific volume v_0	3.27	1.84	3.60
Stress ratio η_0	0.375	0.375	0.375
Degree of structure $1/R^*_0$	9.00	1.70	12.0
Degree of anisotropy ζ_0	0.107	0.107	0.107

As a ground improvement method, vacuum consolidation method using cap-attached prefabricated vertical drains was picked up. The width of the half cross section of the improved region (in the horizontal direction) was 15 m. In the depth direction, both the ground surface and the bottom

boundary were assigned to serve as seal layers, each being 2 m from the permeable boundary. In the improved region, band-shaped drains having a width a = 0.1 m, a thickness b = 0.005 m and a permeability coefficient $\tilde{k}_w = 10^0$ cm/sec were assumed to be installed in a square pattern at a spacing d = 1.2 m. To investigate the basic effects of the vacuum consolidation method only, the water pressure was reduced by 90 kN/m^2 over a period of one day at the top of each drain, and kept constant without additional embankment loading or water pressure recovery. The macro element method was applied to the improved region. The upper and lower boundaries of the macro elements were designated as permeable and impermeable boundaries, respectively, and a desired negative pressure was imposed on the upper boundary. **Eqs. 4.16** & **4.18** were used to calculate d_e and d_w. In addition, k_w was calculated from **Eq. 4.21** in the case of treating the water pressure in the drain as an unknown. The material constants used in the macro element method are summarized in **Table 4.5**.

The above is the basic setup of the analytical model. Supplemental explanations are provided for cases where changes were made to the above conditions.

Table 4. 5 Material constants of macro element method

Equivalent diameter d_e (m)	1.35
Diameter of circular drain d_w (m)	6.56×10^{-2}
Coefficient of permeability of circular drain k_w (cm/sec)	1.42×10^{-1}

4.4.2. Effect of treating water pressure in the drain as an unknown

First, the effect of treating the water pressure in the drain as an unknown is examined. Therefore, for comparison purposes, analysis results for the case when the water pressure in the drains is given as an analysis condition are also presented. In this case, a water pressure distribution in the drains is specified to have the same gradient as the hydrostatic pressure that would yield a desired negative pressure at the top of drains.

Fig. 4.10 shows the time-settlement relationships of the surface at the center of the improved region. It can be seen that the different treatments of the water pressure in the drain result in substantially different final settlements.

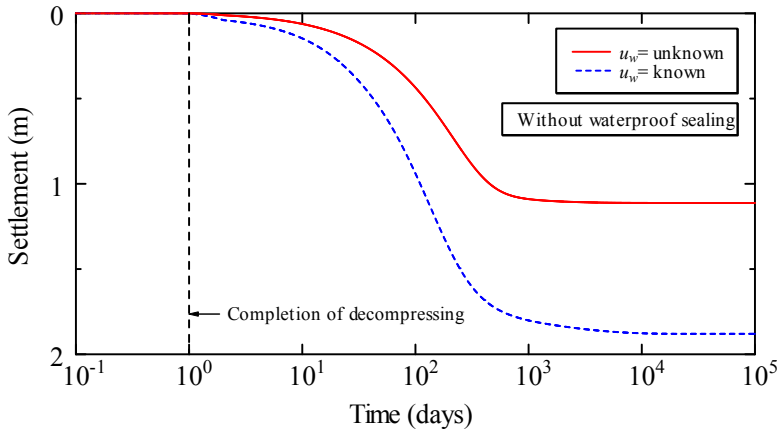

Figure 4.10 Time-settlement relationships (effect of treating the water pressure in the drain as unknown)

Figs. 4.11 and **4.12** show the distribution of the water pressure change in the ground and drain for each method. It is evident that the results differ substantially depending on the treatment of water pressure in the drain. When the water pressure in the drain is treated as an unknown (**Fig. 4.11**), the desired reduction in the water pressure in the drain and the pore water pressure in the ground does not occur. However, when the water pressure in the drains is treated as an analysis condition (**Fig. 4.12**), the pore water pressure of even the deep ground is significantly reduced, regardless of the presence of the middle sand layer because the water pressure in the drain is uniformly reduced across the entire improved region. It is this difference in depressurization that causes the obvious difference in the settlement behavior. Thus, in cases where drains suck large quantities of water from a middle sand layer, the efficacy of vacuum consolidation can be overestimated in simulations unless the water pressure in the drain is treated as an unknown.

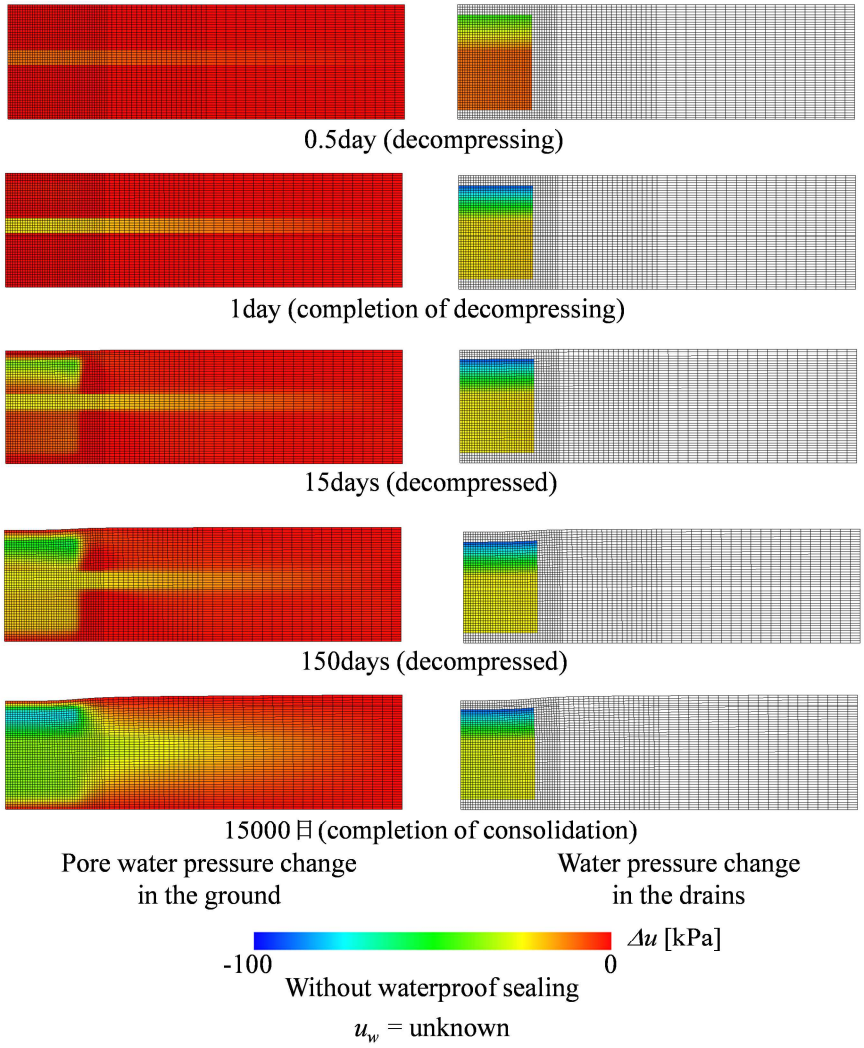

Figure 4.11 Distribution of water pressure in the ground and drain (When water pressure in the drain is treated as an unknown)

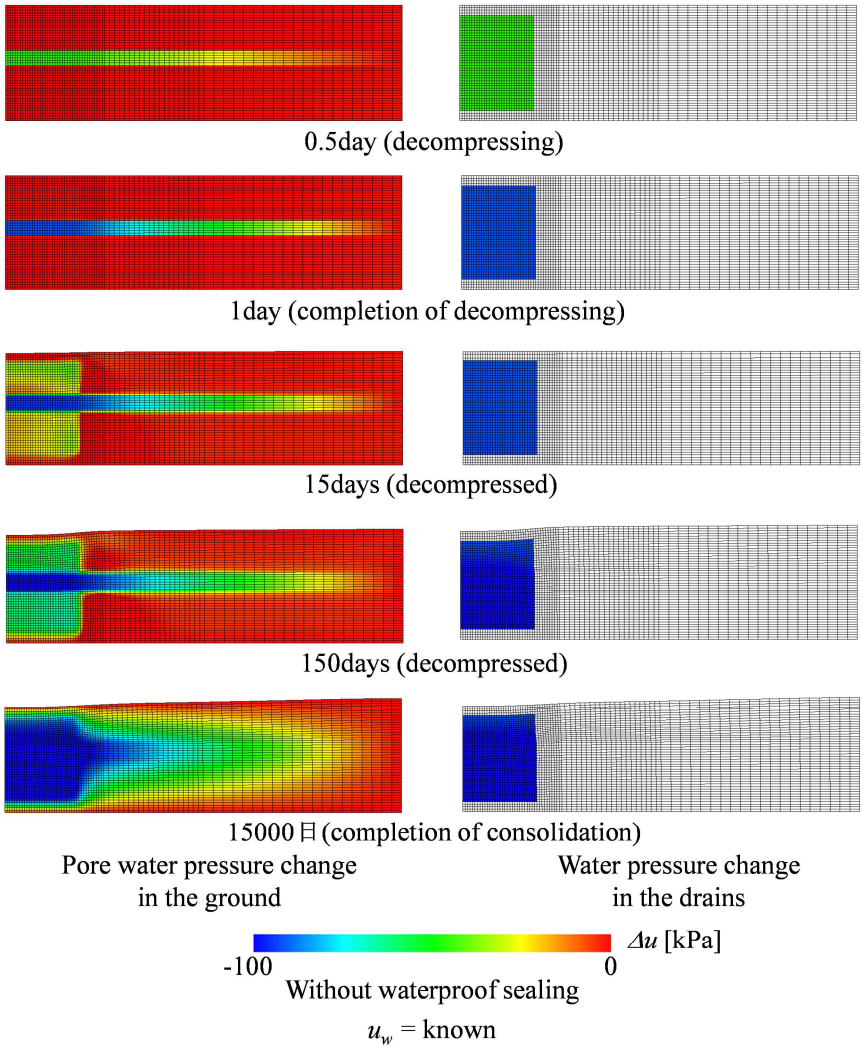

Figure 4.12 Distribution of water pressure in the ground and drain (When water pressure in the drain is assigned as analysis condition)

Hirata et al. (2010b) proposed a method in which a well resistance coefficient by Yoshikuni (1979) is added to the macro element method to simply account for the delay in consolidation resulting from well resistance. In their method, the water absorption function of the drains is reduced and a delay in consolidation occurs, by means of the addition of the well resistance coefficient to the denominator of the flow coefficient term κ in **Eq. 4.12**. One of the difficulties of this method lies in how the so-called 'drainage length' included in the well resistance coefficient is assigned. For example, when the ground contains a seal layer or a middle sand layer, as in the case of the present problem, it is difficult to determine how best to specify the drainage length. Even if there was an agreed upon way to specify the drainage length, so long as the water pressure in the drain is user-specified, the method cannot be applied to problems such as the present one that does not result in an obvious distribution for the water distribution in the drain upon completion of consolidation. Treating the water pressure in the drain as an unknown is useful for solving problems in which it is not obvious that the ground containing the drain exhibits a steady hydraulic head field. From this point onward,

only analysis results for the case in which the water pressure in the drain is treated as an unknown are presented.

4.4.3. Effect of waterproof sealing as an countermeasure for sucking from the middle sand layer

When applying the vacuum consolidation method using cap-attached prefabricated vertical drains, if the presence of a middle sand layer is known in advance, a commonly employed advance countermeasure is to wrap waterproof sealing material on the surface of drains passing through the middle sand layer. The author next investigates whether the effects of this countermeasure can be reproduced using the proposed macro element approach. As illustrated in **Fig. 4.9**, a seal is positioned so that it extends 1 m above and below the sand layer. This waterproof sealing is represented in the macro element method by assigning a value of zero to κ in **Eqs. 4.13** and **4.14**. In the manner, it is possible to eliminate only the water absorption function while preserving the discharge function of the drains.

Fig. 4.13 shows the time-settlement relationships of the ground surface at the center of the improved region. The final settlement increases by waterproof sealing to the part of the drain corresponding to the middle sand layer.

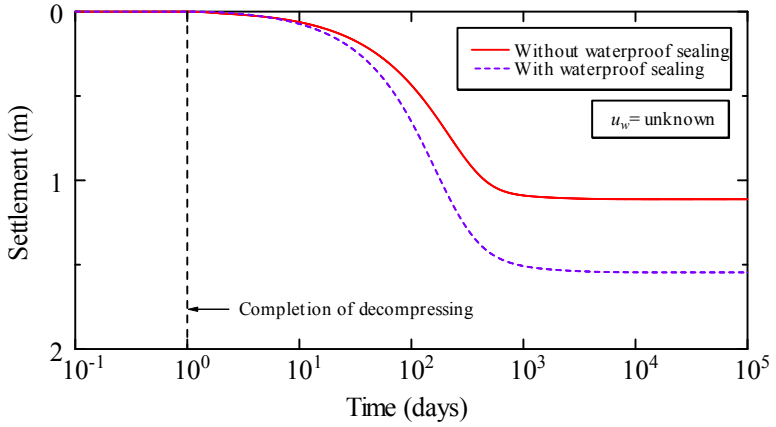

Figure 4.13 Time-settlement relationships (effect of waterproof sealing)

Fig 4.14 shows the distribution of water pressure change in the ground and drain when waterproof sealing is applied. This can be directly compared to **Fig. 4.11**, for which no waterproof sealing is applied. In the case of no waterproof sealing, a pressure reduction begins to appear in the sand layer early on, and is transmitted to the sand layer beyond the improved region. Even after depressurization is completed, the water pressure in the drain has not fallen to the desired level. Although the pore water pressure in the clayey ground gradually declines, because the water pressure in the drain does not fall to a sufficiently low level, the effect of depressurization in the clayey ground is inadequate. In contrast, as shown in **Fig. 4.14**, when waterproof sealing is applied, the early decline in water pressure

in the middle sand layer does not occur. As a result of preventing sucking of water from the middle sand layer by means of the waterproof sealing, the water pressure in the drains decrease to the designated value by the time depressurization is completed at the head of drains. The pore water pressure in the clayey ground also declines gradually, and eventually even in the deep ground, the desired depressurization effect is obtained. Furthermore, even after the passage of a substantial amount of time, the water pressure in the middle sand layer declines only negligibly even though the pore water pressure in the clay layers lying above and below it decreases. This is because water is supplied by the sand layer in the surrounding ground.

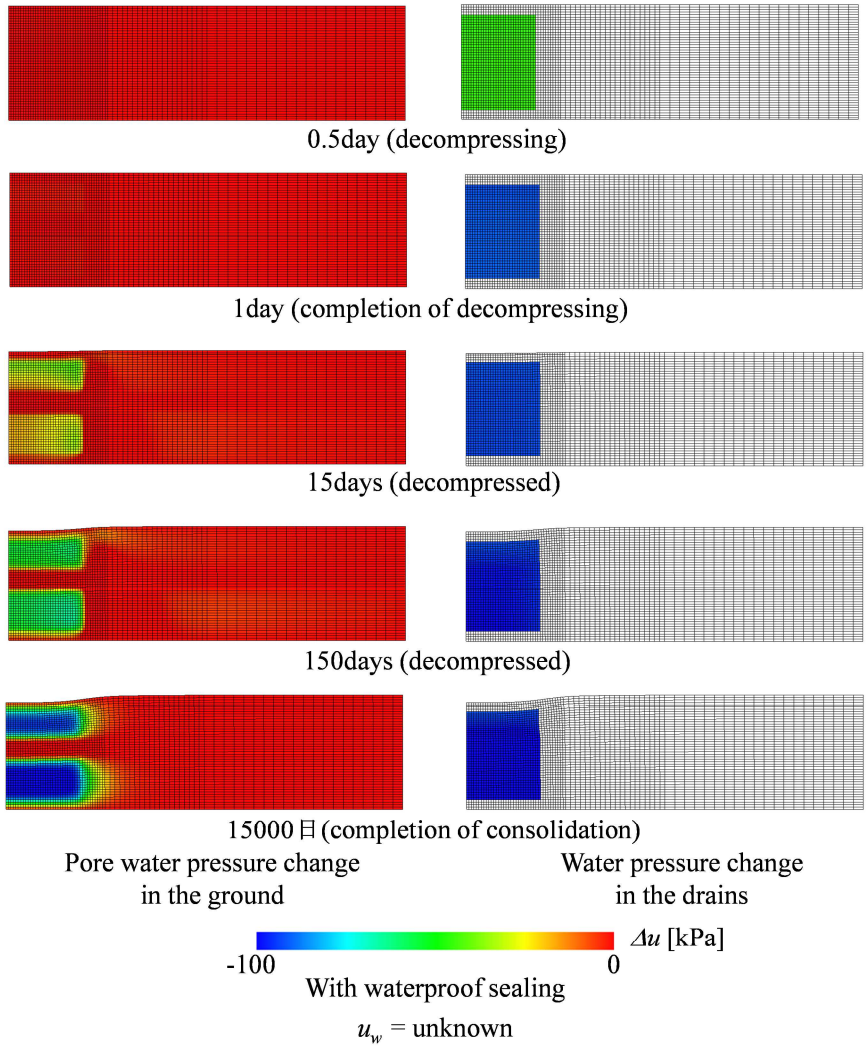

Figure 4.14 Distribution of pore water pressure change in the ground and drain (when waterproof sealing is applied)

Fig. 4.15 shows the distribution of specific volume change in the ground after consolidation has been completed. When waterproof sealing is applied, volume compression occurs even in the deep ground.

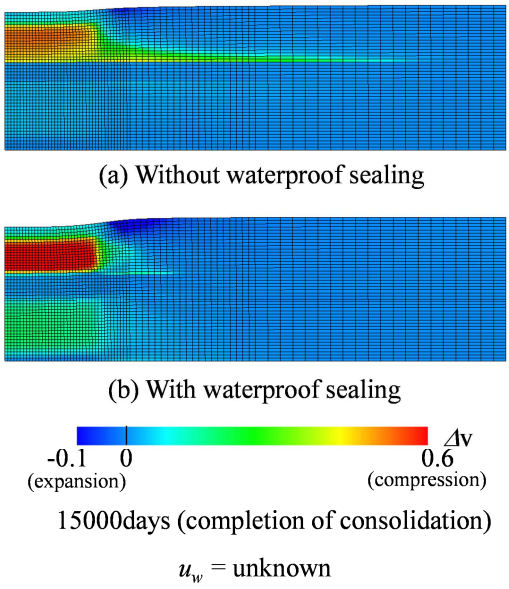

Figure 4.15 Distribution of specific volume change (effect of waterproof sealing)

Fig. 4.16 shows the lateral displacement of the ground along the right-hand edge of the improved region. It is evident that greater lateral displacement occurs when waterproof sealing is applied. If an embankment is constructed in conjunction with the vacuum consolidation method, it is expected that its effect in offsetting the lateral displacement would be even more obvious.

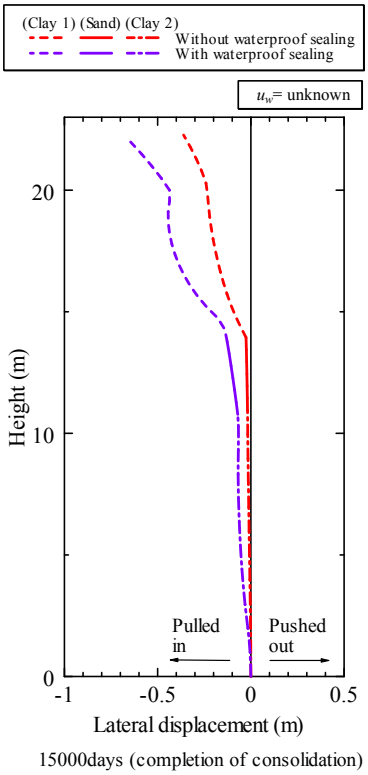

Figure 4.16 Lateral displacement

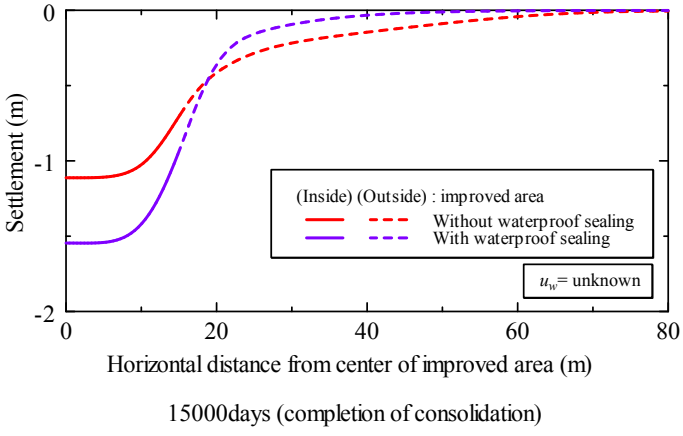

Figure 4.17 Ground surface settlement

Fig. 4.17 shows the settlement shape of the ground surface. When waterproof sealing is not applied, because the effect of depressurization extends beyond the improved region by transmission via the sand layer, the settlement also spreads in the ground surrounding the improved region. It is possible to reduce the settlement of the ground outside the improved region by applying waterproof sealing, although the settlement within the improved region increases.

4.4.4. Mesh size sensitivity

In this subsection, the sensitivity of the solutions obtained using the proposed method to the mesh size is examined. Analyses using meshes that were double and half the size of the mesh illustrated in **Fig. 4.9** were performed. The model analyzed was the same as that described in the previous section, and no waterproof sealing was applied. **Fig. 4.18** shows the time-settlement relationships of the ground surface at the center of the improved region, while **Fig. 4.19** shows the distribution of pore water pressure change after completion of consolidation. Essentially the same results were obtained regardless of the mesh size. From the standpoint of mesh division, it appears that the supplementary conditions for the macro element method suggested by Sekiguchi et al. (1986, 1988) can be removed. Furthermore, in order to appropriately reproduce the effect of a middle sand layer on the vacuum consolidation method, it is necessary to allow for the movement of pore water between transversely adjacent macro elements.

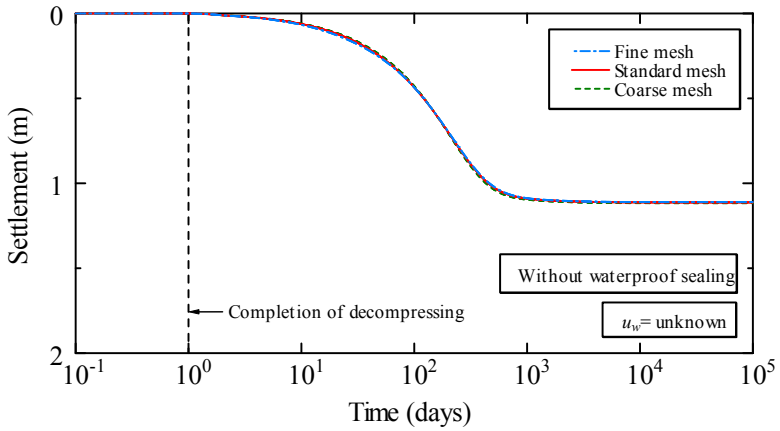

Figure 4.18 Mesh size sensitivity on change of settlement with time

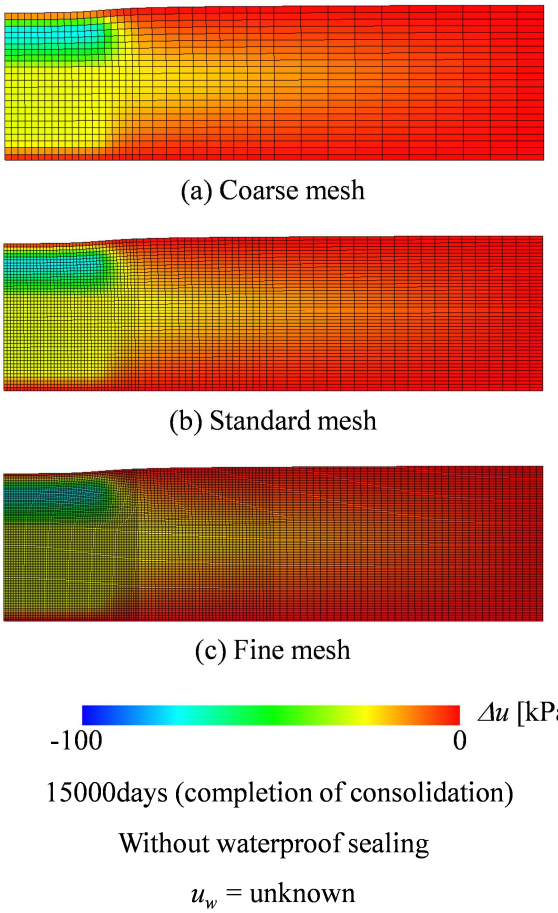

Figure 4.19 Distribution of pore water pressure change (mesh size sensitivity)

4.5. Study on conversion methods of equivalent diameter of band-shaped vertical drain and influences on well resistant phenomenon

In consolidation analysis of soil with vertical drains based on a solution by Barron (1948), band-shaped drain needs to be converted into columnar drain. Hansbo (1979) and Rixner et al.(1986) proposed converstion equations of the equivalent diameter (d_w) as **Eqs. 4.18** and **4.20**, respetively, and these methods have been widely used in practical design. This chapter also sugessted a new estimation method of equivalent diameter based on assumption that the cross-sectinonal area of drain is equal (**Eq. 4.19**). This section numerically compares results of 3D analysis with drainage element and 2D plane strain with macro element to investigat the effects of conversion methods of d_w in addition to vertical drain well resistant phenomenon depending on thickness of band-shaped drain based on the new proposed macro element.

4.5.1. Conversion methods of equivalent diameter of band-shaped vertical drain

A 20m-thick ground that simililar to the section 4.3 but single layer under single drainage condition in which a band-shape drain with typical dimension (width a=100mm, thickness b=4mm) is installed down to the bottom at spacing d=1m in squared pattern was modelled. The permeability

coefficient of ground and vertical drain are k=1.0×10^{-7}cm/s, $\tilde{k}_w$ =5.0×10^{-2}cm/s, respectively. The loading condition and material constants are exactly same as those on section 4.3 previously.

The finite element mesh and boundary conditions for 3D model (exact model) and macro 2D plane-strain model (approximate model) are shown in **Fig. 4.20** and **4.21**, respectively. The former discretized the drain and surrounding ground into a finite mesh with higher coefficient assigned to the elements corresponding to the vertical drain than to the elements representing ground. The latter employed the new macro elements for representing virtually the effect of vertical drain, and created a square finite element mesh because the analytical domain in horizontal direction does not influence to results, which is one of advantage of the new macro element method.

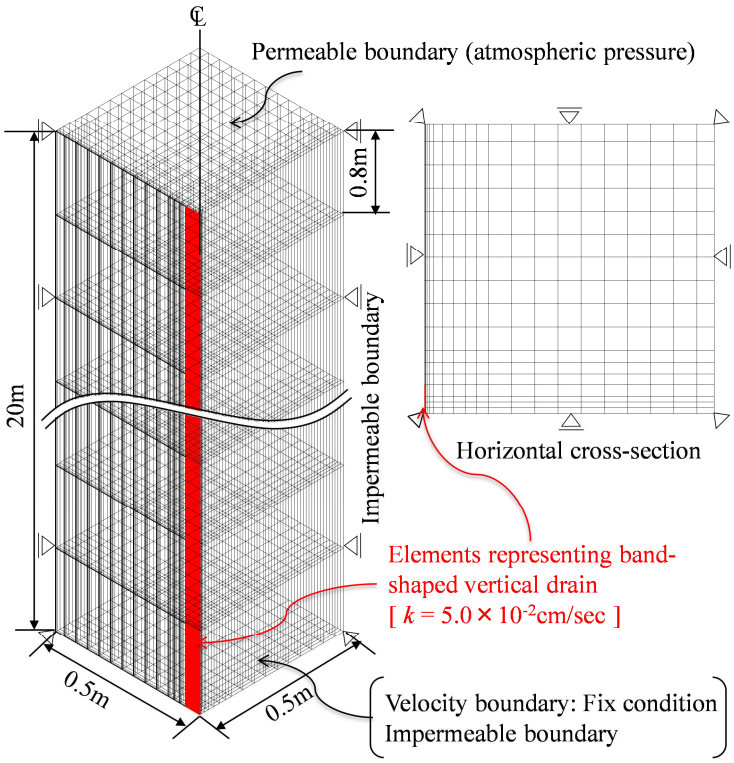

Figure 4.20 Finite element mesh and boundary conditions (exact model, scale Hor.:Ver. = 1:3)

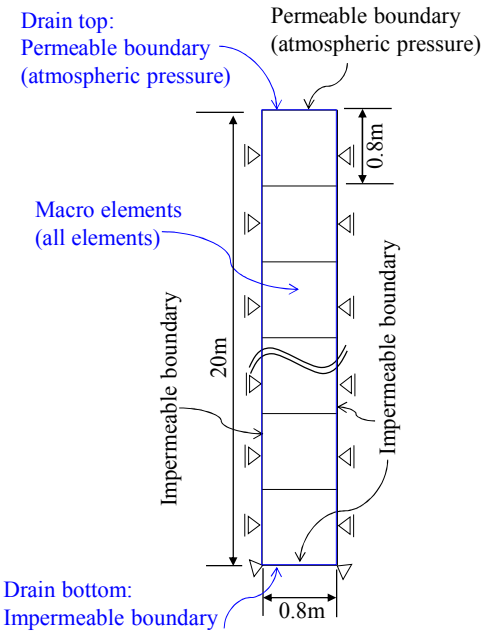

Figure 4.21 Finite element mesh and boundary conditions (approximate model)

In these analyses, the influence of condition of equal drainage capacity before and after converting d_w based on **Eq. 4.21** was investigated by carrying out two case studies. Case a does not apply **Eq. 4.21**, and case b contrary applies that permeability coefficient conversion as tabulated in **Table 4.6**.

Table 4. 6 Case studies on conversion method of d_w

		Permeability coefficient of drain k_w (cm/s)	
Conversion methods of d_w	d_w (m)	Case a (Not using **Eq. 4.21**)	Case b (Using **Eq. 4.21**)
(1) Equal circumference (**Eq. 4.18**)	0.0662	5.0×10^{-2}	5.80×10^{-3}
(2) Average thickness and width (**Eq. 4.20**)	0.0520	($k_w=\tilde{k}_w$)	9.42×10^{-3}
(3) Equal cross-section area **(Eq. 4.19)**	0.0226		5.0×10^{-2}

The numerical calculation results from cases and b that consisted of settlement-time curves and isochrones of pore water pressure in the ground as well as water pressure within vertical drain during consolidation process (at 100 days from the initial state) area shown in **Figs. 4.22a & b**, respectively. In case a, although there is slightly delayed consolidation in settlement curve, converting d_w by assuming equal cross-sectional area of drain in approximate model predicted essentially the closest settlement-time curve and distribution of water pressure to the exact 3D model. Meanwhile conversion of d_w using **Eqs. 4.18** and **4.20** show the similar results to each other, and those are faster consolidation than that of the exact model in 3D condition; this means that over-estimation could be given due to less well resistant effects. In an opposing manner, case b does not result significant

differences in calculation results from the 2D plane-strain approximate model not only among method of conversion d_w but also with 3D exact model, as the demonstrated in **Fig. 4.22b**. When utilizing the condition of constant discharge capacity given to a single drain through cross-sectional area of the influenced region (**Eq. 4.21**), careful attention on the method to convert d_w is generally unnecessary. However, the conversion methods proposed by Rixner et al. (1986), and Hansbo (1979) can achieve results as good as the exact model in 3D condition.

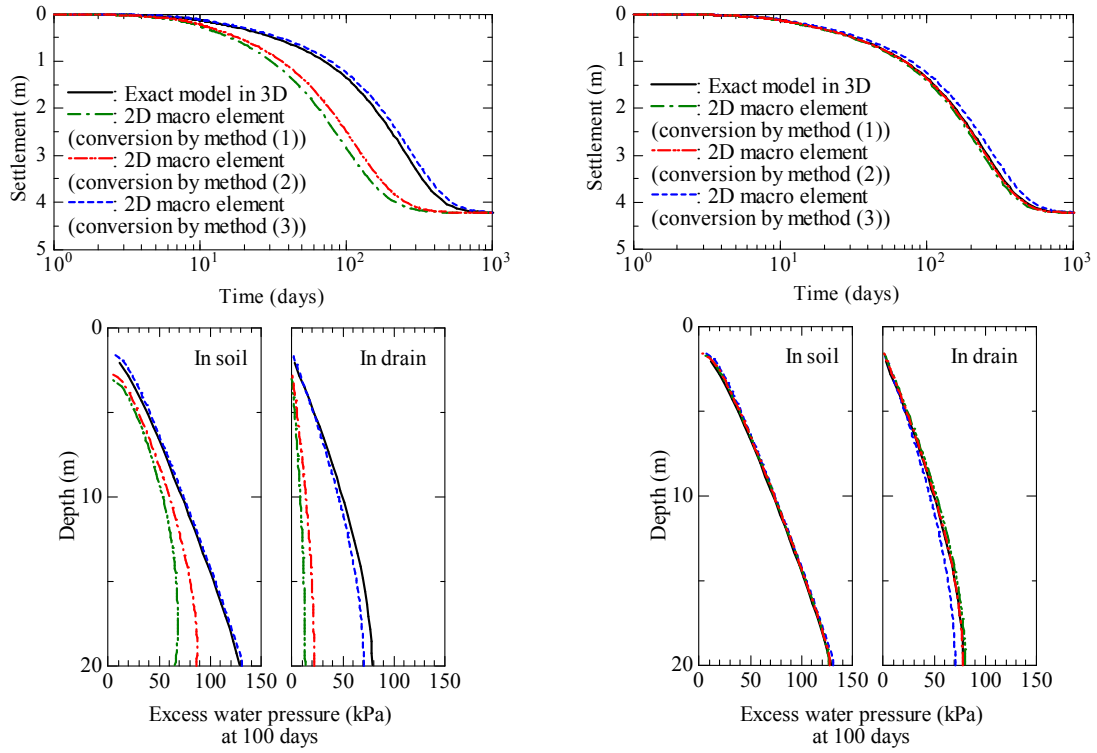

(a) Case a (not convert k_w by **Eq. 4.21**) (b) Case b (convert k_w by **Eq. 4.21**)

Figure 4.22 Settlement curves and water pressure

4.5.2. Well resistant phenomenon of band-shaped vertical drain

As mentioned in section 4.2.6, one of the main advantages of the new proposed macro element method is that FEM mesh division width is independent on spacing and thickness of vertical drain. That means it is able to investigate the effects of thickness of band-shaped drain using the same FEM mesh and boundary condition in 2D plane strain shown in **Fig. 4.21** in this section. The width of band-shaped drain is a=100mm and thickness are b=2mm, 4mm, and 8mm respectively.

Table 4.7 presents the case studies, in which cases 2 and 3 have smaller permeability coefficient of vertical drain than that of case 1; that is the condition of occurrence of well resistant phenomenon. In addition, whereas cases 1 and 2 do not convert permeability of vertical drain based on **Eq. 4.21**, this equation is applied for case 3. In case 3, using conversion method (1) and (2) for equivalent diameter of band-shaped drain, the permeability coefficients reduce, but use method (3) to convert this equivalent diameter, the permeability coefficient of vertical drain does not change between before

and after conversion, that is because the discharge condition in **Eq. 4.21**. Therefore, converting equivalent diameter of vertical drain (d_w) by methods (1) and (2), the effect of well resistance in case 3 is more than that of case 2.

Table 4. 7 Analysis cases

					Case 1		Case 2		Case 3	
Permeability coefficient of drain k_w					Large ($\tilde{k}_w = 1.0\times10^{2}$ cm/s)		Small ($\tilde{k}_w = 5.0\times10^{-2}$ cm/s)		Small ($\tilde{k}_w = 5.0\times10^{-2}$ cm/s)	
Conversion of k_w (**Eq. 4.21**)					No		No		Yes	
Conversion d_w	b (mm)	Legend	d_w (m)	$F(n)$	k_w (cm/s)	k_w/n^2 (cm/s)	k_w (cm/s)	k_w/n^2 (cm/s)	k_w (cm/s)	k_w/n^2 (cm/s)
(1) Equal circumference (**Eq. 4.18**)	2	———	0.0649	2.12	1.0×10^{2} ($\tilde{k}_w = k_w$)	3.30×10^{-1}	5.0×10^{-2} ($\tilde{k}_w = k_w$)	1.65×10^{-4}	3.02×10^{-3}	9.97×10^{-6}
	4	———	0.0662	2.10		3.44×10^{-1}		1.72×10^{-4}	5.80×10^{-3}	1.99×10^{-5}
	8	———	0.0688	2.06		3.71×10^{-1}		1.85×10^{-4}	1.08×10^{-2}	3.99×10^{-5}
(2) Average thickness and width (**Eq. 4.20**)	2	– · –	0.0510	2.35		2.04×10^{-1}		1.02×10^{-4}	4.90×10^{-3}	9.97×10^{-6}
	4	– · –	0.0520	2.34		2.12×10^{-1}		1.06×10^{-4}	9.42×10^{-3}	1.99×10^{-5}
	8	– · –	0.0540	2.30		2.28×10^{-1}		1.14×10^{-4}	1.75×10^{-2}	3.99×10^{-5}
(3) Equal cross-section area (**Eq. 4.19**)	2	– – –	0.0160	3.51		1.99×10^{-2}		9.97×10^{-6}	5.0×10^{-2}	9.97×10^{-6}
	4	– – –	0.0226	3.17		3.99×10^{-2}		1.99×10^{-5}		1.99×10^{-5}
	8	– – –	0.0319	2.82		7.98×10^{-2}		3.99×10^{-5}		3.99×10^{-5}

Fig. 4.24 illustrates the analyzed results that include the settlement-time curves and isochrones of water pressure inside vertical drain as well as pore water pressure in the ground at certain time of loading (100 days from the initiation of loading). It is obviously that the conversion methods of equivalent diameter d_w affect to the consolidation behavior without depending on the presence or absence of well resistant phenomenon, or utilize **Eq. 4.21** for converting k_w or not. In general, the values of d_w corresponding each conversion method are in the order (3)<(2)<(1), if equivalent soil cylinder (d_e) is constant, by **Eq. 4.9** the corresponding values of $F(n)$ is (3)>(2)>(1), results in absorption function parameters κ (**Eq. 4.12**) becomes the order of (3)<(2)<(1), therefore the consolidation rate is (3)<(2)<(1) depending on conversion method of d_w. Additionally, if the coefficient of permeability k_w has been kept constant after conversion of d_w (cases 1 and 2), from Eq. 4.15 the ratio k_w/n^2 is (3)<(2)<(1), result in the drainage function presenting by β_j also becomes (3)<(2)<(1). But, as shown in **Fig. 4.24a**, the effects of conversion method of d_w on consolidation behavior is quite small in case 1, because the difference due to discharge function does not appear when the well resistance does not occur. By the way of addition, the thickness of drain b is not sensitivity to d_w in the conversion methods (1) and (2). Because of this, even though the thickness is double there are very small differences in results between them in case 2 which is without conversion of k_w. On the other hand, in case 3 which is with conversion of k_w, the well resistance occurs and the effect of the drain thickness on consolidation behaviors appears remarkably when using conversion methods (1) and (2). Besides that, applying conversion to k_w, the drainage function parameters β_j are the same among conversion methods (1), (2), and (3) for one vertical drain thickness, so that the same degree of well resistance occurs regardless to the conversion methods of d_w. Because of this, the effect of band-shaped drain thickness b on consolidation rate has appeared well as irrespective to the

conversion of d_w in case 3, while the well resistant effects could be overlooked in case 2 when coefficient of permeability did not applied.

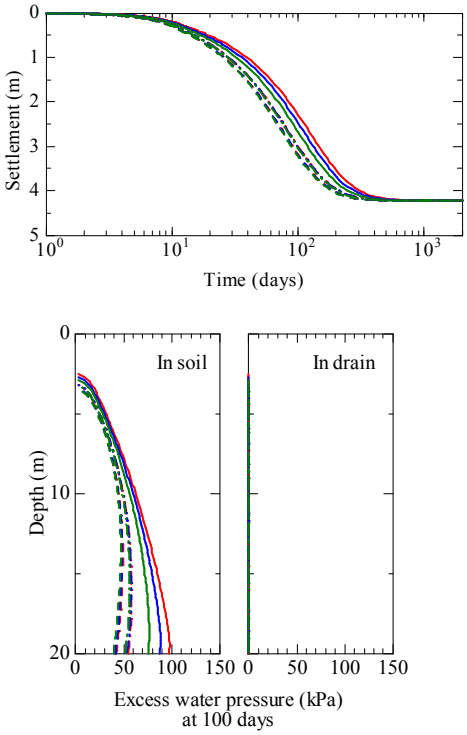

(a) Case 1 (Large and no convert k_w)

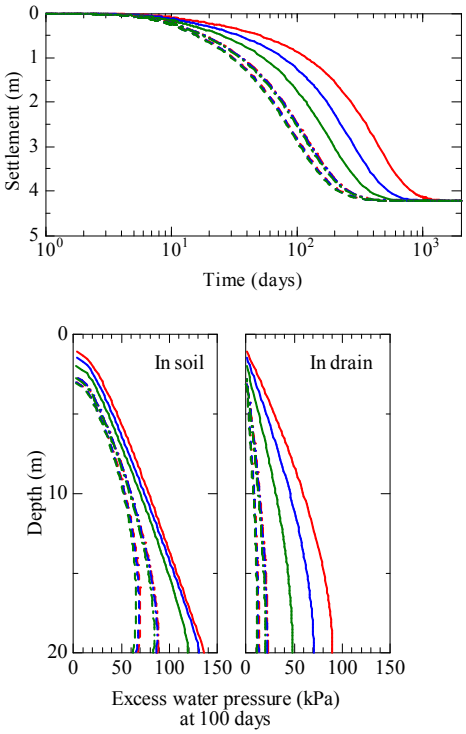

(b) Case 2 (Small and no convert k_w)

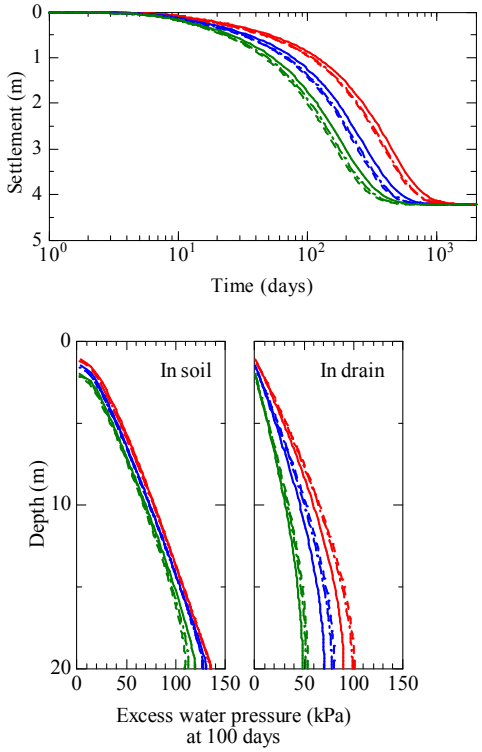

(c) Case 3 (Small and convert k_w)

Figure 4.23 Calculation results (see legend in Table 1)

4.6. Brief summary

This *Chapter* attempted to newly extend the capabilities of macro element method for vertical drains. Specifically, by treating the water pressure in the drain as an unknown and adding a continuity equation for the drains to the governing equations, a discharge function of the drains was newly added while retaining the water absorption function of the drains contained in previous versions of the macro element method. After applying the proposed macro element method to a quasi-static soil-water coupled elasto-plastic finite element method based on finite deformation theory, the basic performance and approximation accuracy of the extended method were verified. In addition, numerical analyses on the application of the vacuum consolidation method to clayey ground containing a middle sand layer were performed. The findings obtained in this *Chapter* are summarized as follows:

1) The results of analyses using the proposed method showed that the well-resistance phenomenon occurs automatically, depending on the analytical conditions. In addition, the proposed method is capable of highly accurate approximation in problems involving material and/or geometrical nonlinearity and multilayered ground.
2) It is known that inadequate depressurization and settlement of surrounding ground can occur when vacuum consolidation is applied to clayey ground containing a middle sand layer. Analysis based on the proposed approach is capable of reproducing the phenomena adequately.
3) As an advance countermeasure to middle sand layers, waterproof sealing material is often wrapped to the surface of drains passing through the parts. The effects of such countermeasures can be appropriately reproduced using the proposed approach.
4) Following the formulation used in this paper makes it unnecessary to perform mesh division width to match the drain arrangement and spacing. Furthermore, the proposed approach yields solutions that are insensitive to the mesh size.
5) The study on modelling of band-shaped vertical drain indicates that the new proposed macro element method could be able to simulate ground behaviors including settlement and water pressure without depending on the conversion method of equivalent diameter if the permeability coefficient of drain was also converted by equalizing the discharge capacity of vertical drain before and after conversion.

Finally, comparison the simulation results with those of actual measurements will be presented in next *Chapter*. After applying the proposed approach to analytical methods for dealing with inertial forces, the stability problems and pore-pressure dissipation methods as a countermeasure to liquefaction has been investigated (Noda et al., 2015).

Chapter 5

Evaluation of improvement effects by vertical drains/vacuum consolidation on peaty ground under embankment loading based on the newly proposed macro element method

5.1. Introduction

When embankments are constructed on soft ground, slip failure during embankment loading or substantial residual settlement can occur after the entry into service. Such large-scale deformation can have a long-term and widespread impact on the surrounding ground.

To date, the members of Geotechnical laboratory in Nagoya University have simulated the mechanical behavior of a wide range of soft soils from naturally deposited clay to high water content peat using the same theoretical framework as for other soil materials such as sand and intermediate soil, namely the elasto-plastic constitutive SYS Cam-clay model based on the soil skeleton structure concept (Asaoka et al., 2002). In addition, they have simulated and predicted long-term settlement and also identified the determinants of and proposed countermeasures to phenomena including slip failure and residual settlement related to the construction of embankments on soft ground using soil-water coupled finite deformation analysis (Noda et al., 2005b; Takaine et al., 2010; Tashiro et al., 2011, 2015). The series of research has yielded the following insights: (1) slip failure and long-term settlement occur in ground comprising of soft soils that possess low-permeability and can easily cause rapid plastic compression with softening when subjected to loads exceeding their consolidation yield stress (i.e., in terms of the SYS Cam-clay model, highly structured soils that undergo rapid structural degradation); (2) when loading ground containing such soft soil with loads exceeding its consolidation yield stress, the implementation of appropriate pre-countermeasures such as ground improvement or slow banking is effective in reducing total costs, including maintenance and management costs, over the entirety of the embankment lifecycle; and (3) ground improvement by installing vertical drains is an effective pre-countermeasure to increase ground stability and to reduce residual settlement.

In recent years, vacuum consolidation has come to be widely applied in combination with vertical drains in cases when embankments have to be loaded quickly to shorten construction period or when ultra-soft soils such as peat or reclaimed clay exist near the ground surface (Cognon et al., 1994; Bergado et al., 1998; Chai et al., 2005, 2006, 2008; Rujikiatkamjorn et al., 2007; Ariyarathna et al., 2010; Mersi and Khan, 2012; Karunawardena and Toki, 2013; Osorio et al., 2010; Kosaka et al., 2011). A remarkable feature of vacuum consolidation is the inward deformation (towards the center of the improved area) resulting from the application of negative excess pore water pressure. It is expected that, in addition to strengthening through preloading, this deformation will contribute to increased stability by offsetting the outward deformation that occurs during embankment loading. At

the same time, depending on the ground condition, this deformation can affect a large area of the surrounding ground. For this reason, it is necessary to accurately model the pertinent aspects of the construction method and, based on predictions of ground behaviors that are likely to occur, to set appropriate construction conditions including drain spacing, improvement area, and the duration of vacuum loading, etc.

In the practical design of vacuum consolidation, the reduction in pore water pressure due to vacuum loading is often replaced by an equivalent surcharge load, which enables the use of the simple, one-dimensional consolidation calculation based on the solution by Barron (1948). However, in order to account for the inward deformation characteristic of vacuum consolidation, it is desirable to perform finite element analysis in multiple dimensions. In multiple-dimensional finite element analysis, directly simulating the vertical drain by employing a fine mesh (Indraratna et al., 2004, 2005; Saowapakpiboon et al., 2011) requires a considerable number of elements. For this reason, a macroscopic method is needed to describe the improved effect depending on drain spacing and permeability.

The most common macroscopic method to represent the effect of vertical drains is the mass-permeability method (Asaoka et al., 1995) whereby permeability of the ground including vertical drains is expressed in an inverse analysis as a mass property. In contrast, the macro-element method proposed by Sekiguchi el al. (1986) allows the effect of a vertical drain to be accounted for even under two-dimensional plane strain conditions by adding a water absorption function of the drain to each element in the improved area. Endeavoring to further extend the function of the macro-element method, a new proposal of macro-element method is previously discussed in *Chapter 4* and Yamada et al. (2015), in that proposal water absorption and discharge functions of the drain by treating the water pressure in the drain as an unknown and adding a continuity equation for the drain to the governing equations and implemented this method (Noda et al., 2015) in the ***GEOASIA*** soil-water coupled finite deformation analysis code (Asaoka & Noda, 2007; Noda et al., 2008a) capable of accounting for inertial forces (see **Appendix A2**). The accuracy of the proposed macro element method was verified by comparing the simulation results with those by "exact model" in which a drain is directly modelled by finite element meshes with higher permeability. In addition, the proposed analysis method was applied to simulate vacuum consolidation on a virtual ground with clay and sand. This method resulted in natural reproduction of the well-resistance phenomenon under specific conditions by solving the water pressure in the drain. Additionally, an advantage of this proposed method macro element method is that the mesh width does not have to matched to the drain spacing; i.e., the total number of finite elements could be remarkably reduced and the effects of drain spacing could be evaluated using the same mesh.

The first objective of this *Chapter* was to validate the ability of the proposed method to accurately simulate "actual" behavior observed at section B in Mukasa area. Simulation results were compared with actual measurements for the loading of a soft peat ground improved with vertical drains and vacuum consolidation. After simulating the construction history, permeability of the drain was sought

as the single fitting parameter to reproduce the observed ground settlement. As a result, it was found that the proposed method was able to comprehensively and closely reproduce the ground behavior including deformation of the surrounding ground and pore water pressure distribution in the ground profile. In addition, at the actual embankment site, widespread settlement of the area surrounding the test embankment was observed following vacuum loading. It was believed this settlement could be attributed to the existence of a middle sand layer spanning the entire improvement area. In fact, the ground at this section had been experienced an embankment loading of approximate 3.0 m for 6 years before installation of vertical drains remarked as the first embankment in this study. Due to this pre-loading the stiffness of the shallow soft clay and peat increased probably. As such, in this *Chapter*, the effects of a middle sand layer in vacuum consolidation in addition to evaluation of effective countermeasures were also analyzed using proposed method. Through the comparison with the conventional macroscopic method such as the mass-permeability method and the macro element method that treats the water pressure in the drains as a known, the superiority of the proposed method to simulate the multi-layered ground especially in case of including middle sand layer was shown. Additionally, the further calculation carried out on same ground condition to analyze the effect of loading history.

The second objective of this *Chapter* was to investigate numerically the effects of vertical drains and vacuum consolidation when embankment loading on a soft ground, focusing particularly on the influence of drain spacing. In this case, a softer ground than that of the actual embankment site with alternating peat and clay layers up to the ground surface was modeled to represent typical ground to which vacuum consolidation would be applied. As a result of calculations by above-verified propose method, it was found that, although vacuum consolidation is effective in cases where there is a need to limit deformation of the surrounding ground, vertical drains alone can reduce residual settlement to the same degree as vacuum consolidation, provided that the drain spacing is appropriately reduced.

Furthermore, the content of this *Chapter* will be published on Nguyen et al. (2015).

5.2. Validation of the accuracy of the proposed method based on simulating an actual embankment loading

5.2.1. Overview of the ground being modelled

In order to validate the ability of the proposed method to accurately simulate actual ground behavior, in this *Chapter*, an actual soft peat ground improved with vertical drains and vacuum consolidation was simulated. **Fig. 2.9** shows a cross-section of ground in the Mukasa area (construction started in 2005; road put into service in 2014) of the Maizuru-Wakasa Expressway that was modeled. As description in *Chapter 2*, the ground in this area comprises thick deposits of peat and clay and represents an ultra-soft ground that is rare even in Japan. A test embankment (left side or section A of **Fig. 2.9**) was constructed on the site in 2006 in order to identify countermeasures to potential problems associated with embankment loading on soft ground. In the case of this test embankment, massive settlement exceeding 11 m occurred, which also had a substantial effect on the

surrounding ground. In *Chapter 3*, using the analysis code ***GEOASIA*** with the mass-permeability method, the authors performed numerical analysis to describe the elasto-plastic behavior of peat, reproduce and predict the large-scale settlement up to that point and in the future, and also to propose countermeasures to prevent settlement. In this *Chapter*, simulations were conducted for the peat ground underlying an embankment located approximately 300 m from the Tsuruga side of the test embankment (right side or section B of **Fig. 2.9**) that was subjected to vacuum consolidation in conjunction with vertical drains in January of 2012 in order to reduce construction time.

The massive settlement in excess of 11 m occurred because the test embankment loading created a stress state that substantially exceeded the consolidation yield stress of these deep peat layers. Based on the results of the numerical analysis in Tashiro et al. (2015), it is predicted that residual settlement on the order of 1.5 m will continue over the next 60 or so years. However, it was confirmed in *Chapter 2* by investigation data analysis is only minimally affected by the artesian conditions in this section B and, therefore, that the deep peat layers possess sufficiently large consolidation yield stress. In addition, it was confirmed that alternating clay and sand layers exist in the middle of the ground profile. Considering the points above, *Chapter 2* concluded that, although there may be problems associated with the stability and settlement of the shallow ground layers, there is little possibility that the target embankment above peaty ground in section B simulated in this study will undergo the same kind of large-scale delayed settlement as the test embankment.

5.2.2. Analysis conditions

The cross-section of the ground profile and the finite element mesh and the boundary conditions used in the analysis are shown in **Figs. 5.1** and **5.2**. Although the thickness of the layers in the actual profile were observed to differ slightly from left to right, given that the settlement amount and pore water pressure were only measured near the center of the embankment, for simplicity, the ground directly under the center of the embankment was modelled and all the layers were assumed to be horizontally stratified. The loading history for the center of the embankment was reproduced as faithfully as possible. In the actual embankment, a vacuum consolidation method with airtight sheet (Association of Vacuum Consolidation Technology, 2013) was utilized to reduce construction time. Plastic board drains (PBD) with a width of 100 mm and thickness of 7 mm were installed to a depth of 20 m in a square pattern with a drain spacing of 0.7 m. One month after the start of vacuum loading at approximately 60 kPa, the embankment was built up at a rate of embankment thickness 8 cm/day to a total height of 8 m. Vacuum loading was stopped approximately 2 months thereafter. In the analysis, the embankment and underlying ground were assumed to be fully saturated, and embankment loading was simulated by adding elasto-plastic elements on top of the ground elements (Takaine et al., 2010). To simulate the ground improvement due to vertical drains, the macro-element method was applied to elements corresponding to the drain-improved area. The diameter of equivalent soil cylinder d_e and the equivalent diameter of drain d_w were both converted based on cross-sectional area. The vacuum consolidation was simulated by assigning a permeable boundary condition that reduces water pressure

to the boundary corresponding to inside (the ground side to which the macro-element method is applied) of the airtight sheet (green line in **Fig. 5.2**) and assigning an impermeable boundary to the outside of the sheet (embankment side).

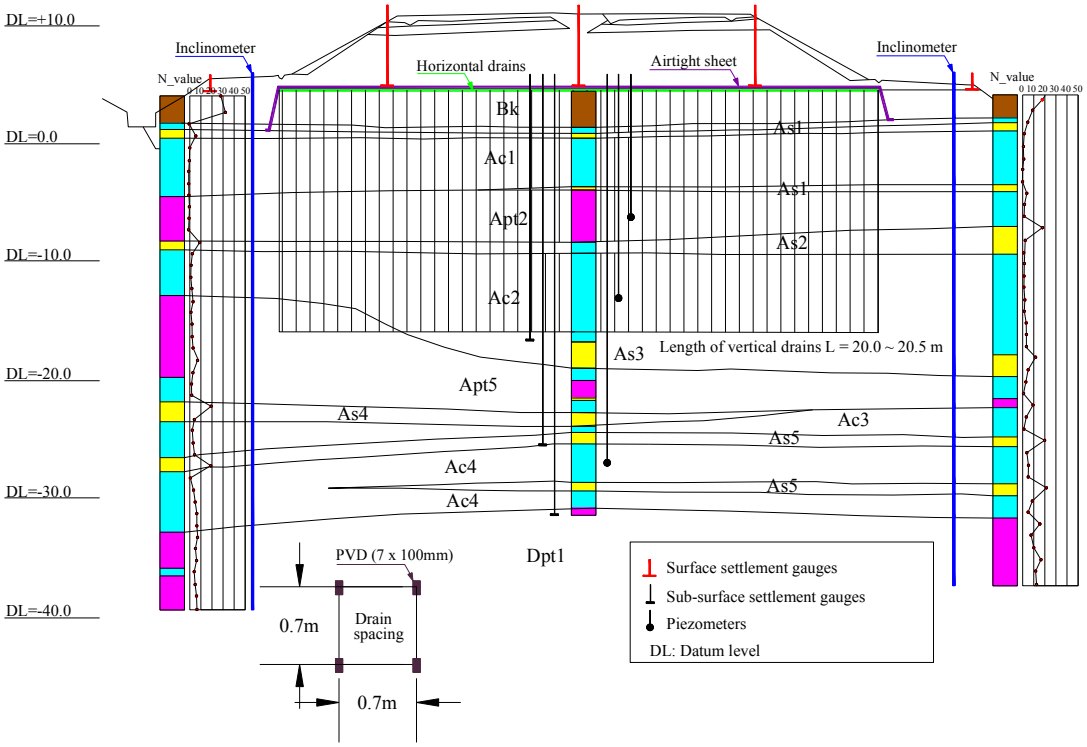

Figure 5.1 Soil profile and measurement points (cross-section)

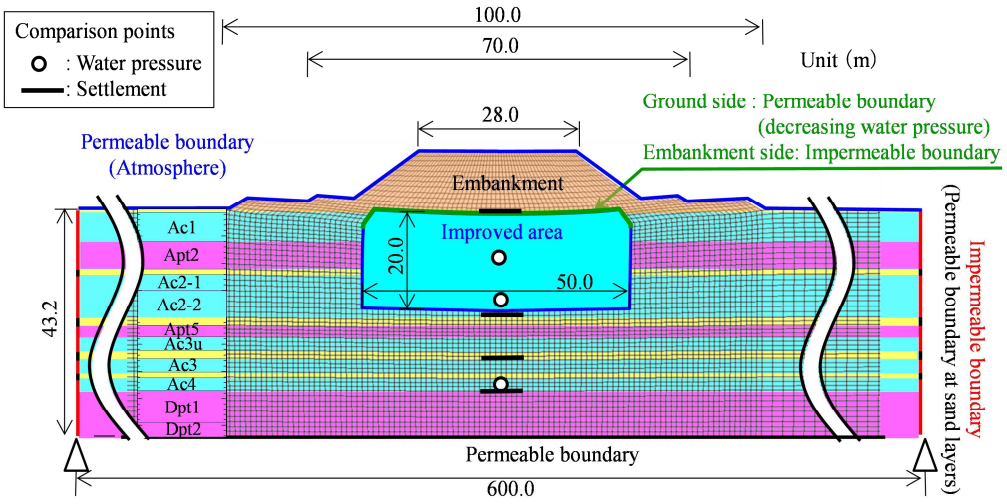

Figure 5.2 Finite element mesh and boundary conditions (after construction of main embankment)

In *Chapter 2*, the material constants and initial conditions of the ground were determined based on laboratory experiments conducted on samples collected from the in-situ by simulation using SYS

Cam-clay model. Material constants are shown in **Table 2.7**, and the distribution of estimated initial conditions is presented in **Fig. 2.19** in *Chapter 2*. For simplicity, it was assumed that the permeability coefficient k for each ground layer to be isotropic and logarithmically related to the void ratio e in the manner expressed in the same **Eq. 3.1** in *Chapter 3* that simulated ground deformation induced by test embankment. As shown in **Table 5.1**, coefficient of permeability change C_k, initial coefficient of permeability k_0, and initial void ratio e_0 were determined based on the results of consolidation tests on undisturbed samples (Taylor, 1948).

In this analysis, after setting all other ground parameters, the permeability coefficient of the drain k_w was utilized as the lone fitting parameter. Based on specifications for PBD (Association of Vacuum Consolidation Technology, 2013), the value of k_w resulting in the best fit to the observed settlement at the center of the embankment was sought from within the range of 1.0×10^{-2} to 1.0×10^{1} cm/s. Incidentally, the influence on consolidation such as disturbance resulting from the drains installation could be automatically considered when permeability of coefficient of drain (k_w) is determined by back analysis, although "the smear effect" of the drain itself is not taken a account into the proposed macro element method.

Table 5. 1 Permeability of the ground used in soil-water coupled finite deformation analysis

	k_0 (cm/sec)	e_0	C_k		k_0 (cm/s)	e_0	C_k
Embankment	1.0×10^{-5}		Constant k	Apt5	1.0×10^{-7}	4.6	0.500
Ac1	5.0×10^{-7}	3.1	0.260	Ac3u, Ac3, Ac4	1.0×10^{-6}	2.5	0.160
Apt2	1.5×10^{-6}	2.5	0.220	Dpt1	1.0×10^{-6}	3.7	0.450
Ac2-1	1.5×10^{-6}	2.5	0.220	Dpt2	1.0×10^{-6}	2.6	0.350
Ac2-2	8.0×10^{-8}	2.9	0.298	Sand layers	3.0×10^{-3}		Constant k

5.2.3. Simulation results to validate accuracy of the proposed method

Figs. 5.3 and **5.4** show the results of simulations. For comparison, the simulation results using the three following methods are also shown. **Table 5.2** presents the material parameters expressing the improvement effect of the vertical drains used in each of these methods.

(1) The vertical drain improvement is expressed using a single equivalent coefficient of permeability for the ground (mass-permeability method).

(2) As with the conventional macro-element method (Sekiguchi et al., 1986), the drain permeability is approximated to be infinity (i.e., macro-element method where drain permeability is treated as a known).

(3) The newly proposed macro-element method with water absorption and discharge functions, which provides a solution for the water pressure in the drain (i.e., macro-element method where drain permeability is treated as an unknown).

Table 5. 2 Parameters representing improvement effect by vertical drains

		(1) Mass-permeability	(2) Conventional macro-element	(3) Newly proposed macro-element
Equivalent coefficient of permeability of improved area	k_E (cm/s)	2.5×10^{-4}	—	—
Coefficient of permeability of vertical drains	k_w (cm/s)	—	equivalent to $k_w \approx \infty$	4.0×10^{-2}

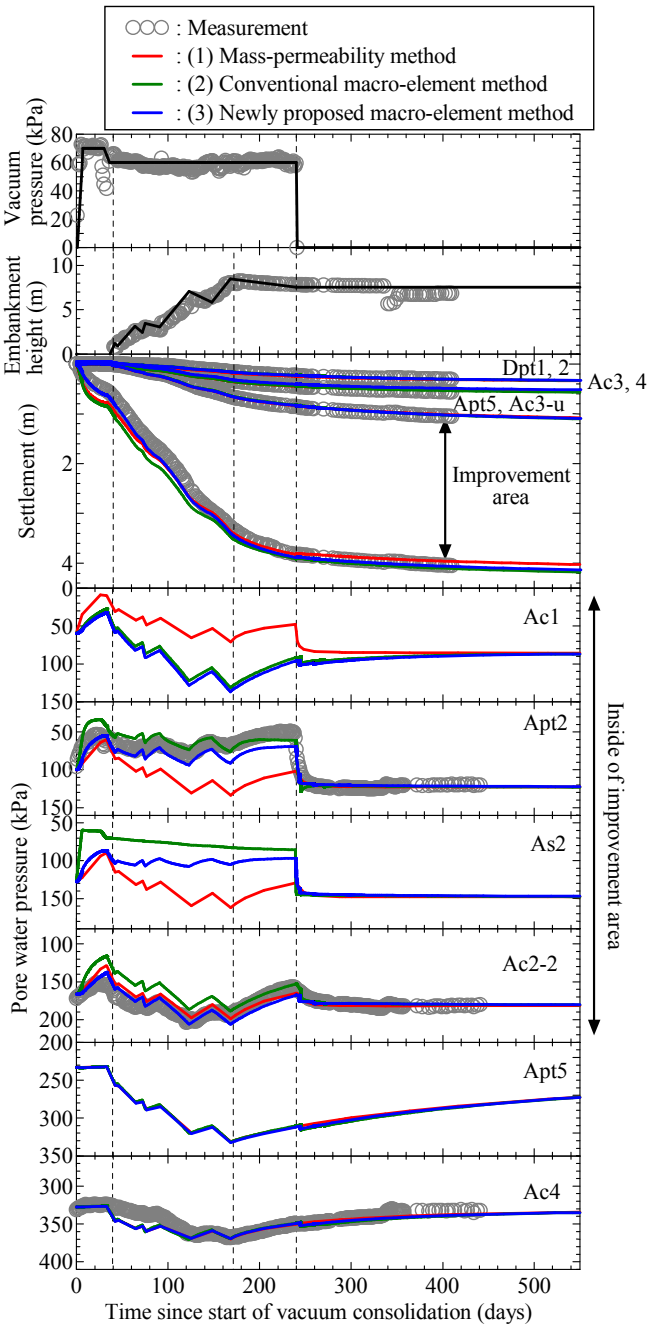

Figure 5.3 Time-settlement/pore water pressure relations at the center of embankment

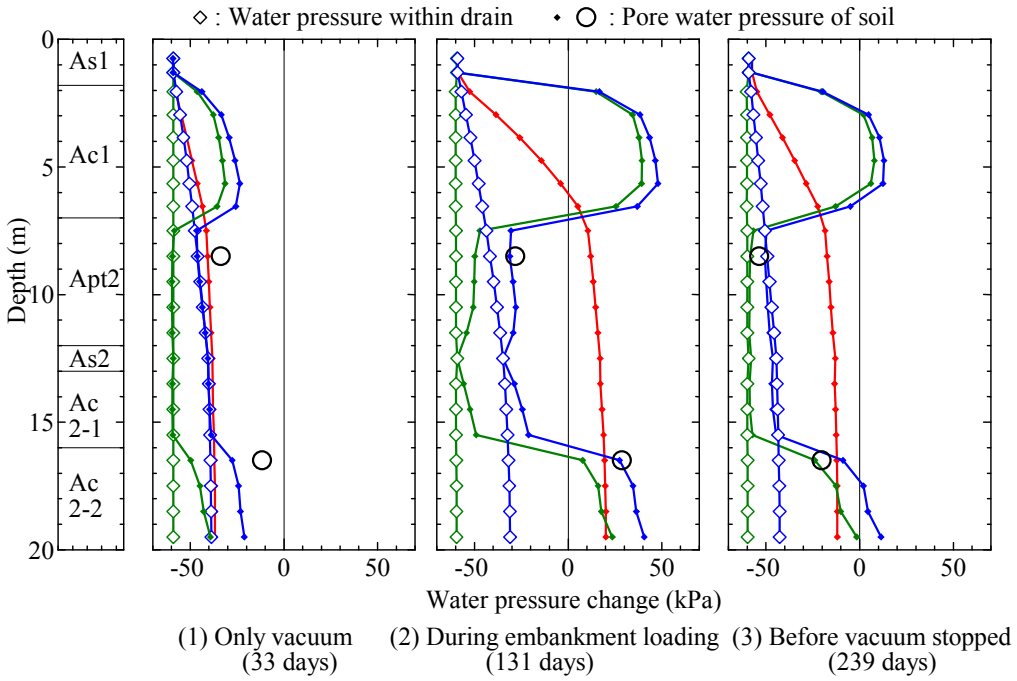

(a) Isochrones of water preesure change inside of improvement area

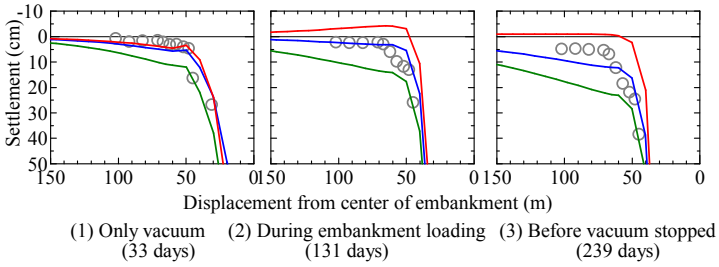

(b) Settlement of the surrounding ground

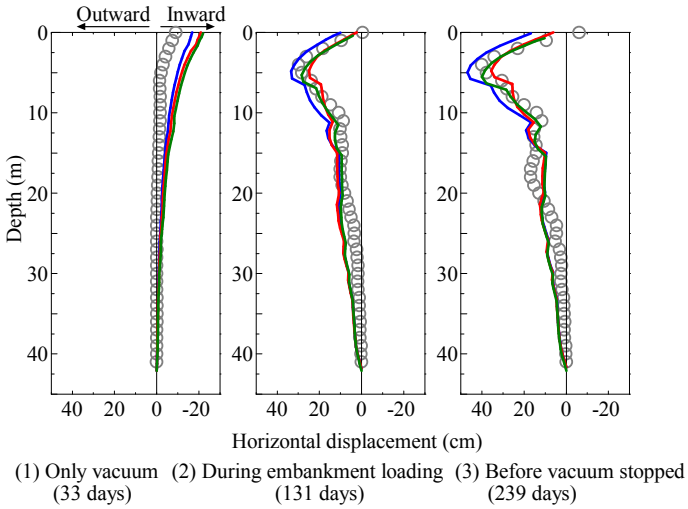

(c) Lateral displacement at the toe of embankment slope

Figure 5.4 Validation of reproducibility

Each of these methods is already capable of simulating settlement of the ground surface. However, because the (1) mass-permeability method does not describe the transmission of vacuum pressure through the vertical drain, the effect of the vacuum loading on the shallow layers of the improved area is overestimated, whereas the effect on the deep layers is underestimated. When thinking about ground stability problems, such a result would be on the dangerous side. Furthermore, the method does not simulate the widespread settlement of the ground surrounding the improved area. Meanwhile, both macro-element methods (2) and (3) simulated a permeability-dependent reduction in pore water pressure in all ground layers down to the deep layers of the improved area by vacuum loading. In particular, the macro-element method proposed in *Chapter 4* and validated here (3) naturally simulated a type of well-resistance phenomena in which the reduction in pore water pressure becomes increasingly difficult in deeper layers. In addition, it was confirmed that the method more comprehensively and accurately simulates all types of observed ground behaviors including the temporal change in pore water pressure, the horizontal displacement directly under the toe of the embankment slope, and settlement of the surrounding ground.

When the simulation of the target embankment was allowed to continue using the same parameters, it was found that consolidation within the vertical drains was completed early on. Although residual settlement of the unimproved deep layers was observed to occur, the settlement amount was predicted to be sufficiently small so as not to be problematic at the time the embankment would be put into service (approximately 2 years after completion of embankment construction).

5.2.4. Impact of the middle sand layers in vacuum consolidation and effective countermeasures

After starting vacuum consolidation on the target embankment, the settlement up to 5 cm was observed over a wide area approximately 50 m far from the toe of the embankment. Subsequent investigation indicated that this settlement may have been due to the presence of thin middle sand layers (As1 and As2) spanning the entire improvement area.

In order to demonstrate that the settlement of the surrounding ground was indeed due to the presence of these middle sand layers, simulations were performed using the proposed macro-element method (3), the simulation accuracy of which was validated above, after replacing the two sand layers (As1 and As2) with the underlying clay layers (Ac1 and Ac2-1). **Figs. 5.5** and **5.6** respectively show the settlement of the surrounding ground and distribution of the vacuum pressure (negative pore water pressure) during vacuum consolidation. It was demonstrated that the transmission of vacuum pressure to a wide area beyond the improved area through the middle sand layers results in settlement, and not uplift, of the surrounding ground even during embankment loading. In this circumstance, the efficacy of vacuum consolidation inside the improved region is usually reduced and unexpected settlement can cause engineering problems on infrastructures surrounding the embankment. On the other hand, the capacity of vacuum pump system is needed to enhance for keeping the designed negative pressure within improved area.

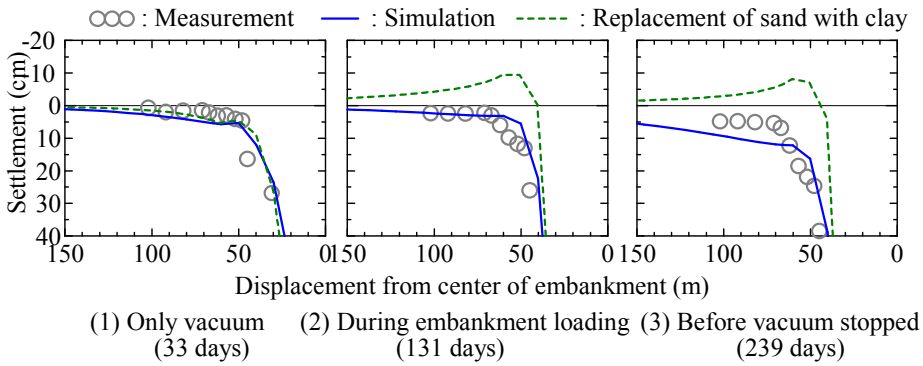

Figure 5.5 Effect of middle sand layer on the surrounding settlement

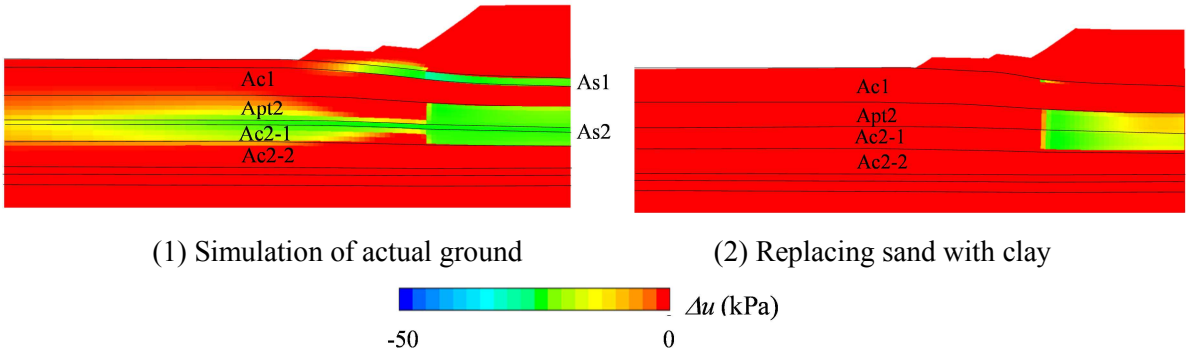

Figure 5.6 Distribution of negative pore water pressures during vacuum consolidation and embankment loading

Association of Vacuum Consolidation Technology (2013) recommended utilizing sheet-pile (well-known as cut of wall or impervious wall) installing downward over the end of middle sand layer or wrap waterproof sealing material on surface of drains passing through the middle sand layer as countermeasures to prevent the transference of vacuum pressure to outside of the improved area. The efficiency of these countermeasures were evaluated by carrying out simulations considering the presence of impervious wall or water proof, and then compare results with the basic case for actual construction conditions. The new proposed macro element (3) is incorporated in these simulations. In case of installing sheet-pile, the undrain boundary is set from ground surface under the embankment edges to the end of PBDs' depth; meanwhile similar to previous calculation in the section **4.4.3**, the waterproof is represented by the macro elements in which the water absorption function is eliminated but the discharge function of the drain is preserved.

Fig. 5.7 shows behaviors of the ground under the centerline including settlement and pore water pressure varying with time and isochrones of excess water pressure inside soil and vertical drains. It is clearly seen that the behaviors are almost similar for all layers except for pore water pressure in the middle sand layer (As2), and excess water pressure within vertical drains. Instead of reduction due to vacuum pressure in actual condition and impervious wall cases in which excess pore water pressure

presented, positive excess pore water pressure occurred in layer As2 due to effects of waterproof sealing (**Figs. 5.7(b)** & **(c)**). In addition, the excess water pressure within the drains or magnitude of negative water pressure in the actual construction condition is slightly smaller than those resulting from the cases of utilizing impervious wall and water proof sealing because of avoiding transfer vacuum pressure to surrounding area through As2 layer, in other word, these countermeasures enhance slightly the efficiency of vacuum consolidation in comparing to the actual condition. Because the thickness of As2 is quite small (about 1m), the loss of vacuum pressure or lack of drainage condition (due to waterproof sealing) does not impact significantly on total and residual settlements of the peaty ground.

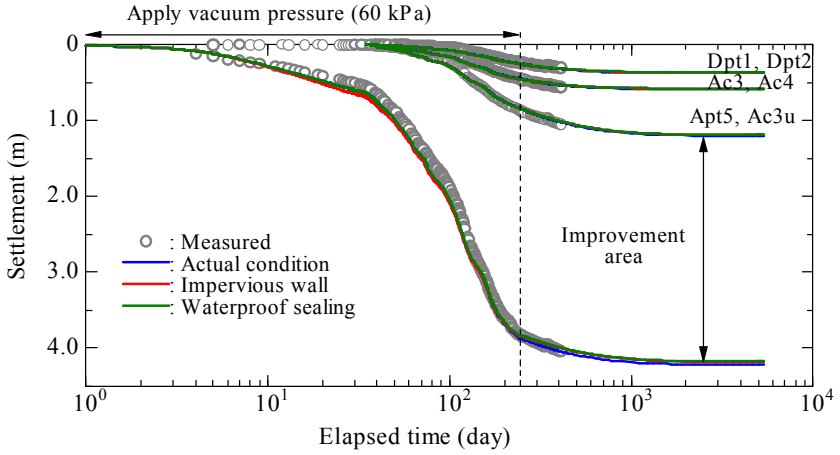

(a) Time-settlement below curves

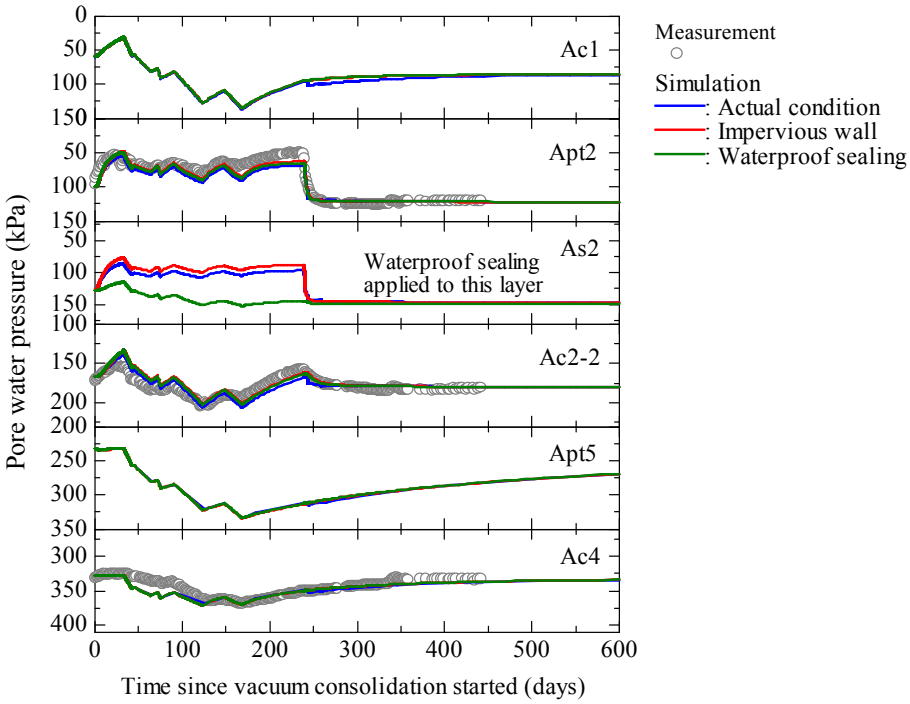

(b) Time-pore water pressure curves

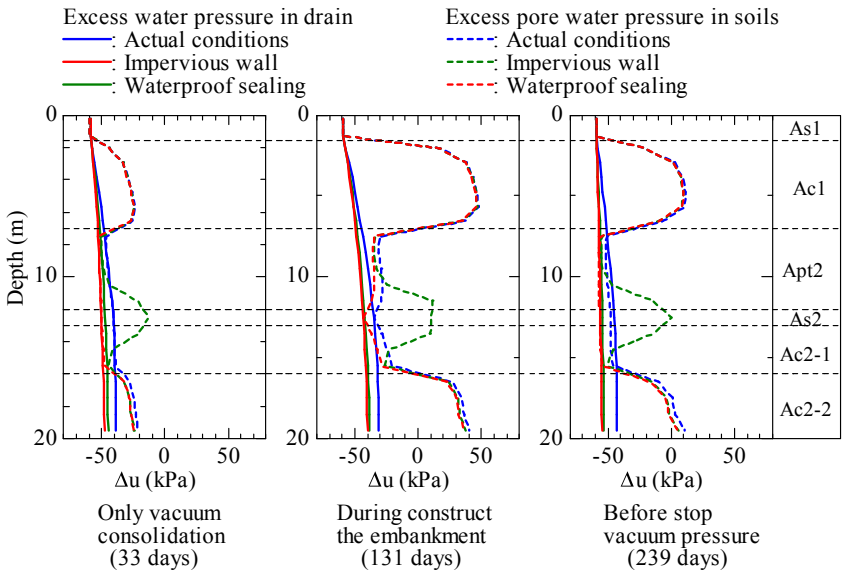

(c) Isochrones of excess water pressure

Figure 5.7 Behavior of ground below center of the embankment

The effectiveness of those countermeasures can be seen in **Fig. 5.8** which shows the deformation of the area nearby the embankment, and **Fig. 5.9** demonstrates the distribution of negative water pressure in the ground. The results illustrated that a decrease of outward lateral displacement means increasing the safety of the embankment due to the enhancement of vacuum consolidation in the improvement region. The surrounding ground is upheaval when using impervious wall or sealing although the later method produces somewhat less upheaval than that of the former. The uplift of the surrounding ground maybe explained that the transferring vacuum pressure to a wide area beyond the improved area is prevented by using cut of wall or waterproof sealing as countermeasures.

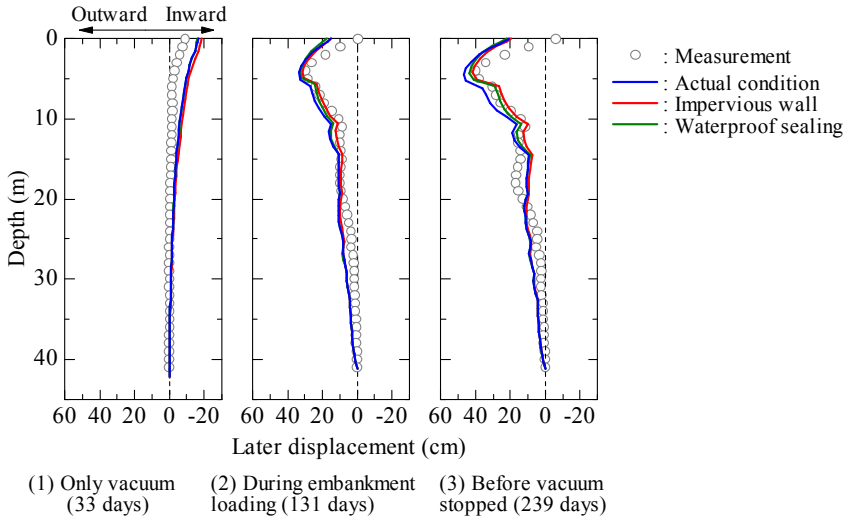

(a) Lateral displacements below the edge of the embankment

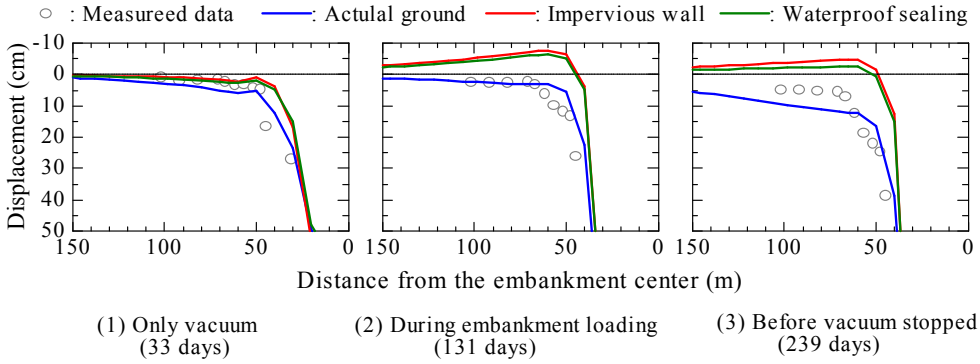

(b) Surface settlements on the surrounding ground

Figure 5.8 Effects of sheet-pile and waterproof sealing on the surrounding ground

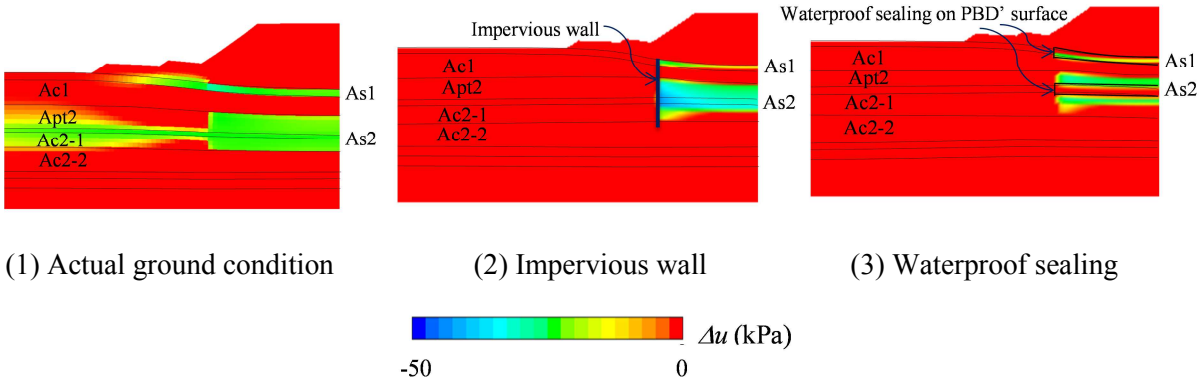

(1) Actual ground condition (2) Impervious wall (3) Waterproof sealing

Figure 5.9 Effects of sheet-pile and waterproof sealing on negative water pressure distribution

5.2.5. Effect of the loading history

The actual construction of this embankment over the soft peaty ground in section B reported two distinguished embankment loading period. The first period or the first embankment, approximate 3 m thick and 100 m wide, had been constructed since 2006 then kept for 6 year. Due to a long period, the ground could consolidate completely under the certain load and then the first embankment is considered as pre-loading step. The main embankment had been constructed in the second period since 2012 with the height of 8 m from the surface of the first embankment as description in section **5.2.2**. This section is going to investigate the effects of the pre-loading on the deformation of the soft ground. To avoid influences of other factors, the calculations were performed on the actual condition without any ground improvement method. Two analysis cases were done; case (a) followed the actual loading history while case (b) shortened the first loading period from 6 years to 30 days.

These calculation results are illustrated on **Fig. 5.10** including settlement at the centerline, surrounding deformation and shear strain distribution in case (b). In spite of same amount of embankment load, the settlement that occurs in case (b) is smaller during loading but higher

inclination, and then tend to higher at the end of consolidation than that in case (a). It is also obvious demonstrated that case (b) produces the large uplift deformation and outward lateral displacement indicating the higher failure potential. In fact, large shear deformation has occurred in shallow weak soil layers (Ac1, Apt2), and the cracking could has developed after completion of embankment loading (**Fig. 5.10(d)**) in case (b) meanwhile similar behaviors do not appear in case (a) . It is revealed that the pre-loading is an effective countermeasure for both reducing settlement and increasing stability when construction of the embankment on soft ground. If very long construction period is allowable, the pre-loading can be an appropriated countermeasure due to not only safely but also low cost.

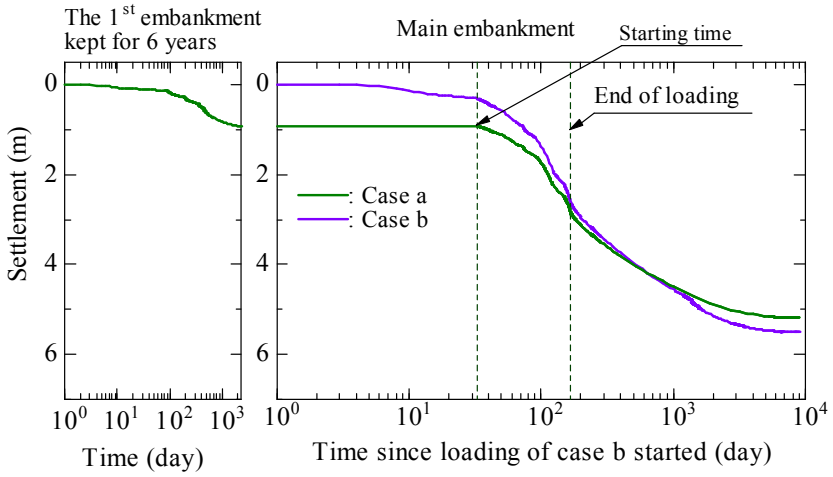

(a) Time-settlement curves below the embankment center

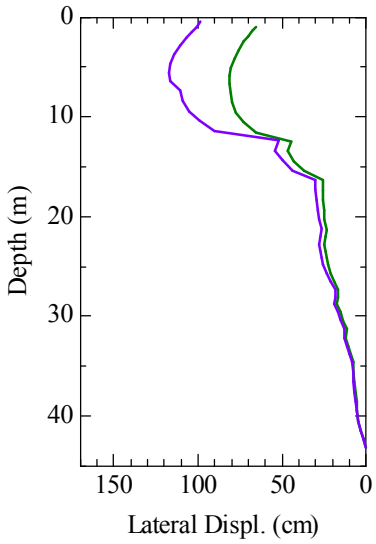

(b) Lateral displacement

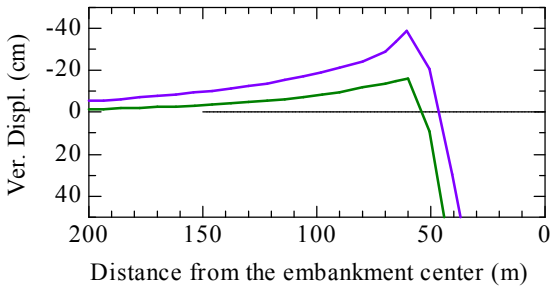

(c) Surrounding uplift

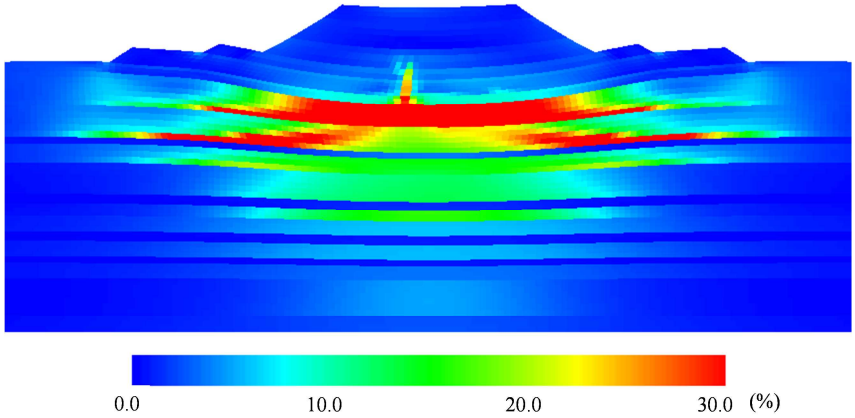

(d) Distribution of shear strain

Figure 5.10 Effect of loading history

5.3. Effects of drain spacing on the ground improvement using vertical drain/vacuum consolidation

An advantage of the proposed macro-element method, the simulation accuracy of which was verified in the previous section, is that the mesh width does not have to be matched to drain spacing. In other words, it is possible to evaluate the effect of drain spacing using the same mesh. Therefore, in this section, calculations were conducted to investigate the influence of drain spacing on the outcome of ground improvement using vertical drains and vacuum consolidation during embankment loading of a soft ground.

5.3.1. Analysis conditions

Here, a softer ground than that in the previous simulations with alternating peat and clay layers up to the ground surface was modelled, to represent the typical ground where vacuum consolidation would be applied. Specifically, all the sand layers of the ground shown in **Fig. 5.2**, which were subject to the analysis in the previous section, were replaced by their underlying clay or peat layers, resulting in the ground model shown in **Fig. 5.11**. Simulations were performed and the results were compared for the following 5 cases:

Case 1: no ground improvement,

Case 2: vertical drains with 1.5 m spacing,

Case 3: vertical drains with 1.0 m spacing,

Case 4: vertical drains with 0.7 m spacing,

Case 5: vertical drains with 1.0 m spacing, combined with vacuum consolidation (70 kPa).

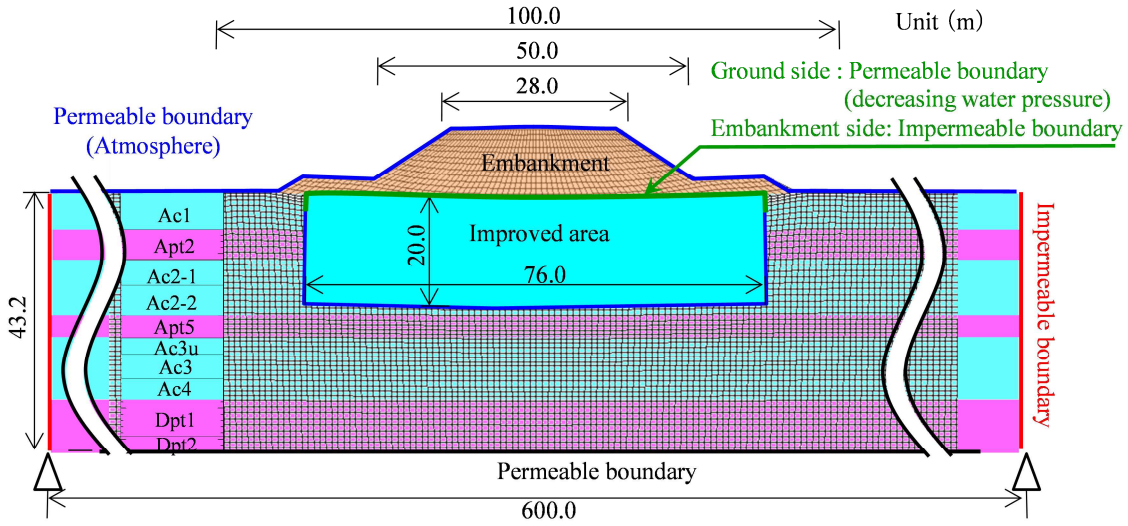

Figure 5.11 Model ground assumed to be softer conditions

For simplicity, a simpler embankment shape and loading history than for the analyses in the previous section were assumed. As in the previous analyses, the depth of the improved area was set at 20 m. The width of the improved was set to the entire embankment width including the counterweight fill. As can be seen from the Case 1 simulation results (**Fig. 5.13**(**a**)), this was done because large-scale shear deformation of the softer ground being modeled occurs even under the counterweight fill. The final embankment level (height from initial ground level) is usually controlled without considering the amount of settlement during loading in practical construction. However in order to compare the final settlement directly under a same total load for each case, the embankment thickness (embankment height + settlement) at completion of embankment construction were set to be the same for each case. The material constants and initial values of the ground, and vertical drain permeability coefficients from the simulations in the previous section were used in the present calculations without modification.

5.3.2. Calculation results

Fig. 5.12 compares the ground surface settlement at the center of the embankment predicted for each of the cases. In Case 1 where no ground improvement is employed, there is a rapid increase in settlement rate during embankment loading, accompanied by the occurrence of large-scale circular shear deformation in the shallow, low-permeability, low-strength Ac1 and Apt2 layers, which can be seen in **Fig. 5.13**(**a**). Although the main focus of this section is on the quasi-static problem of consolidation, by using a code with an inertia term that is capable of handling dynamic problems, depending on the circumstances, it is possible to describe such slip failure under load-controlled condition (Noda et al., 2008b; Takaine et al., 2010; Nakano et al., 2010; and Yamada and Noda, 2013; Tashiro et al., 2015).

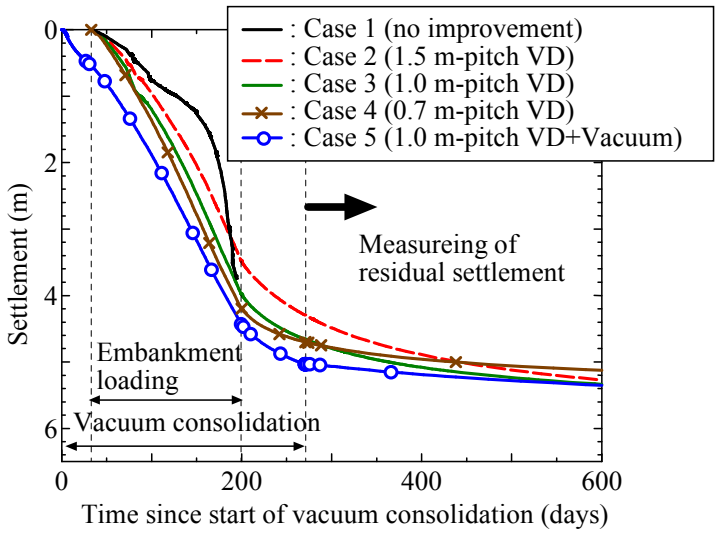

Figure 5.12 Comparison of ground settlements beyond embankment center

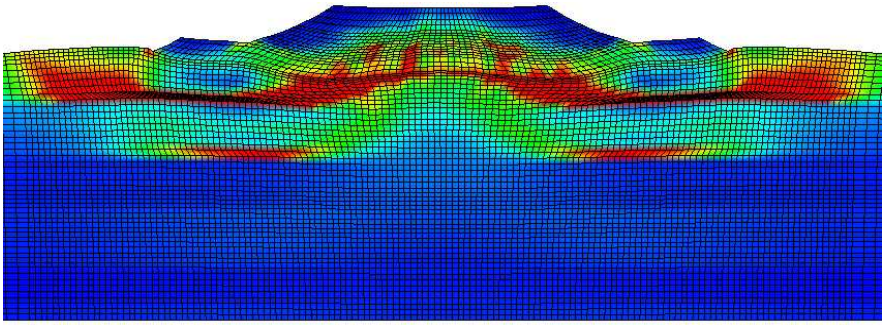

(a) Case 1: No improvement (Circular slip during embankment loading)

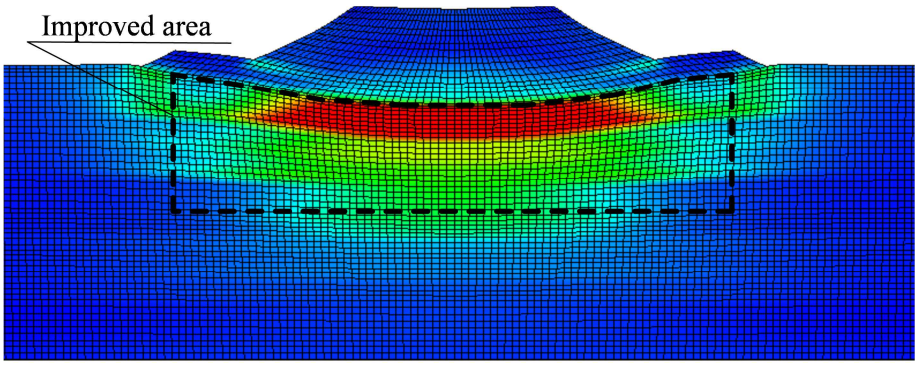

(b) Case 4: 0.7 m-spacing PVD (End of consolidation)

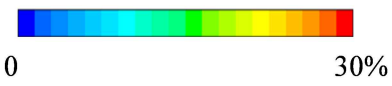

Figure 5.13 Distribution of shear strain

Meanwhile, it was demonstrated that ground improvement using vertical drains is effective in preventing slippage during loading. In cases such as Case 2, where the drain spacing is too wide to provide adequate drainage, although it is possible to prevent fatal slip failure during loading, as can be seen in **Fig. 5.14**, large-scale outward horizontal displacement and uplift of the ground adjacent to the improved area occurs as a result of large shear deformation of the shallow layers in the improved area. As can be seen in **Table 5.3** and **Fig. 5.14**, by reducing the spacing between vertical drains, total settlement, residual settlement, and deformation of the surrounding ground are reduced, enabling more stable construction. In the ground modeled in this study, reducing the drain spacing from 1.0 to 0.7 m (Case 4) yielded the same reduction in residual settlement as combining vacuum consolidation (Case 5). However, even when drain spacing was sufficiently narrow, due to the lack of inward consolidation associated with vacuum consolidation, ground improvement using vertical drains alone did not necessarily reduce the outward horizontal displacement to the same degree as ground improvement using both vertical drains and vacuum consolidation.

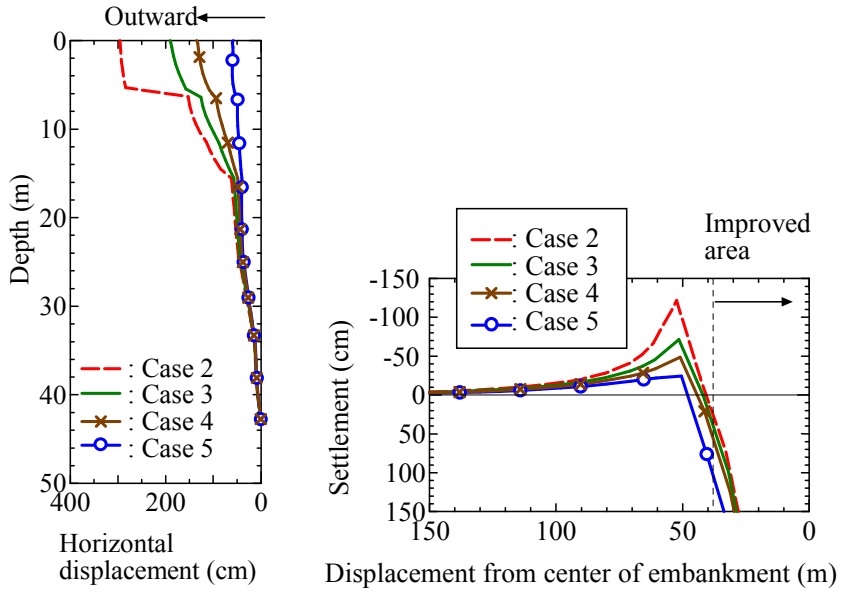

Figure 5.14 Comparison of surrounding deformations at the end of loading

Table 5. 3 Comparison of settlements

Case	Drain spacing (m)	Total settlement (m)	Residual settlement * (cm)
2	1.5	6.03	173
3	1.0	5.92	126
4	0.7	5.63	93
5	1.0 (+Vacuum)	5.88	85

* Defined as the settlement measured 72 days after the end of embankment loading (corresponding to the end of vacuum consolidation).

5.4. Discussion

In this section, the results presented in **Sections 5.2** and **5.3** were discussed with the aim of coming up with practical recommendations for the application of vacuum consolidation during the embankment loading on soft ground.

Given the same drain spacing, the use of vacuum consolidation in combination with vertical drains reduces much more residual settlement than using vertical drains alone. Nevertheless, because the ground does not completely return to its previous state even after vacuum loading is stopped, the total settlement amount is greater. Meanwhile, when employing ground improvement using vertical drains alone, if sufficiently narrow drain spacing is utilized, so that the drains provide adequate drainage relative to the ground's permeability, it is possible to not only enhance ground stability but also reduce residual settlement and total settlement.

Table 5.4 shows the estimated construction costs for Cases 2 through 5 discussed in Section 3, based on the actual construction costs for the target embankment simulated in Section 2. It was assumed that PBD cost 200 JPY/m and that vacuum consolidation costs an additional 10,000 JPY/m^2. Under the conditions simulated in this study, comparing Cases 4 and 5, which yielded the same magnitude of settlement reduction, the additional use of vacuum consolidation approximately doubles construction costs. Furthermore, although reduction in construction time through rapid loading is often touted as one of the advantages of vacuum consolidation, in reality, vacuum consolidation requires substantial set-up time prior to the application of vacuum load in order to lay the airtight sheet, set up the vacuum pump, etc. If, in the end, the construction time is the same, it would be better to install vertical drains at a high density and to employ slow banking.

Table 5. 4 Comparison of construction cost (per unit area)

Case	Drain spacing (m)	Drain length (m)	Construction cost (thousand yen/m^2)
2	1.5	20	1.8
3	1.0	20	4.0
4	0.7	20	8.1
5	1.0 (+Vacuum)	20	14.0

However, because vertical drains alone do not cause inward deformation, they are not able to reduce horizontal displacement to the same extent as vacuum consolidation used in combination with vertical drains, even if vertical drains are installed at a high density. For this reason, vacuum consolidation is effective when there are structures near the area to be improved that must be protected or when the aim is to minimize the impact on the surrounding ground.

Another consideration when deciding whether to also use vacuum consolidation is whether the soft ground contains a middle sand layer. In general, the presence of a middle sand layer can be expected to accelerate consolidation and to contribute to increased stability. However, when performing vacuum consolidation, depending on the ground conditions, the middle sand layer may

cause the effective vacuum pressure to be lower than the design value. In such cases, it may be necessary to reconsider stability/settlement management including the embankment construction rate and the surcharge embankment height. In addition, as discussed in **Section 5.2**, transmission of the vacuum pressure through the middle sand can cause the wide-scale settlement of the ground surrounding the improved area. As such, when using vacuum consolidation in combination with vertical drains, it is important that more careful ground investigation be conducted prior to ground improvement. When a middle sand layer suspected of being continuous is encountered, it is necessary to implement countermeasures including the application of waterproof sealing material to the surface of drains in the vicinity of the sand layer, the installation sheet piling, or making the more fundamental decision not use vacuum consolidation itself. As demonstrated in this study, one solution to the above is to use vertical drains only with narrow spacing. In addition, the proposed macro element, whose simulation accuracy was validated in this *Chapter*, is an effective method for quantitatively predicting the impact of middle sand layers.

5.5. Brief summary

In this *Chapter*, the simulation accuracy of the macro-element method with water absorption and discharge functions, implemented in a soil-water coupled finite deformation analysis code, was validated by simulating an actual site. In addition, at the target site, widespread settlement of the ground surrounding the embankment was observed after application of vacuum loading, which was believed to due to the presence of a middle sand layer spanning the entire improved area. Therefore, the effect of a middle sand layer was investigated using the proposed method. Additional calculations were conducted using a ground model for softer ground than at the actual site, which represented typical ground to which vacuum consolidation would be generally applied. In these simulations, the effect of vertical drains and vacuum consolidation were investigated, with a particular focus on the influence of drain spacing. The content of this *Chapter* will be published on Nguyen et al. (2015) and the main findings are summarized as follows:

1) The macro-element method with water absorption and discharge functions proposed is capable of comprehensively and closely simulating a range of ground behaviors including the temporal change in pore water pressure, horizontal displacement of the ground under the toe of embankment slope, and the settlement of the surrounding ground in consolidation problems involving the embankment loading of multi-layered ground improved with vertical drains and vacuum consolidation.
2) When a middle sand layer is present across the entire improved area, the mass-permeability method (whereby an equivalent coefficient of permeability is assigned to the ground improved using vertical drains) is unable to simulate the reduction in pore water pressure of the ground adjacent to the improved area and the widespread settlement resulting therefrom. Meanwhile, the macro-element method that treats the water pressure in the drains as a known may overestimate the impact of vacuum consolidation.

3) Both installation of sheet-pile and wrapping waterproof sealing material on the surface of drains are effective countermeasures against the transference of vacuum pressure from the improved area to ground adjacent resulting in enhancement of vacuum consolidation inside the improved region and avoiding unexpected settlement occurring in the surrounding areas of the embankment.
4) Pre-loading method is suitable for the embankment which can be allowed to construct in a long period with low cost. Using it, the settlement of the ground can reduce and its safety can increase.
5) Even in the case of ground improvement using vertical drains alone (i.e., without vacuum consolidation), it is possible to increase stability and reduce deformation of the surrounding ground by selecting an appropriate drain spacing that provides sufficient drainage for the ground's permeability. In addition, the use of vertical drains only with the appropriate spacing can yield the same reduction in residual settlement as the case of vacuum consolidation combined with vertical drains.
6) Vacuum consolidation is effective in cases where it is necessary to minimize residual settlement and deformation (in particular, outward horizontal displacement) of the surrounding ground.
7) When deciding vertical drain spacing and whether to also use vacuum consolidation on a soft ground, it is important to carefully consider not only the ground conditions (ground permeability, the presence of a middle sand layer, etc.) but also the impact on, for example, the ground adjacent to the improved area, construction costs, and construction time. The macro-element method proposed by the authors herein is capable of quantitatively simulating/evaluating the effects of various factors and should prove to be an effective tool for making comprehensive decisions in actual practice.

Chapter 6

Conclusions and future works

6.1. Introductions

The SYS Cam-clay model which is capable of depicting the structure, overconsolidation, and anisotropy of skeleton of all soils including natural deposited clay is used first to describe mechanical behavior of highly compressible peat, as known as a material not suited to foundations in the view of engineering. After that, a finite deformation geo-analysis code ***GEOASIA***-based analysis is carried out to simulate a large-scale deformation of an ultra-soft peaty ground improved by SD method under an embankment loading, and to investigate effective countermeasures against residual settlement and failure. This FEM code was mounted with the SYS Cam-clay model as an elasto-plastic constitutive equation together on a motion's equation with an inertial term rather than a fore equilibrium equation. In this numerical analysis, for simplify, the influence of SD on the improvement region was analyzed by using "Mass-permeability concept" without an investigation of water flow between soil and drain. Next, a new macro element method is proposed in order to increase the accuracy in simulating the ground improvement effect not only by vertical drain but also vacuum consolidation method. In which, water pressure inside vertical drain is considered the unknown parameter and equipped with water absorption and discharge function for vertical drain, then well resistance phenomena can be taken into account naturally. Finally, this new proposed macro element method has been validated after incorporated into ***GEOASIA*** by comparing simulation results to observed data in an actual construction site of an embankment on peaty ground improved by vacuum consolidation. After validation of the accuracy, this method is employed to investigate improvement effects of vertical drain at varying spacing and vacuum consolidation.

Chapter 2 gives an overview of peat deposit in engineer point of view, the deduction of engineering properties and distinctive sedimentary environment of peaty soil in Mukasa area, Fukui Prefecture, Japan, and then a description of mechanical behaviors of peat. The main findings are following:

1) Peat is a highly organic soil consisting of partly decomposed vegetable fragments generated in humid areas where the rate of decomposition is usually smaller than that of accumulation. The peat deposition mainly contributes in the cold regions like Canada, United Sate, Russia, Scandinavia, Hokkaido-Japan, and others.
2) In the field of civil engineering, a soil containing more than 20% of organic matter is called as peat or peaty soil. Peat is also classified into fibrous, pseudo-fibrous, and amorphous based on the degree of humification.
3) The distinctive engineering properties of peat are extremely high natural water content, and Atterberg limits; very low density of soil particle; dramatically decreasing of permeability under external load what can be determined by the same testing specifications for inorganic clay.

4) Plenty records of geotechnical problems related to large, long-term settlement, failure of infrastructures constructed on peaty ground due to its low shear strength and extremely compression characteristics. In addition, the effect of gas formation occurred on peat is necessary to consider.
5) In Mukasa area, field of this study, soil characteristics and initial ground conditions containing highly compressible peat and soft clay are evaluated in two sections A and B separately due to further different numerical analyses. In section A, the observed large-scale delayed compression of the deep peat layer could be caused by effect of artesian pressure of 100 kPa which was created through fault motions during Mid-Pleistocene era. In addition, the estimation of initial condition indicates that subsidence of the valley bottom was accompanied by a progressive increase in artesian pressure and that the deep peat layer deposited while maintaining a high void ratio under low effective stress. It was believed that test embankment loading resulted in a stress state readily exceeding the consolidation yield stress, causing a characteristic large-scale compression of the peat layer and a dramatic reduction in permeability due a decrease in the void ratio, leading ultimately to delayed dissipation of excess water pressure. On the other side located at 300 m far from section A, ineffectiveness of the artesian pressure, and occurrence of middle sand layers were found in section B, that cause deep peat layers are overconsolidated state here, then large long-term settlement and failure is less possible to occur.
6) The results of Oedometer and consolidated undrained trial compression tests on peat are able to reproduced by using SYS Cam-clay model, that means its mechanical behaviors can be described in the same framework with other soils either natural deposit or embanking material. As the results, peat could be modelled as a material having a high Poisson ratio, relatively rapidly-developing anisotropy, a small initial consolidation ratio, a high degree of structure, a large compression index, and exhibiting rapid degradation of structure.

Chapter 3 performs the simulation and evaluation focusing on the SD improvement in the test embankment underlain by the thickest soft layer with a depth of approximately 50 m in section A, Mukasa area, using ***GEOASIA***. In this section, the overall settlement exceeded approximately 11 m after 3 years of embankment construction, and did not appear to be approaching convergence due to large-scale delayed compression of the greater than 30-m-deep peat layer, which was assumed in the design stage not to be subject to settlement. The main conclusions of this *Chapter* are listed as following:

1) Mechanical behaviors of peat could be described by using SYS Cam-clay model which is mounted in ***GEOASIA*** as constitutive equation of soil skeleton as concluded in *Chapter 2*. This character is added to the consideration of the sensitivity to disturbance and the heterogeneity of the peat layers, the initial in-situ conditions were deduced by simulating the observed settlement of each layer under the center of the embankment. As a result, it could be demonstrated that the analysis code ***GEOASIA*** was capable of reproducing the observed large-sale ground deformation and pore water pressures during embankment construction and the approximate 2-year period

following construction. The simulation is allowed to continue without changing parameters obtained from the former simulation of the observed behavior resulted in prediction of an additional 1.52 m residual settlement in the next approximately 66 years.

2) The effectiveness of countermeasures against instability and residual settlement was also investigated by continuing using ***GEOASIA*** with the same soil parameters. This FEM code is able to not only simultaneously investigate a long-term settlement behaviors caused by the degradation of soil structure but also circular slips and failures that occur instantaneously. Due to its extremely low consolidation yield stress, when peat is subjected to a substantial load under undrained conditions, large lateral deformation, or in some instances slip failure, can occur. Even under drained conditions, sudden large-scale compression occurs causing to significant deformation of the surrounding ground. Through a series of analyses, it was demonstrated that improvement of the permeability by drains and lowering the loading speed as much as possible or lightening the load are effective not only for increasing stability during construction, but also for reducing residual settlement.
3) Based on the results of the analyses in this *Chapter*, the reparation was carried out on the test embankment, and the remaining highly compressible peaty ground was improved by installation of deeper vertical drain combined with vacuum consolidation prior construction of an embankment to reduce the residual settlement. The field observation data of both embankments presented in this *Chapter* emphasize the importance of implementing countermeasures aimed to ensure stability during construction and future maintenance, and reduce residual settlement when subjecting soft ground containing clay and/or peat to loads exceeding consolidation yield stress of the ground.

Chapter 4 attempts to extend capabilities of macro element method for vertical drains. A discharge function of the vertical drain was newly added while remaining the water absorption function as the conventional macro element, by solving unknown water pressure in drain and adding a continuity equation for the drain to the governing equation. This new proposal was verified by mounting to a quasi-static soil-water coupled elasto-plastic finite element method based on finite deformation theory. After verification, numerical analyses on the application of the vacuum consolidation method to clayey ground containing a middle sand layer were performed. At last, 3D finite deformation analysis was carried out to verify the estimation methods of the equivalent diameter of band-shaped vertical drain used in new method. The following is a summary of findings:

1) Analysis results found that well resistance phenomena often occurring when soft ground improved by vertical drain can be simulated as a natural manner, and depending on analysis condition. Additionally, the new proposed method has a capacity to investigate the problems involving material and/or geometrical nonlinearity and multilayered ground in highly accurate approximation.
2) When applying vacuum consolidation method to improve the soft clayey ground containing a sand seam interleaved, the insufficient reduction of water pressure due to propagating vacuum

pressure through the sand seam thus cause the settlement of surrounding ground. The new proposed approach is capable of simulating the phenomena adequately.

3) In order to prevent the loss of vacuum pressure through middle sand layer, the water proof sealing material is often recommended to wrap to the surface of drain where passing through the parts. The effects of this countermeasure are able to understand by using the new macro element method.
4) In the new proposal of macro element, the water-flow coefficient representing the flow between soil and drain is formulated by using volume of element. The formulation makes it unnecessary to create mesh division with to match the drain arrangement and spacing. Furthermore, the proposed approach yields solutions that are insensitive to element size of the FEM mesh.
5) By verification with 3D analysis, the ground behaviors including settlement and pore water pressure could be simulated numerically without depending on the conversion methods of equivalent diameter of band-shaped vertical drain when its discharge capacity through a cross-sectional area is constant before and after the conversion.

Chapter 5 first validates the new macro-element method with water absorption and discharge functions proposed in *Chapter 4*, by implementing in a soil-water coupled finite deformation analysis code ***GEOASIA***, to reproduce observational data in an actual site. In this site, a widespread settlement of the ground surrounding the embankment was observed after application of vacuum loading, which was believed to cause by the presence of a middle sand layer over the whole improved area. Therefore, the effect of a middle sand layer and the effective countermeasures were investigated using the same method for the drains. Next, the effect of vertical drains and vacuum consolidation were investigated, particularly focusing on the influence of drain spacing on a ground model for softer ground than that of actual site which represents a typical ground to which vacuum consolidation would be generally applied. These analyses give following conclusions:

1) The proposal of the new macro element method with water absorption and discharge functions has capacity to carry out comprehensively and closely simulations of a range of ground behaviors improved by vertical drain combined with vacuum consolidation. The behaviors includes the change of pore water pressure, horizontal displacement of the ground under embankment toe, and the settlement of surrounding ground in consolidation problems involving the embankment loading on multi-layered ground.
2) In this soft ground with presence of middle sand layers crossing the entire improved area, the macro element method treating water pressure inside drains as a known constant may do overestimate the impact of vacuum consolidation. Meanwhile the mass permeability method that used in *Chapter 3* is unable to simulate the reduction of pore water pressure adjacent to the improved region, and widespread settlement caused by this point.
3) The evaluation of the countermeasures indicates that using either impervious wall (sheet-pile) or waterproof sealing material are effective against the pass of vacuum pressure through middle sand layer; in the consequence, the efficacy of vacuum pressure is only concentrated inside improved

area thus avoids the settlement occurring in the surrounding area. The ground behaviors between the two countermeasures are slightly different.

4) The ground in this analysis had been experienced the first embankment loading for long time before the construction of the main embankment at a desired height of 8 m. The ground is considered as completely consolidated under first loading step, as known "pre-loading". The analysis results in assumption of ground without improvement show that pre-loading is effective for construction in a long period because this method can reduce the residual settlement and potential of failure.
5) When the very soft ground without middle sand layers is improved by vertical drain only, the reduction of residual settlement and increase of stability could be achieved by selecting an appropriate drains spacing. Moreover, the vertical drain only can yield the similar amount of residual settlement with vacuum consolidation method if using a suitable spacing.
6) Comparison to vertical drain only, the vacuum consolidation method is advantage in the case that needs to minimize the residual settlement and surrounding ground deformation.
7) When choosing improvement method for highly compressible soft ground to use whatever vertical drains with suitable spacing and vacuum consolidation method, it is important to carefully take into account not only ground condition but also the impacts on, for instead, the vicinity area, time and cost of construction. The new proposed macro element method herein should be an effective tool for making comprehensive decisions in engineering practice because it is capable of quantitatively simulating/evaluating the influence of various factors.

6.2. Future works

1) In section A, the very soft peaty ground was improved by SD installation. Although the large-scale deformation of this ground under embankment loading was well simulated by applying mass permeability concept for the influence of SD as discussed in *Chapter 3*, the lateral displacement and ground upheaval were fairly obtained due to limitation of mass permeability method. Future numerical study should be performed using the new proposed macro element method to again simulate the large-scale ground behaviors in which effect of artesian pressure is taken into account.
2) The new macro element method was validated comprehensively as seen in the early part of *Chapter 5*; however, water pressure inside vertical drain could not be done due to lack of measurement data. Therefore, additional validation should be carried out in the future whenever the monitoring data of water pressure within vertical drain is available.
3) To prevent the impact of middle sand layer in vacuum consolidation method, the steel sheet-pile is usually applied at actual site. However, only undrain condition at improvement region boundary assumed for simplicity that could not evaluate total roles of this countermeasure. Future numerical study should be executed by replacing soil-water elasto-plastic material with elastic steel sheet-pile material at the finite elements at the boundary improvement area.

4) Although the comparison between vacuum consolidation and vertical drain only methods was investigated clearly, the loading condition was equal only at final stage of construction. This evaluation should not apply for reclamation or pre-loading projects where external load often has been decided before the construction, then apart of surcharge fill will be removed to desired embankment level. According to this construction sequence, the case using vertical drain only should be further simulated with an additional surcharge fill that is equivalent to amount of applied vacuum pressure; in addition, the surcharge removal should be included in this future simulation.

References

1) Adams, J. (1965). The engineering behavior of Canadian Muskeg. *6th International Conference on Soil Mechanic and Foundation Engineering*, (pp. 3-7). Montrael, Canada.
2) Akai, K. and Tamura, T. (1978). Numerical analysis of multi-dimensional consoliation accompanied with elasto-plastic consitutive equation . *Proceeding of JSCE*. No. 269, (pp. 95-104).
3) Ajlouni, M. A. (2000). *Geotechnical properties of peats and related engineering problems.* Urbana, Illinois: Ph.D thesis, Univerisrty of Illinois at Urbana-Champain.
4) Andrejko, M.J., Fiene, F., Cohen, A.D. (1983). Comparison of ashing techniques for determination of inorganic contents in peats. *Testing of peats and organic soils. ASTM Special Technical Publication 820*, 5-20.
5) Arai, A., Takeyama, T., Aoki, T., Nakamura, K., Honda, S., Ohta, H. (2008). Application of macro-element method to vacuum consolidation (part 2). *43rd Anual Conference of Japan Society of Cilvil Engineering (JSCE)* (pp. 889-890). (in Japanese).
6) Ariyarathna, P. R. C., Thilakasiri., H. S., Karunawardena., W. A. (2010). Vacuum consolidation of Sri Lanka peaty soil. *Annual Transactions of The Institution of Engineers, Sri Lanka*, 27-37.
7) Asaoka, A. (2003). Consolidation of clay and compaction of sand, - an elasto-plastic description -. Keynote lecture. *12th Asian Regional Conference on Soil Mechanic and Geotechnical Engineering* , (pp. 1157-1195). Singapore.
8) Asaoka, A., Nakano, M., Noda, T. (1994). Soil-water coupled behaviour of saturated clay near/at critical state. *Soils and Foundations.* Vol. 34(1), 91-106.
9) Asaoka, A., Nakano, M., Fernando, G.S., Nozu, M. (1995). Mass permeability concept in the analysis of treated ground with drains. *Soils and Foundations*. Vol. 35(3) 43-53.
10) Asaoka, A., Nakano, M., Noda, T. (1997a). Soil-water coupled behaviour of heavily overconsolidated clay near/at critical state. *Soils and Foundations.* Vol. 37(1), 13-28.
11) Asaoka, A., Noda, T., Fernado, G.S.K. (1997b). Effects of change in geometry on the linear elastic consolidation deformation. *Soils and Foundations.* Vol. 37(1), 29-39.
12) Asaoka, A., Nakano, M., Noda, T. (1998). Superloading yield surface concept for the saturated structured soils. *4th European Conference on Nummerical Methods in Geotechnical Engineering*, (pp. 233-242). Udine, Italy.
13) Asaoka, A., Noda, T., Yamada, E., Kaneda, K., Nakano, M. (2002). An elasto-plastic decription of two distinct volume change mechanisms of soils. *Soils and Foundations*. Vol. 42(5) 47-57.
14) Asaoka, A., Noda, T. (2007). All soils all states all round geo-analysis integration. *International Workshop on Constitutive Modelling-Development, Implementation, Evaluation, and Application*, (pp. 11-27). Hong Kong, China.
15) Association of vacuum consolidation technology. (2013). *Technical material: Koushinku N&H method-Vacuum consolidation method, kairyogata (in Japanese).*
16) Barron, R. (1948). Consolidation of fine-grained soil by drain wells. *Trans. ASCE.* Vol. 113, 718-742.

17) Bergado, D. T., Chai, J. C., Minura, N., Balasubramaniam, A. S. (1998). PVD improvement of soft Bangkok clay with combined vacuum and reduce sand embankment loading. *Proceeding of the Institution of Civil Engineering-Geotechnical Engineering* , 95-122.

18) Borges, J. (2008). Three-dimesional analysis of embankments on soft soils incorporating vertical drains by finite element method. *Computers and Geotechnics.* Vol. 31(8), 665-676.

19) Boulanger, R. W., Arulnathan, R., Harder Jr, L. F., Torres, R. A., Driller, M. W. (1998). Dynamic properties of Sherman Island Peat. *Geotechnical and Geoenvironmental Engineering.* Vol. 124. No. 1, 12-20.

20) Brawner, C. O. (1958). The muskeg problem in British Colombia highway construction. *4th Muskeg Reseach Conference., NRC, ACSSM,* Technical memorandum 54 (pp. 45-53). Ottawa, Canada: National Reseach Council of Canada.

21) Brinkgreve, R.B.I., Vermeer, P.A., Vos, E. (1994). Consitutive aspects of an embankment widening project. *Advances in understanding and modelling the mechanical behaviour of peat* (pp. 143-158). Delft, Netherlands: A.A. Balkema.

22) Chai, J. C., Carter, J. P., Hayashi, S. (2006). Vacuum consolidation and its combination with embankment loading. *Canadan Geotechnical Journal*. Vol. 43(10) 985-996.

23) Chai, J.C., Carter, J.P., Hayashi, S. (2005). Ground deformation induced by vacuum consolidation. *Journal of Geotechnical and Geoenvironmental Engineering*. Vol. 131(12) 1552-1561.

24) Chai, J.C., Miura, N., Bergado, D.T. (2008). Preloading clayey deposit by vacuum pressure with cap-drain: analyses versus performance. *Geotextiles and Geomembranes*. Vol. 26(3) 220-230.

25) Chai, J.C., Shen, S.L., Miura, N., Bergado, D.T. (2001). Simple method of modelling PVD improved subsoil. *Journal of Geotechnical and Geoenviromental Engineering, ASCE*. Vol. 127(11) 965-972.

26) Christian, J.T. and Boehmer, J.W. (1970). Plane strain consolidation by finite elements. *Proceeding of ASCE, SM 4*, (pp. 1435-1457).

27) Cogno, J. M., Juran, I., Thevanayagam, S. (1994). Vacuum consolidaion technology-principles and field experience. *The Conference on Vertical and Horizontal Deformations of Foundations and Embankment, College Station, TX, USA* (pp. 1237-1248). New York, USA: Geotechnical Special Publiaction 40.

28) Cola, S., Cortellazzo, G. (2005). The shear strength behavior of two peaty soils. *Geotechnical and Geological Engineering (Springer)*, 679-695.

29) Craig, R. (1992). *Soil mechanics. 5th edition.* London: Chapman & Hall.

30) Edil, T. B., Simon-Gilles, D. A. (1986). Settlement of embankments on peat: Two case histories. *Advances in Peatland Engineering* (pp. 147-154). Carleton University, Ottawa, Canada: National Research Council of Canada.

31) Gould, R.A., Philip, Bedell, R., Muckle, J.G. (2002). Construction over organic soils in an urban. *Canadian Geotechnical Journal*. Vol. 39 345-356.

32) Hanrahan, E. T. (1954). An investigation of some physical properties of peat. *Geotechnique.* Vol. 4, 108-121.

33) Hanrahan, E. T. (1964). A road failure on peat. *Geotechnique*, Vol. 14 185-202.

34) Hartlen. J., Wolski, W. (1996). *Embankments on organic soils - Developments in Geotechnical Engieering.* Vol. 80. Amsterdam: Elservier.

35) Hashiguchi, K. (1978). Plastic constitutive equations of granular materials. *US-Japan Seminar on Continuum Mechanics and Statistical Approaches in the Mechanics of Granular Materials* (pp. 321-329). Sendai, Japan: JSSMFE.

36) Hashiguchi, K. (1989). Subloading surface model in uncoventional plasticity. *International Journal of Solids and Structures.* Vol. 25, 917-945.

37) Hashiguchi, K., Chen, Z.P. (1998). Elasto-plastic constitutive equations of soils with subloading surface and rotational hardening. *International Journal of Numerical Analysis Method on Geomechanics.* Vol. 22, 197-227.

38) Hayashi, H., Nishimoto, S., Takahashi, M. (2011). Field performance of PVD combined with reinforced embankment on peaty ground. *Soils and Foundations*. Vol. 51(1) 191-201.

39) Hayashi, H., Yamazoe, N., Mitachi, T., Tanaka, H., Nishimoto, S. (2012). Coefficient of earth pressure at rest for normally and overconsolidated peat ground in Hokkaido area. *Soils and Foundations*. Vol. 52 (2) 299-311.

40) Hirata, M., Kitho, M., Yamada, K., Iizuka, A., Arai, K. (2010a). Deformation behavior and countermeasure of expressway embankment on super-soft ground. *Journal of Japan Society of Civil Engineers C*. Vol. 66 (2) 356-369 (in Japanese).

41) Hirata, M., Shimizu, H., Fukuda, J., Yamada, K., Kawaida, M. (2010b). F.E. Simulation for vertical drain placing ground using expanded maco-element method. *Journal of applied mechanics, JSCE.* Vol. 13, 431-442.

42) Hird, C.C., Pyrah, I.C., Russell, D. (1994). Finite element modelling of vertical drains beneath embankments on soft ground. *Geotechnique*.Vol. 42(3), 499-511.

43) Hobbs, N. B. (1986). Mire morphology and the properties and behaviour of some British and foreign peats. *The Quaternary journal of engineering geology.* Vol 19 (1), 7-80.

44) Huat, B. B. K., Prasad, A., Asadi, A., Kazemian, S. (2014). *Geotechnics of organic soils and peat.* London: CRC Press/Balkema.

45) Inagaki, M., Nakano, M., Noda, T., Tashiro, M., Asaoka, A. (2010). Proposal of a simple method for judging naturally deposited clay grounds exhibiting large long-term settlement due to embankment loading. *Soils and Foundations*, Vol. 50, 109-122.

46) Indraratna, B., Bamunawita, C., Khabbaz, H. (2004). Numerical modelling of vacuum preloading and field applications. *Canadian Geotechnical Journal*. Vol. 41 1098-1110.

47) Indraratna, B., Rujikiatkamjorn, C., Sathananthan, I. (2005). Analytical and numerical solutions for a single vertical drain including the effects of vacuum preloading. *Canadian Geotechnical Journal*. Vol. 42 994-1014.

48) Japan Highway Public Corporation. (1998). *Design guideline (Sekkei youryou), Earthwoks-Countermeasures for soft ground (in Japanese).*

49) Japanese Geotechnical Society. (2004). *The story of peat (Deitan no ohanashi)*. Geotech-note 14 (in Japanese).

50) Karlsson, R., Hansbo, S. (1981). *Soil classification and identification.* Stockholm: Swedish council for building research D8:81.

51) Karunawardena, W. A. (2007). *Consolidation analysis of Sri Lanka peaty soil using elasto-viscoplastic theory.* Kyoto, Japan: PhD Thesis, Kyoto University.

52) Karunawardena, A., Toki, M. (2013). Design and Performance of Highway Embankments Constructed Over Sri Lanka Peaty Soils. *The 18th International Conference on Soil Mechanics and Geotechnical Engineering* (pp. 2949-2952). Paris, France: Presses des Ponts.

53) Kazemian, S., Huat, B.B.K., Prasad, A., Barghchi, M. (2011). A state of art review of peat: Geotechnical engineering perspective. *International journal of physical sciences.* Vol. 6 (8), 1974-1981.

54) Kjellman, W. (1952). Consolidation of clay soil by means of atmospheric pressure. *Proceeding of a Conference on Soil Stabilization* , (pp. 258-263). Massachuset Institute of Technology, Boston.

55) Kosaka, T., Kawakita, M., Inagaki, M., Teerachaikulpanich, N. (2011). Performance of Vacuum Consolidation for High Embankment of Expressway Construction on an Extremely Soft Ground. *The International Conference on Geotechnics for sustainable development (Geotec Hanoi 2011)*, (pp. 65-74). Hanoi, Vietnam.

56) Landva, A. O., Korpijaakko, E. O., Pheeney, P. E. (1983). Geotechnical classification of peats and organic soils. *Testing of peat and organic soils. ASTM special technical publication 820.* Vol. 17, 37-51.

57) Lea, N.D., Brawner, C.O. (1963). Highway design and construction over peat deposits in the lower Bristish Colombia. *Highway Research Record*, No. 7, pp. 1-32.

58) Lefebvre, G., Langlois, P., Lupien, C., Lavallee, J.G. (1984). Laboratory testing and in situ behavior of peat as embankment foundation. *Canadian Geotechical Journal*, 322-337.

59) MacFarlane, I. C. (1969). *Engineering characteristics of peat. Muskeg engineering handbook.* Toronto, Canada: Univerity of Toronto Press, Canada.

60) Mersi, G., Ajlouni, M. (2007). Engineering properties of fibrous peats. *Journal of Geotechnical and Geoenviromental Engnieering*, Vol. 133(7) 850-866.

61) Mersi, G., Khan, A. Q. (2012). Ground improvement using vacuum loading together with vertical drains. *Jounal of Geotechnical and Geoenvironmental Engineering*. Vol. 138(6) 680-689.

62) Mersi, G., Stark, T.D., Ajlouni, M.A., Chen, C.S. (1997). Secondary compression of peat with and without surcharging. *ASCE Journal of Geotechnical and Geoenvironmetal Engineering*. Vol. 123(5) 411-420.

63) Miyakawa, I. (1960). *Some aspects of road construction on peaty or marshy areas in Hokkaido, with particular reference to filling methods.* Civil Engineering Research Institute, Hokkaido Development Bureau, Saporo, Japan.

64) Mochinaga, R., Kurihara, N., Sezai, T. (1984). Historical aspects of countermeasures for expressway's embankmentworks on the soft ground. *Journal of Japan Society of Civil Engineers*. No. 349, 6 (1) , 74-83 (in Japanese).

65) Nakano, M., Sakai, T., Asaoka, A. (2010). Soil-water coupled finite deformation analysis of seismic deformation and failure of embankment on horizontal and inclined ground. *Soil Dynamics and Earthquake engineering*, *Geotechnical special publication No. 201, ASCE*, (pp. 139-144). Shanghai, China.

66) Nakae, S., Komatsubara, T., Naito, K. (2002). *Geology of Nishizu District, Quadrangle Series, 1:50 000, Geological Survey of Japan.* AIST (in Japanese with English abstract 3p.).

67) Nguyen, H.S., Tashiro, M., Inagaki, M., Yamada, S., Noda, T. (2015). Simulation and evaluation of improvement effects by vertical drains/ vacuum consolidation on peat ground under embankment loading based on a macro-element method with water absorption and discharge functions. *Soils and Foundations*. Vol. 55 (4), (In press)

68) Noda, T., Asaoka, A., Yamada, S. (2005a). Elasto-plastic behaviour of naturally deposited clay during/after sampling. *Soils and Foundations.* Vol. 45(1), 51-64.

69) Noda, T., Asaoka, A., Nakano, M., Yamada, E., Tashiro, M. (2005b). Progressive consolidation settlement of naturally deposited clayey soil under embankment loading. *Soils and Foundations*. Vol. 45 (5), 39-51.

70) Noda, T., Asaoka, A., Nakano, M. (2008a). Soil-water coupled finite deformation analysis based on a rate-type equation of motion incorporating the SYS Cam-clay model. *Soils and Foundations*, Vol. 48. 6., 771-790.

71) Noda, T., Nakai, K., Asaoka, A. (2008b). Delayed failure of a clay foundation-embankment system after the occurence of an earthquake. Theoretical and applied mechnanics Japan. Vol. 57, 41-47.

72) Noda, T., Yamada, S., Nonaka, T., Tashiro, M. (2015). Study on the pore water pressure dissipation method as a liquefaction countermeasure using soil-water coupled finite deformation analysis equipped with a macro element method. *Soils and Foundations*. (Accepted).

73) Noto, S. (1991). Geotechnical engineering of peat (Deitan jiban kougaku). *Gihodo (in Japanese)*.

74) Osorio, J. P., Farrell, E. R., O'Kelly, B. C., Casey, T. (2008). Rampart roads in the peat lands of Ireland: genesis, development and current performance. *The 1st International conference on transportation geotechnics* (pp. 227-233). Nottingham, UK: CRC Press.

75) Osorio, J. P., Farrell, E. R., O'Kely, B. C. (2010). Peat improvement under vacuum preloading: A novel approach for bog roads in Ireland. *Proceeding of the Joint Symposium on Bridge and Infrastructure Research in Ireland and Concrete Reseach in Ireland (BCRI 2010)*, (pp. 255-262). Cork, Ireland.

76) Pigott, P., Hanrahan, E. T, Somers, N. (1992). Major canal reconstruction in peat areas. *Proceeding or the ICE - water maritime and energy.* Vol. 96 (3), 141-152.

77) Porbaha, A., Hanzawa, H., Kishida, T. (2000). Analysis of a failed embankment on peaty ground. *Geo-Denver 2000* (pp. 281-293). August 5-8, Denver, Colorado, United State: American Society of Civil Engineers (ASCE).

78) Radforth, N. (1969). *Classification of Muskeg. In: MacFarlane, I. C. Muskeg engineering handbook. Canadian building series.* Toronto: University of Toronto Press.

79) Rixner, J.J., Kaemer, S.R., Smith, A.D. (1986). Prefabricated vertical drains 1, *Federal Highway Administration*, FHWA-RD-86/168

80) Root, A. (1958). California experience in construction of highway across mash deposits. *Washington DC, United State: Highway Research Board*, Bull. 173.

81) Roscose, K.H., Burland, J.B. (1968). On the generalized stress-strain behaviour of "wet" clay. *Engineering Plasticity (edit by Heyman, J. and Leckie, F.A* (pp. 535-609). Cambridge University Press.

82) Rujikiatkamjorn, C., Indararatna, B., Chu, J. (2007). Numerical modelling of soft soil stabilized by vertical drains, combining surcharge and vacuum preloading for a storage yard. *Canadian Geotechnical Journal*. Vol. 44 326-342.

83) Santagata, M., Bobet, A., Johnston, C.T., Hwang, J. (2008). One-dimension compression behavior of a soil with high organic matter content. *Journal of geotechnical and geoenvironmental engineering ASCE.* Vol. 134 (1), 1-13.

84) Saowapakpiboon. S., Bergado . D. T., Voottipruex. P., Lam. L. G., Nakakuma. K. (2011). PVD improvement combined with surcharge and vacuum preloading including simulations. *Geotextiles and Geomembranes*. Vol. 29, 74-92.

85) Sekiguchi, H., Ohta, H. (1977). Induced anisotropy and times dependency in clays. *9th International Conference on Soil Mechanics and Foundation Engineering*, (pp. 229-238). Tokyo.

86) Sekiguchi, H., Shibata, T., Fujimoto, A., Yamaguchi, H. (1986). A macro element approach to analyzing the plane strain behavior of soft foundation with vertical drains. *Proceeding of 31st symposium* (pp. 111-116). Japanese Geotechnical Society (in Japanese).

87) Sekiguchi, H., Shibata, T., Mimura, M., Sumikura, K. (1988). Behaviour of the seawall and bridge abutment at the edge of an offshore airport fill. *Annuals Disas. Prev. Res. Inst. Kyoto Univerity.* Vol. 32 (B-2) (pp. 123-145). Kyoto: (in Japanese).

88) Sellmejer, J. (1994). Anisotropic peat model. *Advances in understanding and modelling the mechanical behaviour of peat* (pp. 211-230). Delft, Netherlands: A.A. Balkema.

89) Shinsha, H., Hara., H., Abe, Y., Tanaka, A. (1982). Consolidation settlement and lateral displacement of soft ground improved by sand drains. *Tsuchi-to-Kiso.* Vol. 30(5), 7-12 (in Japanese).

90) Shinsha, H., Yoneya, H., Nagastu, T. (2006). Review of progress in the vacuum consolidation method. *Soil mechanics and foundation engineering, Japanese Geotechnical Engineering society*. Vol. 54(7) 16-18 (in Japanese).

91) Skempton, A. W., Petley, J. (1970). Ignition loss and other properties of peats and clays from Avonmouth King's Lynn and Cranberry Moss. *Geotechnique.* Vol. 20 (4), 343-356.

92) Takaine, T., Tashiro, M., Shiina, T., Noda, T., Asaoka, A. (2010). Predictive simulation of deformation and failure of peat-calcareous layered ground due to multistage test embankment loading. *Soils and Foundations*. Vol. 50 (2), 245-260.

93) Takeyama, T., Aoki, A., Arai, A., Ohta, H. (2008). Application of macro-element method to vacuum consolidation (part1). *43rd Anual Conference of Japan Society of Civil Engineering (JSCE)* (pp. 887-888). (in Japanese).

94) Tan, Y. (2008). Finite element analysis of highway construction in peat bog. *Canadian Geotechnical Journal*. Vol. 45 147-160.

95) Tashiro, M., Noda, T., Inagaki, M., Nakano., M, Asaoka, A. (2011). Prediction of settlement in natural deposited clay ground with risk of large residual settlement due to embankment loading. *Soils and Foundations*. Vol. 51 (1), 133-149.

96) Tashiro, M., Nguyen, H.S., Inagaki, M., Yamada, S., Noda, T. (2015). Simulation of large-scale deformation of ultra-soft peaty ground under test embankment loading and investigation of effective countermeasures against residual settlement and failure. *Soils and Foundations*. Vol. 55 (2), 343-358.

97) Taylor, D. (1948). *Fundamentals of soil mechanic.* New York, USA: John Wiley & Sons.

98) Termaat, R., Topolnicki, M. (1994). Biaxial tests with natural and artificial peat. *Advances in understanding and modelling mechanical behaviour of peat* (pp. 241-252). Delft, Netherlands: A.A. Balkema.

99) Terzaghi, K. P. (1996). *Soil mechanics in Engineering pratice.* New York: John Wiley & Sons Inc.

100) The Geological Survey of Japan. (2001). *1:50 000 Geomorphological land classification map "Nishizu Kumagawa".* Fukui Prefecture, Japan.

101) Tran, T.A., Mitachi, T. (2008). Equivalent plane strain modelling of vertical drains in soft ground under embankment combined with vacuum preloading. *Computers and Geotechnics*. Vol. 35 655-672.

102) Ulusay, R., Tuncay, E., Hasancebi, N. (2010). Geo-engineering properties and settlement of peaty soils at an industrial site (Turkey). *Bulletin of Engineering geology and the enviroment.* Vol. 69 (3), 397-410.

103) Van Baars, S. (2005). The horizontal failure mechanism of the Wilnis peat dyke. *Geotechnique*. Vol. 55(4) 319-323.

104) Vonk, B. F. (1994). Some aspects of the engineering pratice regarding peat in small polder dikes. *Advances in Understanding and Modelling the Mechanical Behaviour of Peat* (pp. 389-402). Delf, Netherlands: A.A Balkema.

105) Whitlow. (2010). *The geology of the Gold Coast Region.* Gold Coast, Australia: Report prepared for Gold Coast City.

106) Wilson, N.E., Radforth, N.W., Macfarlane, I.C., Lo, M.B. (1965). The rates of consolidation for peat. *6th International Conference on Soil Mechanic and Foundation Egnieering*, (pp. 407-411). Montrael, Canada.

107) Yamada, S., Noda, T. (2013). Simulation of delayed failure in naturally deposited clay ground by soil-water coupled finite deformation analysis taking inertial forces into consideration. *18th Internation Conference on Soil Mechnanics and Foundation Engineering* , (pp. 841-844). Paris.

108) Yamada., S., Noda., T., Tashiro., M., Nguyen, H.S. (2015). Macro element method with water absorption and discharge functions for vertical drains. *Soils and Foundations*. (Accepted)

109) Yamaguchi, H., Hashizume, Y., Ikenaga, H. (1992). Change in pore size distribution of peat in shear processes. *Soils and Foundations*. Vol. 32(4) 1-16.

110) Yamaguchi, H., Ohira, Y., Kogure, K. (1985a). Volume change characteristics of undisturbed fibrous Peat. *Soils and Foundations*. Vol. 25(2) 119-134.

111) Yamaguchi, H., Ohira, Y., Kogure, K. and Mori, S. (1985b). Undrained shear characteristics of normally consolidated peat under triaxial compression and extension conditions. *Soils and Foundations*. Vol. 25(3) 1-18.

112) Yamaguchi, H., Zushi, M., Ohira, Y., and Kogure, K. (1987). A few considerations on triaxial shear properties of Peat (only abstract in English). *Japanese Society of Soil Mech. and Foud. Eng., 7 (6)*, (pp. 111-120). Tokyo, Japan.

113) Yan, S.W, Chu, J. (2005). Soil improvement for a storage yard using the combined vacuum and fill preloading method. *Canadian Geotechnical Journal*. Vol. 42(4) 1094-1104.

114) Yoshikuni, H. (1979). Design and construction control of vertical drain methods. *Foundation Engineering Series (in Japanese).* Gihodo Publishing Co.

115) Yoshikuni, H., Nakanodo, H. (1974). Consolidation of soils by vertical drain wells with finite permeability. *Soils and Foundations.* Vol. 14(2), 35-46.

116) Zwanenburg, C. (2005). *The influence of anisotropy on the consolidation behavior of Peat*. PhD Thesis. Delft University of Technology: Delft University Press.

117) Zwanenburg, C., Den Haan, E. J., Kruse, G. A. M., Koelewijn, A. R. (2012). Failure of a trial embankment on Peat in Booneschans, the Netherlands. *Géotechnique*. Vol. 62 479-490.

Appendix A1

Physical model for the static soil-water coupled governing equations

The physical model for the following soil-water coupled equation is given based on Asaoka et al. (1994, 1997b).

$$-\int_v \mathrm{tr}\boldsymbol{D}dv = \int_a \boldsymbol{v}' \cdot \boldsymbol{n}da\,, \tag{A1}$$

where $\boldsymbol{D}$ denotes the stretching tensor of soil skeleton.

The flow rates $\boldsymbol{v}_1'$ and $\boldsymbol{v}_2'$ shown in **Fig. A1** are approximated using the following equations (although the figure depicts a 2-dimensional analysis, it is the same for 3 dimensions):

$$\boldsymbol{v}_1' = -k_1 \frac{h_c - h}{l_1} \frac{\boldsymbol{l}_1}{l_1} \tag{A2}$$

$$\boldsymbol{v}_2' = -k_2 \frac{h_i - h_c}{l_2} \frac{\boldsymbol{l}_2}{l_2} \tag{A3}$$

where k_1 and k_2 are the permeability coefficients for elements 1 and 2, respectively. If $\boldsymbol{v}'^i = \boldsymbol{v}_1' = \boldsymbol{v}_2'$ is set, then $\boldsymbol{v}'^i$ can be expressed as follows:

$$\boldsymbol{v}'^i = -k^i \frac{h_i - h}{l^i} \frac{\boldsymbol{l}^i}{l^i} \tag{A4}$$

$$k^i = \frac{k_1 k_2 (l_1 + l_2)}{k_1 l_2 + k_2 l_1} \tag{A5}$$

where k^i is an apparent permeability coefficient incorporated to approximate the flow from element 1 to element 2. Furthermore, the right side of **Eq. (A1)** can be approximated using $\boldsymbol{v}'^i$ as follows:

$$\int_a \boldsymbol{v}' \cdot \boldsymbol{n}da = \sum_{i=1}^{m} \boldsymbol{v}'^i \cdot \boldsymbol{n}^i s^i \tag{A6}$$

where m is the number of faces composing the element. By discretizing the left side of **Eq. (A1)** into finite elements and substituting **Eq. (A4)** into **Eq. (A6)**, the following physical model for Eq. (A1) is obtained.

$$-\mathrm{L}\left\{\boldsymbol{v}^{\mathrm{N}}\right\}=\sum_{i=1}^{m}\alpha_i(h-h_i) \tag{A7}$$

$$\alpha_i=\frac{k^i}{l^i}\frac{\boldsymbol{l}^i}{l^i}\cdot\boldsymbol{n}^i s^i \tag{A8}$$

Here, $\left\{\boldsymbol{v}^N\right\}$ is the node velocity vector, L is the matrix for converting $\left\{\boldsymbol{v}^N\right\}$ to the element's volume change rate, and α_i is the coefficient of pore water flow through boundary surface i to the adjacent element.

When boundary surface i is designated as an impermeable boundary surface, there is no flow of pore water through that surface and α_i is set to zero. On the other hand, when boundary surface i is designated as a permeable boundary, in addition to assigning h_i to the center of the boundary surface, $\boldsymbol{l}^i$ and k^i in Eq. (A8) are specified in the following manner to calculate α_i.

$\boldsymbol{l}^i$: vector from the center of the element to the center of boundary surface i.

k^i : permeability coefficient for the element.

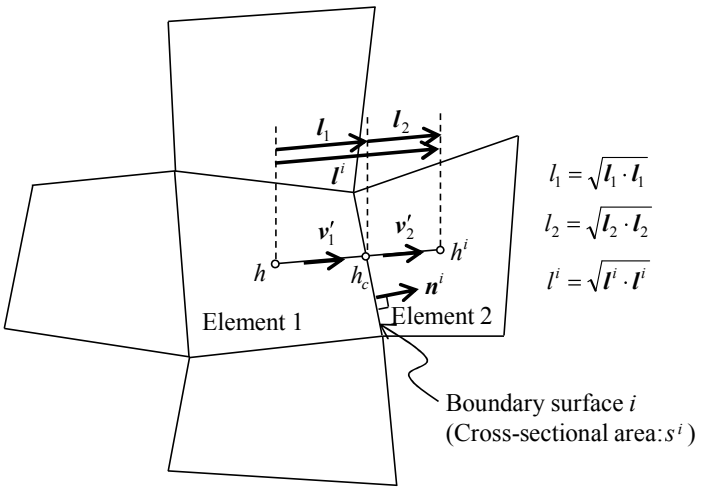

Figure A1. Comparison of ground settlements beyond embankment center

Appendix A2

Governing equations of the dynamic soil-water finite deformation analysis applied with the macro element method with water absorption and discharge functions for vertical drains (For details, referred to Noda et al., 2015)

The soil-water finite deformation analysis with inertia terms developed by Noda et al. (2008a) employs a so-called ***u*-*p*** formulation to obtain the nodal displacement velocity vector $\{\boldsymbol{v}^N\}$ and representative pore water value u for each element by solving the space-discretized rate-type equation of motion and soil-water coupled equation given by

$$\mathrm{M}\{\dot{\boldsymbol{v}}^N\}+\mathrm{K}\{\boldsymbol{v}^N\}-\mathrm{L}^{\mathrm{T}}\dot{u}=\{\dot{\boldsymbol{f}}\} \tag{A1}$$

$$\frac{k}{g}\mathrm{L}\{\dot{\boldsymbol{v}}^N\}-\mathrm{L}\{\boldsymbol{v}^N\}=\sum_{i=1}^{m}\alpha_i(h-h_i)\rho_w g \tag{A2}$$

where M is the mass matrix, K is the tangent stiffness matrix, L is the matrix for converting $\{\boldsymbol{v}^N\}$ to the element volume change rate, $\{\dot{\boldsymbol{f}}\}$ is the nodal force rate vector, $\{\dot{\boldsymbol{v}}^N\}$ and $\{\ddot{\boldsymbol{v}}^N\}$ denote the nodal acceleration and jerk vectors, and h and h_i represent the total heads corresponding to the representative values for water pressure for an element and adjacent elements, respectively, k is the permeability coefficient for the ground, g is the magnitude of the gravitational acceleration, α_i is the coefficient of pore water flow to adjacent elements, ρ_w is the density of water, and m is the number of boundary surfaces for each element. The first term on the left-hand side of **Eqs. (A1)** and **(A2)** is the one which vanishes when inertia forces does not work.

In the macro element method proposed by Yamada et al. (2015), the water absorption and discharge functions of vertical drains were introduced into the above analytical method by the following procedures;

First, to incorporate the water absorption function of vertical drains into each element, the soil-to-drain pore water flow rate is added to the right-hand side of **Eq. (A2)**, yielding the following expression.

$$\frac{k}{g}\mathrm{L}\{\dot{\boldsymbol{v}}^N\}-\mathrm{L}\{\boldsymbol{v}^N\}=\sum_{i=1}^{m}\alpha_i(h-h_i)\rho_w g+\kappa(h-h_D)\rho_w g \tag{A3}$$

Eq. (A3) is called the soil-water continuity equation and replaces **Eq. (A2)** as a governing equation. Here, h_D is the representative value for total head in the drain for each element. κ is the coefficient of pore water flow from the soil to the drain and given by the following equations:

$$\kappa=\frac{8kV}{F(n)d_e^2\rho_w g}, \tag{A4}$$

$$F(n)=\frac{n^2}{n^2-1}\ln n-\frac{3n^2-1}{4n^2},\quad n=\frac{d_e}{d_w}. \tag{A5}$$

in which V is the current volume of each element. d_e and d_w represent the equivalent diameter and diameter of circular drain, respectively, and are treated as material constants.

Next, to incorporate the discharge function of the drains in the macro element method, the following continuity equation for the drain is introduced to governing equations, on the assumption that the mesh division from the top to the bottom of the improved region is initially divided up approximately vertically:

$$\kappa(h-h_D)\rho_w g=\sum_{j=1}^{2}\beta_j(h_D-h_{Dj})\rho_w g \tag{A6}$$

where β_j is the coefficient of water flow through the virtual drain contained in each element, and h_{Dj} is the total head of the drain contained in the elements above and below the macro element. For the sake of simplicity, it is assumed that water flow through the drain obeys Darcy's law. Bearing in mind that the ratio of the cross-sectional area of the virtual drain to the area of the boundary surface between the elements connected above and below is $1/n^2$, β_j is given by the following equation:

$$\beta_j=\frac{k_w}{l^j}\frac{\boldsymbol{l}^j}{l^j}\cdot\boldsymbol{n}^j\frac{s^j}{n^2} \tag{A7}$$

where each symbol is defined as illustrated in **Fig. A1**. k_w is the permeability coefficient for a circular drain and is treated as a material constant. The boundary conditions for **Eq. (A6)** are handled in the same manner as the hydraulic boundary conditions for **Eq. (A2)**.

Consequently, **Eqs. (A1)**, **(A3)**, and **(A5)** represent the governing equations when the macro element method is applied. Solving these equations simultaneously yields $\{\boldsymbol{v}^N\}$, u, and u_D, which is the water pressure corresponding to h_D.